Università Politecnica delle Marche
Facoltà di Ingegneria
Dipartimento di Meccanica

DOTTORATO DI RICERCA IN INGEGNERIA MECCANICA V CICLO - NUOVA SERIE
SETTORE DISCIPLINARE: ING/IND 12

Developement of the Unbalanced Force Mapping Method for Defect Detection from Surface Velocity Mesureaments in Layered Shell Structure

Coordinator: Chiar.mo Prof. Enrico Evangelista
Supervisors: Chiar.mo Prof. Enrico Primo Tomasini
Prof. Paolo Castellini

PhD Candidate: Roberto Bernetti

,

Contents

I The Mathematical Model **7**

1 The Thick/Thin Shell Structural Model **8**
1.1 Governing Equations for a Composite Plate Under Bending Deformation . . . 8
1.1.1 Equilibrium Equations . . . 8
1.1.2 Constitutive Equations . . . 12
1.1.3 Stress-Strain Relationship . . . 12
1.1.4 Kinematic Relations . . . 15
1.1.4.1 Thin Plate Condition . . . 15
1.1.4.2 Thick Plate Condition . . . 20

2 The Mixed Finite Element Method for Shell/Beam Structure **26**
2.1 The Equations . . . 26
2.2 The Compatibility Equation . . . 27
2.2.1 The Equilibrium Equations . . . 29
2.2.2 The Shear Effect . . . 31
2.3 Finite Element Model . . . 33
2.3.1 The Weak Formulation . . . 33
2.3.2 The Shape Function and the Finite Element Matrix . . . 36
2.3.3 Solution with "Displacement Only Method" . . . 38
2.3.3.1 Applying End Rotations . . . 39
2.3.3.2 Applying End Moments . . . 39
2.3.3.3 Applying End Displacements or Shear Forces 44
2.4 Numerical Tests . . . 45
2.4.1 Eigen Mode Extraction . . . 45
2.4.2 Time Integration . . . 48

3 Spatial Frame Applications of Beam Element **55**
3.1 The column behaviour . . . 55
3.2 Matrix Rotation . . . 57

3.2.1 Coupling Column and Bending Behaviour 59
3.2.2 Local to Global system Transformation 61
3.2.2.1 End Rotations Condition 64
3.3 Numerical Example 67

II The Experimental Data Post-Processing 71

4 Laboratory Test Normal Surface Displacement Determination 72
4.1 Introduction 72
4.2 Sample building 72
4.3 measurement chain 74

5 The Finite Element Model 78
5.1 Introduction 78
5.2 The Elements 78
5.3 Typical analysis results 80

6 Experimental vs Virtual Laboratory results 82
6.1 The Input Force 82
6.2 Experimental results 83
6.2.1 Eigen-frequencies comparison 83
6.2.2 Frequency Response to Impulsive Input 84

7 Unbalanced Force Mapping Method 92
7.1 Unbalanced Force Mapping Method (UF2M) 92

8 Test of UF2M Performances 95
8.1 Introduction 95
8.2 The Virtual Laboratory 95
8.3 The Displacements Frequency Response 96
8.4 The Unbalanced Force Calculation 99
8.5 Conclusion 105

Foreward

In the last few years use of composite material is increased because their mechanical properties outperform the ones of classical material thanks to the ratio between stiffness and weight. The most useful application fields are in aeronautics, automotive and naval where there are critical operating conditions (for instance: high temperature) and low weight is required. Considering the performance of the composite they are substituting the other material as aluminum, or steel in many applications, above all, because their fibers can be oriented along the stress directions.

Due to their high end application Defect Detection is a main activity in composite making and maintenance, in particular Non Destructive Tests (NDT) is highly wanted. It is widely used in the mechanical industries to monitor own products both along the production process and at the end of it: integrity of mechanical structure is most wanted by the factories. Above all NDT is used in the maintenance operation, because the residual life of the products should be estimated, without using invasive test; i.e. changing geometric or physical properties. Here attention is posed on the detection of delamination defect both at the end of production line and during operation, due to fatigue or other load condition, requiring to determine both the in-plane defect position and extension.

In the present work a method is developed that, using the vibration data gathered from the surface measurement of displacements or velocities, is able to analyze them and to assess the position and length of the structural anomalies of a beam or shell layered structure.

The key idea is to use a standard linear Finite Element Model (hereafter FEM) of the structure to reproduce the balance effect between the inertial and elastic forces in the free vibrating area of the structure.

The linear matrix application, representing the FEM, will map the vector space of the measured nodal displacements to the vector space of the applied external nodal forces. From a theoretical point of view the resultant forces must be zero in the nodes under free vibration condition and as a consequence the applied external nodal force vector must be a null vector.

A gap between the mathematical model and the real physical model in an homogeneous structure will anyway be present and will results in a force vector different from zero with a constant in space mean error distribution. This non-zero value represents the unbalanced forces between the inertial and elastic component due to the model uncertainty. For this reason the resulting vector is called Unbalanced Force Vector.

The nodal components of the Unbalanced Force Vector which show a peak, respect to the mean value, highlights the area where it is possible to guess the

presence of a deviation from the standard mechanical or geometric characteristics.

To reduce the error associated with the differentiation of the measured displacements a Mixed Finite Element approach has been adopted to decrease to a minimum the degree of the derivative present in the mathematical operator representing the dynamic vibration of the structure. The performance of the Mixed Finite Element Method in dynamic condition has been tested versus standard Finite Element Method. The Mixed formulation clearly outperforms the standard formulation in the stress and internal action calculation in modal or transient analysis.

The need for a variety of delamination condition has been highlighted to better test the method, giving rise to the development of a virtual laboratory which overtakes the practical difficulties in the realization of a controlled delamination defect into the beam or shell structure.

Following the previous considerations two main advantages can be highlighted:

1. no requirements for accurate knowledge of the mechanical characteristic of the structure

2. no needs of contact measurements (except for the excitation area) or part dis-assembling

The results obtained support the hypothesis at the basis of the method. In fact in almost all the test cases the mean unbalanced force "noise" value to the peak value ratio is alway less then 20%, allowing for a clear identification of the possible defected area. Moreover it has been possible to associate a clear pattern with the presence of delamination defect.

The thesis is divided in two part:

1. the first part describes the mathematics used to model the physics of the natural phenomenon

2. the second part describes the laboratory measurement method used to verify the FEM model used to generate the measurement data and the post-processing technics used to detect the anomalies present in the structure.

The first part is divided into two chapters:

1. one concerns the mathematical model used to simulate the structural behaviour of the beam/shell

2. the other describe the deduction of the numerical model.

The second part is divided into four chapters:

1. the laboratory experiment used to validate the FEM model
2. the FEM model used to reproduce the virtual laboratory
3. the comparison between laboratory tests and FEM calculation
4. the Unbalanced Forces Mapping Method,
5. and the last one the results of the test of the unbalanced force method.

Acknowledgments

At the end of this job I wish to thank for the unvaluable support Prof. Enrico P. Tomasini, Prof. Nicola Paone, Prof. Paolo Castellini, Prof. Marco Revel, the whole staff and all the PhD students of the "Dipartimento di Meccanica" of the Università Politecnica delle Marche.

Part I

The Mathematical Model

Chapter 1

The Thick/Thin Shell Structural Model

To better understand the effect of the presence of anomalies or delamination it is necessary to develop a mathematical model for the structure composed by two or more "laminas" bonded together to form a laminated composite.

This non-homogeneous anisotropic plate should now be consider a whole structure and the main aim is to define its response to external loads as a whole rather then a multicomponent structure.

This development will start with the definition of the stress-strain relationship and then the introduction of the classical equations for the flexural behaviour of thin/thick plate, then adding consideration about the shear effects on the deflection surface and concluding with the influence of the principal failure mechanism, the "delamination"

1.1 Governing Equations for a Composite Plate Under Bending Deformation

The governing equations are obtained by combining the constitutive relations and the equilibrium equations. The constitutive relations take under consideration of anisotropic behaviour of the component materials in the form of the stress-strain relationship, while the equilibrium equations consider the way in which the laminas are bonded together to form the structure.

1.1.1 Equilibrium Equations

As common in the small deformation analysis the following assumption has been hold valid in the following developments:

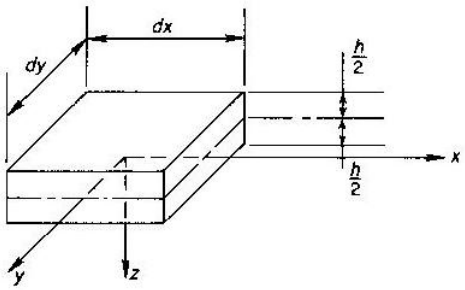

(a) Reference frame

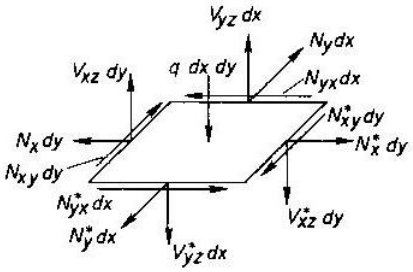

(b) Vertical equilibrium

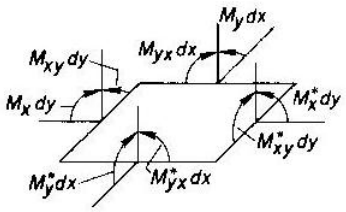

(c) Rotational equilibrium

Figure 1.1: equilibrium diagram for vertical translation and rotation

- initial and final configuration can be considered identical from the point of view of the equilibrium equations

The figure 1.1 shows an infinitesimal element of the plate structure with the accompanying reference frame in which the following position has been done:
in which:

$$M_x = \int_{-\frac{h}{2}}^{\frac{h}{2}} \sigma_x z dz$$

$$M_y = \int_{-\frac{h}{2}}^{\frac{h}{2}} \sigma_y z dz$$

$$M_{xy} = \int_{-\frac{h}{2}}^{\frac{h}{2}} \tau_{xy} z dz$$

$$V_{xz} = \int_{-\frac{h}{2}}^{\frac{h}{2}} \tau_{xz} dz$$

$$V_{yz} = \int_{-\frac{h}{2}}^{\frac{h}{2}} \tau_{yz} dz$$

$$V_{xz}^* = V_{xz} + \frac{\partial V_{xz}}{\partial x} dx$$

$$V_{yz}^* = V_{yz} + \frac{\partial V_{yz}}{\partial y} dy$$

$$M_x^* = M_x + \frac{\partial M_x}{\partial x} dx$$

$$M_y^* = M_y + \frac{\partial M_y}{\partial y} dy$$

$$M_{xy}^* = M_{xy} + \frac{\partial M_{xy}}{\partial x} dx$$

It is worthwhile to recall that:

M_x is the moment vector parallel to y axis

M_y is the moment vector parallel to x axis

In the previous equation the plane $z = 0$ is assumed to be placed in the middle surface of the plate, and the mechanical and geometrical characteristics of the structure are symmetric respect to that plane. This assumption allow to satisfy the condition for decoupling the *"out of plane deformation"* from the *"in plane deformation"*.

From a general point of view the reference surface, in the presence of bonded laminas with different mechanical characteristic or dimensions, could not be effectively defined to avoid bending and normal stresses coupling due to the fact that one parameter z_0, the position of the reference surface, should

satisfy the condition that constant strain state, through the thickness, have to results in zero bending and torsional moment, which results in:

$$\begin{aligned}\sum_{k=1}^{N}\int_{z_{k-1}}^{z_k}(C_{11}^k\varepsilon_x^0+C_{12}^k\varepsilon_y^0)zdz &= 0\\ \sum_{k=1}^{N}\int_{z_{k-1}}^{z_k}(C_{21}^k\varepsilon_x^0+C_{22}^k\varepsilon_y^0)zdz &= 0\\ \sum_{k=1}^{N}\int_{z_{k-1}}^{z_k}C_{44}^k\gamma_{xy}^0zdz &= 0\end{aligned}$$

in which:

C_{ij}^k the stiffness matrix of the $k-th$ lamina

N the number of laminas

ε_x^0 constant deformation in the x direction

ε_y^0 constant deformation in the y direction

γ_{xy}^0 constant shear in the $x-y$ plane

In the same way the internal action can be rewritten as:

$$M_j=\sum_{k=1}^{N}\int_{z_{k-1}}^{z_k}\sigma_j z dz \qquad j=x,y \qquad M_{xy}=\sum_{k=1}^{N}\int_{z_{k-1}}^{z_k}\tau_{xy}zdz \tag{1.1}$$

$$V_{xz}=\sum_{k=1}^{N}\int_{z_{k-1}}^{z_k}\tau_{xz}dz \qquad V_{yz}=\sum_{k=1}^{N}\int_{z_{k-1}}^{z_k}\tau_{yz}dz \tag{1.2}$$

in which $z_k$are the coordinate of the plane bounding each lamina.

The figure 1.1 (b) and (c) show the equilibrium diagram for the translation and rotational forces and momentum. The summation of force in the z direction has to be zero:

$$\frac{\partial V_{xz}}{\partial x}dxdy+\frac{\partial V_{yz}}{\partial y}dydx+qdxdy=0$$

simplifying:

$$\frac{\partial V_{xz}}{\partial x}+\frac{\partial V_{yz}}{\partial y}=-q \tag{1.3}$$

the same results for the moment summation around x and y axis, in which third order infinitesimal quantity has been dropped:

$$V_{yz}dxdy - \frac{\partial M_y}{\partial y}dydx - \frac{\partial M_{xy}}{\partial x}dxdy = 0$$

simplifying the incremental quantity:

$$V_{yz} = +\frac{\partial M_y}{\partial y} + \frac{\partial M_{xy}}{\partial x} \tag{1.4}$$

and:

$$V_{xz}dydx - \frac{\partial M_x}{\partial x}dydx - \frac{\partial M_{xy}}{\partial y}dydx = 0$$

after simplifying:

$$V_{xz} = \frac{\partial M_x}{\partial x} + \frac{\partial M_{xy}}{\partial y} \tag{1.5}$$

The substitution of equation 1.4 and 1.5 into equation 1.3 determines the following equations:

$$\frac{\partial^2 M_x}{\partial x^2} + 2\frac{\partial^2 M_{xy}}{\partial x \partial y} + \frac{\partial^2 M_y}{\partial y^2} = -q(x,y) \tag{1.6}$$

1.1.2 Constitutive Equations

The constitutive equations, connecting the deformation to the internal actions, are obtained combining:

1. the stress-strain relationship, connecting strains and stresses induced by the deformation displacements
2. the kinematic relationships connecting the structure displacements with the material strains.

1.1.3 Stress-Strain Relationship

From elementary elasticity, the generalized Hooke's law can be used to connect the stress to the strain in a material:

$$\sigma_{ij} = C_{ijmn}\varepsilon_{mn} \tag{1.7}$$

in which:

ε_{ij} the linear deformation tensor

C_{ijmn} the Stiffness tensor

σ_{mn} the stress tensor

From hereon it is better, in the view of the Finite Element formulation, to use a vector notation rather then a tensorial one and the engineering strain. So the strain vector can be obtained in the following manner:

$$\boldsymbol{\varepsilon} = \begin{bmatrix} \varepsilon_x \\ \varepsilon_y \\ \varepsilon_z \\ \gamma_{xy} \\ \gamma_{yz} \\ \gamma_{xz} \end{bmatrix} = \begin{bmatrix} \varepsilon_{11} \\ \varepsilon_{22} \\ \varepsilon_{33} \\ 2\varepsilon_{12} \\ 2\varepsilon_{23} \\ 2\varepsilon_{13} \end{bmatrix}$$

in the same guise for the stress:

$$\boldsymbol{\sigma} = \begin{bmatrix} \sigma_x \\ \sigma_y \\ \sigma_z \\ \tau_{xy} \\ \tau_{yz} \\ \tau_{xz} \end{bmatrix} = \begin{bmatrix} \sigma_{11} \\ \sigma_{22} \\ \sigma_{33} \\ \sigma_{12} \\ \sigma_{23} \\ \sigma_{13} \end{bmatrix}$$

Following the previous position the stiffness tensor can be represented by a matrix:

$$\boldsymbol{C} = [C_{ij}]$$

The matrix $\boldsymbol{C}$ is, in general, fully populated but according to usual assumptions the 36 elements of the matrix can be reduced. The assumptions used hereafter are:

1. orthotropic Material
2. plane stress

The orthotropic assumption can reduce to 12 the non-zero elements, in fact if the shear deformation cannot induce normal stresses the matrix $\boldsymbol{C}$ assumes the following form:

$$\boldsymbol{C} = \begin{bmatrix} C_{11} & C_{12} & C_{13} & 0 & 0 & 0 \\ C_{12} & C_{22} & C_{23} & 0 & 0 & 0 \\ C_{13} & C_{23} & C_{33} & 0 & 0 & 0 \\ 0 & 0 & 0 & C_{44} & 0 & 0 \\ 0 & 0 & 0 & 0 & C_{55} & 0 \\ 0 & 0 & 0 & 0 & 0 & C_{66} \end{bmatrix} \tag{1.8}$$

The plain stress assumption require the following non zero vector stresses component:

$$\boldsymbol{\sigma} = \begin{bmatrix} \sigma_x \\ \sigma_y \\ \tau_{xy} \end{bmatrix}$$

as a consequence the stiffness matrix reduces to a 3x3 giving the following stress strain relationship:

$$\boldsymbol{\sigma} = \boldsymbol{C}\boldsymbol{\varepsilon}$$

in detailed form:

$$\begin{bmatrix} \sigma_x \\ \sigma_y \\ \tau_{xy} \end{bmatrix} = \begin{bmatrix} C_{11} & C_{12} & 0 \\ C_{12} & C_{22} & 0 \\ 0 & 0 & C_{44} \end{bmatrix} \begin{bmatrix} \varepsilon_x \\ \varepsilon_y \\ \gamma_{xy} \end{bmatrix} \tag{1.9}$$

If the principal orthotropic material directions $l-t$, are coincident with the $x-y$ coordinate system, the matrix elements can be connected to the usual material parameters:

E_l	Young modulus in the l direction
E_l	Young modulus in the t direction
ν_{lt}	Poisson coefficient
ν_{tl}	Poisson coefficient
G_{lt}	Shearing modulus of elasticity

with the following relations:

$$\begin{aligned} C_{11} &= \frac{E_l}{1-\nu_{lt}\nu_{tl}} \\ C_{12} &= \frac{E_t\nu_{lt}}{1-\nu_{lt}\nu_{tl}} \\ C_{22} &= \frac{E_t}{1-\nu_{lt}\nu_{tl}} \\ C_{44} &= G_{lt} \end{aligned} \tag{1.10}$$

If the material principal directions are not parallel to the coordinate system $x-y$ axis it is necessary to apply a transformation to the stress and strain vectors and to the stiffness matrix. This transformation can be deduced from the second order tensor transformation of the following type:

$$A_{ij} = t_{ik}a_{kl}t_{jl}$$

in which:

a_{ik} is the transformation matrix obtained by the direction cosine of the transformed axis

Transforming the previous relation to the vector form it is possible to obtain for the transformation matrix:

$$\boldsymbol{T} = \begin{bmatrix} cos^2\alpha & sin^2\alpha & 2sin\alpha \cdot cos\alpha \\ sin^2\alpha & cos^2\alpha & -2sin\alpha \cdot cos\alpha \\ -sin\alpha \cdot cos\alpha & sin\alpha \cdot cos\alpha & cos^2\alpha - sin^2\alpha \end{bmatrix} \tag{1.11}$$

The stiffness matrix is the result of the following relationship:

$$\boldsymbol{C}_{glo} = \boldsymbol{T}^{-1}\boldsymbol{C}\boldsymbol{T} \tag{1.12}$$

in which:

$\boldsymbol{C}$ is the stiffness matrix in the material principal directions

$\boldsymbol{C}_{glo}$ is the stiffness matrix in the coordinate system axis

The matrix $\boldsymbol{C}_{glo}$ is fully populated and the equation 1.12 is transformed to:

$$\begin{bmatrix} \sigma_x \\ \sigma_y \\ \tau_{xy} \end{bmatrix} = \begin{bmatrix} c_{11} & c_{12} & c_{13} \\ c_{12} & c_{22} & c_{23} \\ c_{13} & c_{23} & c_{33} \end{bmatrix} \begin{bmatrix} \varepsilon_x \\ \varepsilon_y \\ \gamma_{xy} \end{bmatrix} \tag{1.13}$$

1.1.4 Kinematic Relations

Two different approach has been used to describe the relation between the displacements and the strain:

- thin plate condition (Euler-Bernoulli theory [Calcote 1969])
- thick plate condition (Mindlin-Reissner theory[Auricchio 1994])

The principal difference between the two is the different assumption about the shear deformation in the plane orthogonal to the plate surface.

1.1.4.1 Thin Plate Condition

Whitout loosing in generality now From here on it is considered that the plate is composed by symmetric laminas respect to the middle surface. This assumption allows for the decoupling of the in-plane and out-of-plane deformation into the resolving equations. The small deformation theory has been applied to derive the deformation tensor from the structure displacements. The following assumptions are used for the description of the thin plate deformation from displacements [Calcote 1969]:

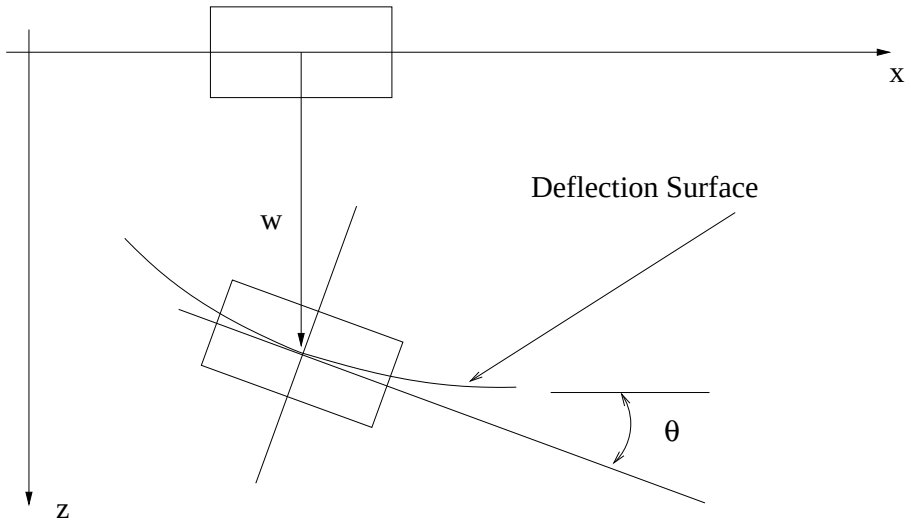

Figure 1.2: Physical quantities in the plate deflection

a) points laying on a normal to the plate middle surface will still lay on the normal to the deformed middle surface

b) the elongation of a line drawn along the thickness, normal to the middle surface can be neglected

Under the action of a load normal to the middle plane of the plate, the structure deformation can be sketched according to figure 1.2.

According to hypotesis b) the displacement in the z direction can be described by the displacement of the middle surface which is function of the x, y coordinate only:

$$w = w(x, y)$$

Following assumption a) the points with positive z coordinate the displacements in the x direction are negative and proportional to the normal rotation θ and can be expressed by:

$$\begin{aligned} u &= z\theta_y \\ v &= -z\theta_x \\ w &= w \end{aligned} \tag{1.14}$$

According to hypothesis a) results:

$$\begin{aligned} \theta_x &= \frac{\partial w}{\partial y} \\ \theta_y &= -\frac{\partial w}{\partial x} \end{aligned} \tag{1.15}$$

The essence of the previous relation is the infinitely shear stiffness of the plate. This statement should be considered in a relative way respect to the bending stiffness, the correct assertion should be: *the bending stiffness is several order of magnitude less the the shear stiffness.* If, for any reason, the shear stifness decreases to a value comparable to the bending one the relationship represented by equation 1.15 is no more valid. According to the previous hypotesis the displacement can be expressed by:

$$\begin{aligned} u &= -z\frac{\partial w}{\partial x} \\ v &= -z\frac{\partial w}{\partial y} \end{aligned}$$

Considering the assumption b) and the small deformation strain tensor definition:

$$\begin{bmatrix} \varepsilon_x \\ \varepsilon_y \\ \gamma_{xy} \end{bmatrix} = -z \begin{bmatrix} w_{,xx} \\ w_{,yy} \\ 2w_{,xy} \end{bmatrix} \tag{1.16}$$

in which the following convention has been used for the coma:

$w_{,xx} = \frac{\partial^2 w}{\partial x^2}$

For a whole vectorial notation it is possible to write:

$$\boldsymbol{\varepsilon} = -z\boldsymbol{w'}$$

in which:

$$\boldsymbol{w'} = \begin{bmatrix} w_{,xx} \\ w_{,yy} \\ 2w_{,xy} \end{bmatrix}$$

Inserting equation 1.16 into the general stress-strain relationship of equation 1.9 it is possible to connect the structure displacements to the internal stress, then inserting the resulted relations into equations 1.1 and 1.2 the final connection between displacements and internal action is obtained. The relation can be written in the following vectorial form:

$$\boldsymbol{M} = \sum_{k=1}^{N} \int_{z_{k-1}}^{z_k} \boldsymbol{C}^k_{glo}(-z)\boldsymbol{w'} \cdot z \cdot dz$$

in which:

$$\boldsymbol{M} = \begin{bmatrix} M_x \\ M_y \\ M_{xy} \end{bmatrix}$$

sorting out constant quantity from the integral sign one obtains:

$$\boldsymbol{M} = \left(-\sum_{k=1}^{N} \boldsymbol{C}_{glo}^{k} \int_{z_{k-1}}^{z_k} z^2 \cdot dz \right) \cdot \boldsymbol{w'}$$

then performing the integration:

$$\boldsymbol{M} = \left(-\sum_{k=1}^{N} \boldsymbol{C}_{glo}^{k} \frac{1}{3} \, z^3 \Big|_{z_{k-1}}^{z_k} \right) \cdot \boldsymbol{w'}$$

or equivalently:

$$\begin{bmatrix} M_x \\ M_y \\ M_{xy} \end{bmatrix} = - \begin{bmatrix} D_{11} & D_{12} & D_{13} \\ D_{12} & D_{22} & D_{23} \\ D_{13} & D_{23} & D_{33} \end{bmatrix} \begin{bmatrix} w_{,xx} \\ w_{,yy} \\ 2w_{,xy} \end{bmatrix} \tag{1.17}$$

where the elements of the matrix $\boldsymbol{D}$ are defined as follow:

$$D_{ij} = \frac{1}{3} \sum_{k=1}^{N} c_{ij}^{k} (z_k^3 - z_{k-1}^3)$$

in which:

c_{ij}^{k} is the stiffness matrix (equation 1.13) in the global reference frame of the $k-th$ lamina

z_k, z_{k-1} are the coordinates of upper and lower planes bounding the $k-th$ lamina

In full vectorial notation:

$$\boldsymbol{M} = -\boldsymbol{D} \cdot w'$$

The deformation described in figure 1.2, pure rotation about the reference surface, can induce in-plane internal action like N_x, N_y and N_{xy}, that are defined by:

$$\boldsymbol{N} = \begin{bmatrix} N_x \\ N_y \\ N_{xy} \end{bmatrix} = \sum_{k=1}^{N} \int_{z_{k-1}}^{z_k} \boldsymbol{C}_{glo}^{k}(-z) \boldsymbol{w'} \cdot dz$$

Integrating along the thickness reads:

$$\boldsymbol{N} = \left(-\sum_{k=1}^{N} \boldsymbol{C}^{k}_{glo} \frac{1}{2} \, z^2 \Big|_{z_{k-1}}^{z_k} \right) \cdot \boldsymbol{w'}$$

The previous integral is equal to zero only *if the plate is symmetrical about its reference surface*, both for structural characteristic $\boldsymbol{C}^k$ and for geometrical dimension z_k. Inserting equation 1.17 into 1.6 it is possible to get the resolving equation:

$$\begin{aligned} -D_{11}w_{,xxxx} - 4D_{13}w_{,xxxy} - 2(D_{12}+2D_{33})w_{,xxyy} + \\ -4D_{23}w_{,xyyy} - D_{22}w_{,yyyy} \quad = \quad -q \end{aligned} \tag{1.18}$$

The equation **??** allows to solve the structural problem of the deflection of a plate from known mechanical characteristic and loads. It is worth, for the following analysis, to highlight that while the equilibrium equation 1.6 is always satisfied by any plate configuration the equation **??** is satisfied only if the ratio between the bending stiffness and the shear stiffness are very low. If the latter happens the following relation should be considered true:

$$\begin{aligned} -D_{11}w_{,xxxx} - 4D_{13}w_{,xxxy} - 2(D_{12}+2D_{33})w_{,xxyy} + \\ -4D_{23}w_{,xyyy} - D_{22}w_{,yyyy} + q \quad \neq \quad 0 \end{aligned}$$

This can happen for example when some defect in lamination of the ply reduce the bonding between the relative sliding of the laminas reducing the shear stiffness and allowing for comparable values between shear and bending. The equation **??** consider static equilibrium, in the case of dynamic excitation the external and elastic forces should be equal to the inertial ones:

$$\begin{aligned} -D_{11}w_{,xxxx} - 4D_{13}w_{,xxxy} - 2(D_{12}+2D_{33})w_{,xxyy} + \\ -4D_{23}w_{,xyyy} - D_{22}w_{,yyyy} + q \quad = \quad \rho_A \frac{\partial^2 w}{\partial t^2} \end{aligned} \tag{1.19}$$

in which $\rho_a$is the mass per unit area of the plate. If the principal material directions of each ply correspond to the $x-y$ coordinate axis the coefficients disappear:

$$D_{13} = 0 \qquad D_{23} = 0$$

and the equation 1.19 is further simplified to:

$$-D_{11}w_{,xxxx} - 2(D_{12}+2D_{33})w_{,xxyy} - D_{22}w_{,yyyy} + q = \rho_A \frac{\partial^2 w}{\partial t^2}$$

1.1.4.2 Thick Plate Condition

The needs to consider more general conditions lead to the Mindlin-Reissner theory [Auricchio 1994]which drops the condition a) of section 1.1.4.1, but holding b) one, assuming that points laying on a straight line before the deformation remain on a straight line.

According to the previous assumption the points laying along the normal to the reference surface before the deformation lay no more on the normal to the deformed surface. For this reason the relations, expressed by equations 1.15, have to be written in a more general form.

According to the sign conventions represented in figure 1.3 it is possible to define:

θ_y rotation of a line normal to the reference surface around the y axis

θ_x rotation of a line normal to the reference surface around the x axis

γ_{xz} angular shear deformation in the $x-z$ plane

γ_{yz} angular shear deformation in the $y-z$ plane

$w_{,x}$ x component of the normal to the deformed surface

$w_{,y}$ y component of the normal to the deformed surface

and drawn the following relationships:

$$\begin{aligned} \theta_y &= \gamma_{xz} - w_{,x} \\ \theta_x &= -\gamma_{yz} + w_{,y} \end{aligned} \tag{1.20}$$

Using the rotation θ_x and θ_y it is possible to express the displacements using the equation 1.14:

$$\begin{aligned} u &= z\theta_y \\ v &= -z\theta_x \\ w &= w \end{aligned}$$

The derivation of the previous equation leads to the following quantity:

$$\boldsymbol{K} = \begin{bmatrix} \theta_{y,x} \\ -\theta_{x,y} \\ \theta_{y,y} - \theta_{x,x} \end{bmatrix} = \begin{bmatrix} \gamma_{xz,x} - w_{,xx} \\ -(\gamma_{yz,y} + w_{,yy}) \\ \gamma_{xz,y} - w_{,xy} - (\gamma_{yz,x} + w_{,yx}) \end{bmatrix}$$

in which:

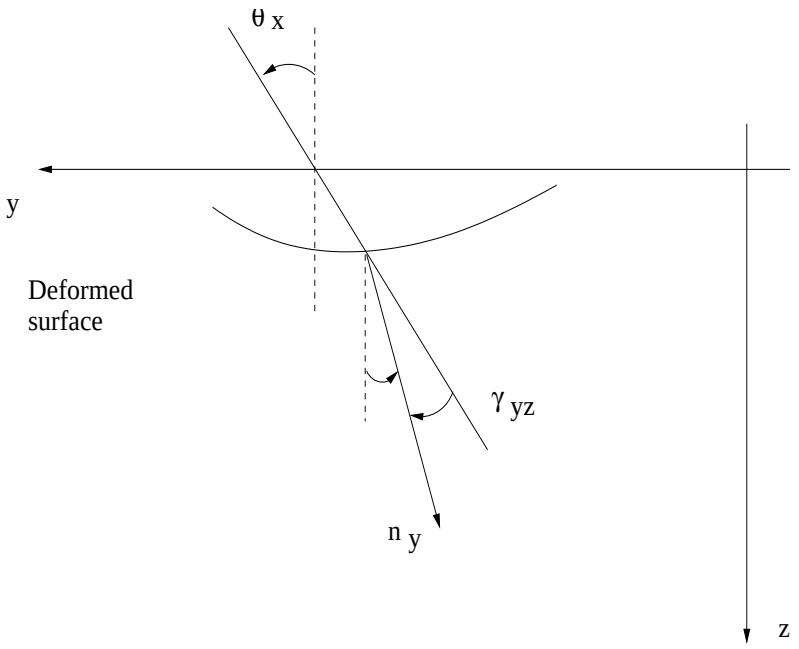

(a) didascalia tetax

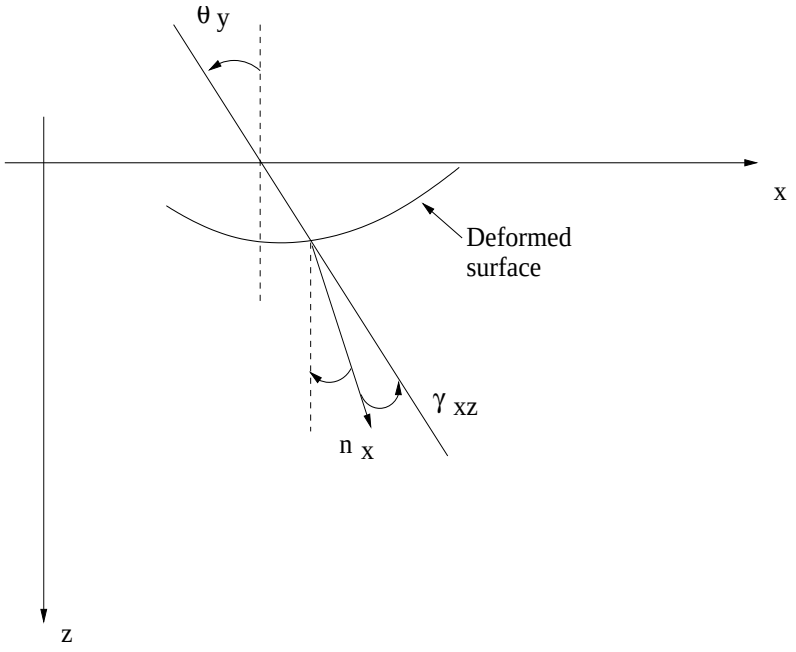

(b) didascalia tetay

Figure 1.3: shear and bending deformation relation

$\boldsymbol{K}$ is the curvature vector

The curvature vector can be easily connected to vector of the internal moments, $\boldsymbol{M}$, using the constitutive relationship 1.9:

$$\boldsymbol{M} = \boldsymbol{D}_b \cdot \boldsymbol{K} \tag{1.21}$$

The same relation can be obtained for the shear, defining:

$$\boldsymbol{V} = \begin{bmatrix} V_{xz} \\ V_{yz} \end{bmatrix}$$

and:

$$\boldsymbol{\Gamma} = \begin{bmatrix} \gamma_{xz} \\ \gamma_{yz} \end{bmatrix}$$

Recalling equations 1.7 and 1.8 it is possible to write the following vector relation:

$$\begin{bmatrix} \tau_{xz} \\ \tau_{yz} \end{bmatrix} = \begin{bmatrix} C_{66} & 0 \\ 0 & C_{55} \end{bmatrix} \cdot \begin{bmatrix} \gamma_{xz} \\ \gamma_{yz} \end{bmatrix}$$

Assuming that the shear deformation γ_{xz} and $\gamma_{yz}$are constant along the plate thickness the definition of equations 1.2 can be used to construct the matrix relationship between vertical shear force and shear deformation.

$$V_{xz} = \sum_{k=1}^{N} \int_{z_{k-1}}^{z_k} C_{66}^k \gamma_{xz} dz \qquad V_{yz} = \sum_{k=1}^{N} \int_{z_{k-1}}^{z_k} C_{55}^k \gamma_{yz} dz$$

Finally:

$$\boldsymbol{V} = \boldsymbol{D}_s \cdot \boldsymbol{\Gamma} \tag{1.22}$$

in which:

$$\boldsymbol{D}_s = \begin{bmatrix} d_{11} & 0 \\ 0 & d_{22} \end{bmatrix}$$

and

$$d_{11} = \sum_{k=1}^{N} C_{66}^k (z_k - z_{k-1}) \qquad d_{22} = \sum_{k=1}^{N} C_{55}^k (z_k - z_{k-1})$$

Now the structural problem can be solved, indeed there are 10 unknowns:

- the three scalar quantities w, θ_x, θ_y
- the 7 components of the vector quantities $\boldsymbol{\Gamma}$, $\boldsymbol{M}$, and $\boldsymbol{V}$

and 10 independent equations:

- the equilibrium equations 1.3, 1.4 and 1.5
- the compatibility equation 1.20
- the constitutive equations 1.21 and 1.22.

It is worthwhile highlight how the equations 1.18 and 1.19 will result applying the previous approach. Combining equation 1.21 into 1.6 that means using the Mindlin-Reissner curvature relationship into the equilibrium equations it results:

$$\begin{aligned}
&[D_{11}(\gamma_{xz,x} - w_{,xx}) + D_{12}(\gamma_{yz,y} - w_{,yy}) + D_{13}(\gamma_{xz.y} + \gamma_{yz,x} - 2w_{xy})]_{xx} + \\
&2\,[D_{13}(\gamma_{xz,x} - w_{,xx}) + D_{23}(\gamma_{yz,y} - w_{,yy}) + D_{33}(\gamma_{xz.y} + \gamma_{yz,x} - 2w_{xy})]_{xy} \\
&\quad [D_{12}(\gamma_{xz,x} - w_{,xx}) + D_{22}(\gamma_{yz,y} - w_{,yy}) + D_{23}(\gamma_{xz.y} + \gamma_{yz,x} - 2w_{xy})]_{yy} \quad = \quad -q
\end{aligned}$$

Separating the two contributions, the pure bending from the pure shear one, it is possible to get:

$$\begin{aligned}
-D_{11}w_{,xxxx} - 4D_{13}w_{,xxxy} - 2(D_{12} + 2D_{33})w_{,xxyy} + \\
-4D_{23}w_{,xyyy} - D_{22}w_{,yyyy} + \\
(D_{11}\gamma_{xz} + D_{13}\gamma_{yz})_{,xxx} + 3D_{23}\gamma_{yz,xyy} + \\
(2D_{33} + D_{12})(\gamma_{yz,xxy} + \gamma_{xz,xyy}) + \\
+3D_{23}\gamma_{yz,xyy} + (D_{22}\gamma_{yz} + D_{23}\gamma_{xz})_{,yyy} \quad = \quad -q \qquad (1.23)
\end{aligned}$$

Comparing equation 1.23 with equation 1.18 it is straight to draw that when the structure is no more infinitely stiff in shear deformation equation 1.18 is no more satisfied due to the presence of the following term:

$$\begin{aligned}
F_s(\gamma_{xz}, \gamma_{yz}) \quad = \quad & (D_{11}\gamma_{xz} + D_{13}\gamma_{yz})_{,xxx} + 3D_{23}\gamma_{yz,xyy} + \\
& +(2D_{33} + D_{12})(\gamma_{yz,xxy} + \gamma_{xz,xyy}) + \\
& +3D_{23}\gamma_{yz,xyy} + (D_{22}\gamma_{yz} + D_{23}\gamma_{xz})_{,yyy} \qquad (1.24)
\end{aligned}$$

If the principal coordinate system of the ply is parallel to the global one the expression simplify to read:

$$\begin{aligned}
F_s(\gamma_{xz}, \gamma_{yz}) \quad = \quad & (D_{11}\gamma_{xz} + D_{13}\gamma_{yz})_{,xxx} + \\
& +(2D_{33} + D_{12})(\gamma_{yz,xxy} + \gamma_{xz,xyy}) + \\
& +(D_{22}\gamma_{yz} + D_{23}\gamma_{xz})_{,yyy}
\end{aligned}$$

The previous expressions represent the force due to shear effect and cannot be neglected when the shear stiffness is comparable to the bending one. For

the purpose of the present research it is important to highlight that *if the shear stiffness is locally reduced, for the presence of incorrect bonding or for any other reason, the displacements field measured will not satisfy, in the defected area, the equation 1.19, due to the presence of the term described in equation 1.24.*

Bibliography

[Calcote 1969] Lee. R. Calcote, "The Analysis of Laminated Composite Plate" Van Nostrand Reinhold Company 1969

[Auricchio 1994] F.Auricchio, R., F., Taylor "A share deformable plate element with an exact thin limit", Computer methods in Applied Mechanics and Engineering vol 118, pagg. 393-412, 1994

[Grigolyuk 1987] E. Grigolyuk, V. Tolkachev, "Contact problems in the theory of plates and shells", MIR, Moscow, 1987

Chapter 2

The Mixed Finite Element Method for Shell/Beam Structure

In numerical approximation methods the primary variables are always more accurate then the derived one, because they are usually obtained as derivative of the primary ones. From an engineering point of view the stress inside the material is of main interest and usually it is obtained deriving the displacements, for this reason the family of Mixed Finite Elements has been developed to increase the accuracy of the more interesting variables. In the Mixed Finite Elements formulation the resulting expression of the total energy of the structural system is describer using lower degrees of derivation. For plate and beam the Mixed Element method assumes as primary variable the displacements and the bending moment, instead of rotations.

2.1 The Equations

The matrixes of the mixed finite element draw from a different choice of the governing equation. In the classical finite element analysis the matrixes are deduced from the governing equation in which the only unknowns are the displacements of the structure, in the approximation procedure the shape functions are build using nodal displacement and rotation as unknown parameter. The stresses are then obtained deriving the displacement and for example in the beam theory two level of differentiation are needed to obtain the moment.

Considering the beam structure as example, in the mixed formulation the moment is assumed as primary variable as the displacement. The final governing equation should be slightly modified to take this change into account, and in the following this formulation is presented.

2.2 The Compatibility Equation

The compatibility equation considers the relationship between bending moment and beam deformation. Hereafter, without loosing in generality from a numerical point of view, the following assumptions have been made:

- the mechanical characteristics of the lamina do not vary along the axis of the beam
- the thickness and principal axis orientation do not vary along the axis of the beam
- the z axis is a symmetry axis for the cross section

No loose in generality is due to the previous assumption from a numerical point of view in which a continuous structure should be divided into finite piece-wise constant stretch.

According the usual theory of beams and using the sketch of figure 2.1 the axial displacements are described by the following:

$$u = z \cdot \theta_y \tag{2.1}$$

in which:

θ_y rotation of a line normal to the x axis before the deformation around the y axis

u the displacement in the x direction

According to the Euler-Bernoulli theory the only non-zero deformation tensor component is:

$$\varepsilon_x = u_{,x} \tag{2.2}$$

Using equation 2.1, 2.2 and the Hooks law the axial stress inside the beam is:

$$\sigma_x = E^k \cdot z \cdot \theta_{y,x}$$

in which:

E^k is the Young modulus of the $k-th$ ply

To get the simplest form of the governing equations it is necessary to uncouple the bending from the axial effect. To this aim, according with the previous assumptions, the x axis of the reference coordinate system is placed along

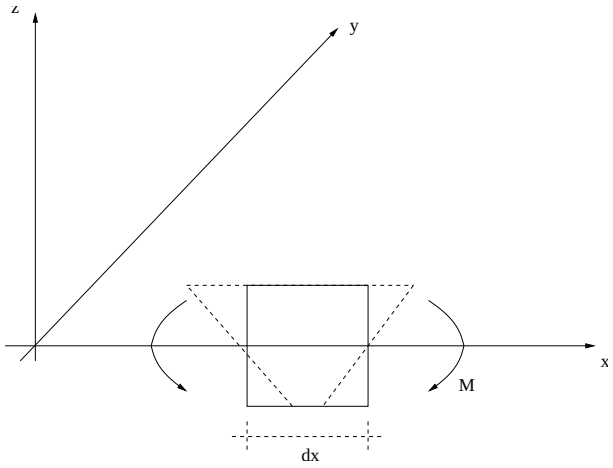

Figure 2.1: Infinitesimal Beam deformation

the line connecting the barycentre of each cross section, determined by the following relationships:

$$\sum_{k=1}^{N} b_k \int_{z_{k-1}}^{z_k} E^k z \cdot dz \quad = \quad 0 \tag{2.3}$$

in which:

b_k width of the $k-th$ ply

According to the equation 2.3 no axial force is induced by a rotation θ_y, in fact:

$$N_x = \sum_{k=1}^{N} b_k \int_{z_{k-1}}^{z_k} E^k \cdot z \cdot \theta_{y,x} dz = 0$$

on the contrary no bending moment will come frome an axial deformation:

$$M_x = \sum_{k=1}^{N} b_k \int_{z_{k-1}}^{z_k} E^k \varepsilon_x^0 \cdot z dz = 0$$

The symmetry condition for the z axis ensures no coupling between torsion and shear in the $x-z$ plane. The condition stated by equation 2.3 will be easy fulfilled if the distribution of the laminas is symmetric respect to the $x-y$ plane. Following the previous discussion the bending moment is:

$$M_x = \sum_{k=1}^{N} b_k \int_{z_{k-1}}^{z_k} E^k \cdot z^2 \cdot \theta_{y,x} dz$$

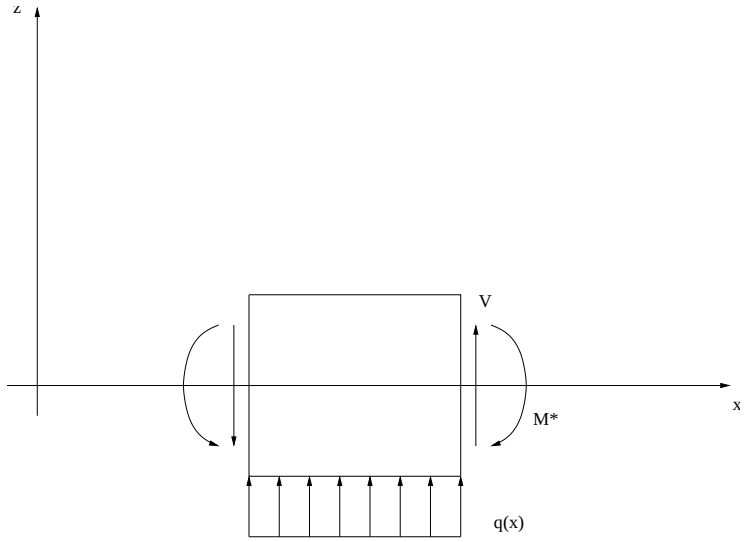

Figure 2.2: Force diagram sketch

Considering a rectangular cross section the following quantity can be defined:

$$E = b \sum_{k=1}^{N} \int_{z_{k-1}}^{z_k} E^k \cdot z^2 \cdot dz \tag{2.4}$$

leading to the final relation:

$$M_x = E\theta_{y,x} \tag{2.5}$$

in which:

M_x is the bending moment in the $x - z$ plane

The convention for positive As is showed in figure assuming a right handed reference system, with the $x$axis the beam central axis, a positive rotation about the y axis correspond to a negative

2.2.1 The Equilibrium Equations

The second equation is the second Newton law of dynamics. The rotational equilibrium reads:

$$-V_{xz}dx - M_x + M_x + \frac{\partial M_x}{\partial x}dx = 0$$

after simplification:

$$V_{xz} = \frac{\partial M_x}{\partial x} \tag{2.6}$$

and the translation in the z direction:

$$-V_{xz} + V_{xz} + \frac{\partial V_{xz}}{\partial x} dx + q(x) = A_c \frac{\partial^2 w}{\partial t^2}$$

after simplification:

$$\frac{\partial V_{xz}}{\partial x} + q(x) = A_c \frac{\partial^2 w}{\partial t^2} \tag{2.7}$$

in which:

w is the transverse beam displacement in the z direction

V_{xz} is the beam shear

$q(x)$ is the applied load per unit length

$A_c = \rho A$ is the mass per unit length of the beam

Combining equations 2.6 and 2.7 it is possible to obtain:

$$\frac{\partial^2 M_x}{\partial x^2} + q(x) = A_c \frac{\partial^2 w}{\partial t^2} \tag{2.8}$$

Assuming no shear deformation the θ_y variation is:

$$\theta_{y,x} = -\frac{\partial^2 w}{\partial x^2}$$

According to the previous statements the system of governing equations results the following one:

$$\begin{cases} M_x + E\frac{\partial^2 w}{\partial x^2} = 0 \\ \frac{\partial^2 M}{\partial x^2} + q(x) - A_c \frac{\partial^2 w}{\partial t^2} = 0 \end{cases} \tag{2.9}$$

The boundary condition shall be added to system 2.9 to uniquely determine the solution. Usually two different sets of conditions are defined:

- **essential boundary conditions** that are applied to the unknown function in the form $w = b_w(t)$ or $M = b_m(t)$ at one or both the beam ends, where $b_w(t)$and $b_m(t)$ are known function;
- **natural boundary conditions** that are applied on the share force and on the rotation in the form $V_{xz} = b_v(t)$or $\theta_{y,x} = b_\theta(t)$ at one or both the beam ends, where $b_v(t)$ and $b_\theta(t)$ are known function;

2.2.2 The Shear Effect

If the shear effect has to be taken into account the first equation of 2.9 should be modified considering the following hypothesis:

- the shear deformation is assumed to be uniform in the cross section of the beam and is called γ_{xz}

As a consequence the relation between the shear stress τ_{xz} and the internal action V_{xz} assumes the following form:

$$V_{xz} = b \int_{z_1}^{z_N} \tau_{xz} dz = \mu \sum_{k=1}^{N} b_k c \int_{z_{k-1}}^{z_k} G_{xz}^k \gamma_{xz} dz$$

in which:

b is the cross section base

μ is the cross section shape factor taking into account for the difference between real shear deformation variation along the thickness and the constant assumption

G_{xz}^k is the shear modulus in the $x-z$ plane of the $k-th$ lamina

Using the assumption of constant shear deformation it is possible to write:

$$G = \sum_{k=1}^{N} b_k \int_{z_{k-1}}^{z_k} G_{xz}^k dz \tag{2.10}$$

the final relation is:

$$V_{xz} = \mu G \gamma_{xz} \tag{2.11}$$

Inserting equation 2.6 into 2.11 reads:

$$\frac{\partial M}{\partial x} = \mu G \gamma_{xz} \tag{2.12}$$

Now deriving respect to x the shear deformation definition:

$$\gamma_{xz,x} = \theta_{y,x} + w_{,xx} \tag{2.13}$$

in which coma stand for derivation, and performing the substitution of equation 2.5 and 2.12 it is possible to write:

$$\frac{1}{\mu G} \frac{\partial^2 M}{\partial x^2} = \frac{M}{E} + w_{,xx}$$

leading to the system of governing equation:

$$\begin{cases} \frac{M_x}{E} - \frac{1}{\mu G}\frac{\partial^2 M_x}{\partial x^2} + \frac{\partial^2 w}{\partial x^2} = 0 \\ \frac{\partial^2 M_x}{\partial x^2} + q(x) - A_c \frac{\partial^2 w}{\partial t^2} = 0 \end{cases} \tag{2.14}$$

in which the shear deformation effect has been taken into account. The boundary conditions are applied in the same manner as in section 2.2.1.

2.3 Finite Element Model

The numerical solution of the system of equations 2.9 can be obtained via the usual Finite Element technique where the transverse displacement function w and the bending moment M_x are assumed as unknowns in both formulation with and without the shear effect. For a coherent approximation theory it is necessary to state a little bit more formally the previous problem as follow:

find $M_x(x), w(x) \in \mathrm{C}^2$ on the interval $[0, L]$satisfying the boundary conditions and the following differential equation:

$$\begin{cases} \frac{M_x}{EI} - \frac{1}{\mu G}\frac{\partial^2 M}{\partial x^2} + \frac{\partial^2 w}{\partial x^2} = 0 \\ \frac{\partial^2 M}{\partial x^2} + q(x) - A_c\frac{\partial^2 w}{\partial t^2} = 0 \\ w(0,t) = 0 \\ \theta_y(0,t) = b_\theta(0,t) \\ M_x(L,t) = 0 \\ V_{xz}(L,t) = b_v(t) \end{cases} \tag{2.15}$$

The previous statement defines the problem with the classical formulation. As consequence it is not always possible to find a solution for the problem due to the restriction imposed to the degree of continuity of the solution.

2.3.1 The Weak Formulation

Finite Element Method, instead of a classical formulation of the problem, starts usually from less restrictive set of possible solution to find then in this new set the approximated solution, this is called "weak formulation". The unknown function can be approximated in a broader set then the classical one C^2. This approximated set, called H^1, is the set of all functions with at least the first derivative square integrable. The next step is to define a subset $\mathrm{H}^1_\mathrm{h} \subset \mathrm{H}^1$ constructed using the base function $N_i(x)$. In the following development the subscript i connects the base function to the node of the elements used to discretize the domain by the following:

$N_i(x)$ is different from zero only on the elements that are attached to or contain the node i

The unknown function can then be expressed by:

$$M^h(x) = M_i N_i(x) \qquad w^h(x) = w_i N_i(x) \qquad i = 1, 2, ..n \tag{2.16}$$

in which the repeating indeces summation convention has been used and:

M^h approximated function of the bending moment

w^h approximated transverse displacement

M_i value of the bending moment at node i

w_i value of the transverse displacement at node i

n total number of nodes

The above relations if substituted in system 2.14 give rise to the following residues:

$$\begin{cases} \frac{M^h}{EI} - \frac{1}{\mu G}\frac{\partial^2 M^h}{\partial x^2} + \frac{\partial^2 w^h}{\partial x^2} = R_1(x,t) \\ \frac{\partial^2 M^h}{\partial x^2} + q(x) - A_c\frac{\partial^2 w^h}{\partial t^2} = R_2(x,t) \end{cases}$$

Now the Finite Element Method looks for a solution of the problem in the subset H^1_h weighting the previous residues with trial functions equal to the $N_j(x)$. This approach was introduced by Galerkin and named "Galerkin method" after him. The aim is to represent the physical problem described by the system of equations 2.15 using a different class of solution functions and it is formulated as follow:

find $M^h(x), w^h(x) \in H^1_h$ on the interval $[0, L]$ satisfying the boundary conditions $w^h(0,t) = 0$, $\theta^h_y(0,t) = 0$ and the following system of equations for each $v^h \in H^1_h$:

$$\begin{cases} \int_0^L \frac{M^h}{EI} v^h dx - \int_0^L \frac{1}{\mu G}\frac{\partial^2 M^h}{\partial x^2} v^h dx + w_i \int_0^L \frac{\partial^2 w^h}{\partial x^2} v^h dx + (\theta^h_y - b_\theta(t))v^h\big|_0 = 0 \\ \int_0^L \frac{\partial^2 M^h}{\partial x^2} v^h dx + \int_0^L q(x) v^h dx - A_c \int_0^L \frac{\partial^2 w^h}{\partial t^2} v^h dx - (V^h_{xz} - b_v(t))v^h\big|^L = 0 \end{cases} \tag{2.17}$$

in which:

(a) the repeated indexes *summation convention* is used

(b) the boundary condition, expressed through the functions $b_\theta(t)$ and $b_\theta(t)$, for the shear force (last term in the left hand member of the second equation) and for the rotation (last term in the left hand member of the first equation), are applied in a weak form called *Natural Boundary Conditions*

(c) the boundary conditions for the displacement and the moment in a strong form, *Essential Boundary Conditions*.

As clearly stated by system 2.17 the Natural Boundary Conditions will be enforced by the solution of the linear system of equations whilst as it results from definition 2.17 Essential Boundary Conditions will be enforced by the appropriately choice of the nodal values.

The relation expressed by equation 2.17 is satisfied if it is true for each base function, leading to:

$$\begin{cases} \frac{M_i}{EI}\int_0^L N_i N_j dx - \frac{M_i}{\mu G}\int_0^L \frac{\partial^2 N_i}{\partial x^2} N_j dx + w_i \int_0^L \frac{\partial^2 N_i}{\partial x^2} N_j dx - (\theta_y^h - b_\theta(t))N_j\big|_0 = 0 \\ M_i \int_0^L \frac{\partial^2 N_i}{\partial x^2} N_j dx + \int_0^L q(x) N_j dx - A_c \frac{d^2 w_i}{dt^2}\int_0^L N_i N_j dx - (V_{xz}^h - b_v(t))N_j\big|^L = 0 \end{cases} \quad j = 1, ..n$$

where use of the equation 2.16 has been done. Applying integration by parts it is possible to highlight the presence of the boundary conditions:

$$\begin{cases} \frac{M_i}{EI}\int_0^L N_i N_j dx + \frac{M_i}{\mu G}\int_0^L \frac{\partial N_i}{\partial x}\frac{\partial N_j}{\partial x} dx - \frac{M_i}{\mu G}\frac{\partial N_i}{\partial x} N_j\big|_0^L + \\ -w\int_0^L \frac{\partial N_i}{\partial x}\frac{\partial N_j}{\partial x} dx + w_i \frac{\partial N_i}{\partial x} N_j\big|_0^L - (\theta_y^h - b_\theta(t))N_j\big|_0 = 0 \\ -M_i \int_0^L \frac{\partial N_i}{\partial x}\frac{\partial N_j}{\partial x} dx + M_i \frac{\partial N_i}{\partial x} N_j\big|_0^L + \int_0^L q(x) N_j dx + \\ -A_c \frac{d^2 w_i}{dt^2}\int_0^L N_i N_j dx - (V_{xz}^h - b_v(t))N_j\big|^L = 0 \end{cases}$$

Referring to equation 2.13 and 2.6 it is possible to write:

$$\theta_y^h = \frac{M_i}{\mu G}\frac{\partial N_i}{\partial x} - w_i \frac{\partial N_i}{\partial x}$$

$$V_{xz}^h = M_i \frac{\partial N_i}{\partial x}$$

Except for the boundary node the base function The approximated system of equations finally is:

$$\begin{cases} \frac{M_i}{EI}\int_0^L N_i N_j dx + \frac{M_i}{\mu G}\int_0^L \frac{\partial N_i}{\partial x}\frac{\partial N_j}{\partial x} dx - w_i \int_0^L \frac{\partial N_i}{\partial x}\frac{\partial N_j}{\partial x} dx \\ \quad - (\frac{M_i}{\mu G} - w_i)\frac{\partial N_i}{\partial x} N_j\Big|_0^L - (\theta_y^h - b_\theta(t))N_j\big|_0 = 0 \\ -M_i \int_0^L \frac{\partial N_i}{\partial x}\frac{\partial N_j}{\partial x} dx + \int q(x) N_j dx + -A_c \frac{d^2 w_i}{dt^2}\int_0^L N_i N_j dx \\ \quad + M_i \frac{\partial N_i}{\partial x} N_j\big|_0^L - (V_{xz}^h - b_v(t))N_j\big|^L = 0 \end{cases}$$

and

$$\begin{cases} \frac{M_i}{EI}\int_0^L N_i N_j dx + \frac{M_i}{\mu G}\int_0^L \frac{\partial N_i}{\partial x}\frac{\partial N_j}{\partial x} dx - w_i \int_0^L \frac{\partial N_i}{\partial x}\frac{\partial N_j}{\partial x} dx + \\ \quad + \theta_y^h N_j\big|_0 - (\theta_y^h - b_\theta(t))N_j\big|_0 - \theta_y^h N_j\big|^L = 0 \\ -M_i \int_0^L \frac{\partial N_i}{\partial x}\frac{\partial N_j}{\partial x} dx + \int_0^L q(x) N_j dx - A_c \frac{d^2 w_i}{dt^2}\int_0^L N_i N_j dx + \\ \quad + V_{xz}^h N_j\big|^L - (V_{xz}^h - b_v(t))N_j\big|^L - V_{xz}^h N_j\big|_0 = 0 \end{cases}$$

Considering now the boundary conditions the shape function is zero, for the displacement at $x = 0$, with $N_j(0,t) = 0 \; \forall \quad j$ and for the moment at $x = L$ with $N_j(L,t) = 0 \; \forall \quad j$, canceling out the relevant terms. Finally the system of equations reads:

$$\begin{cases} \frac{M_i}{EI}\int_0^L N_i N_j dx + \frac{M_i}{\mu G}\int_0^L \frac{\partial N_i}{\partial x}\frac{\partial N_j}{\partial x} dx - w_i \int_0^L \frac{\partial N_i}{\partial x}\frac{\partial N_j}{\partial x} dx + \\ \quad + b_\theta(t)N_j\big|_0 = 0 \\ -M_i \int_0^L \frac{\partial N_i}{\partial x}\frac{\partial N_j}{\partial x} dx + \int_0^L q(x) N_j dx - A_c \frac{d^2 w_i}{dt^2}\int_0^L N_i N_j dx + \\ \quad + b_v(t)N_j\big|^L = 0 \end{cases} \tag{2.18}$$

The previous equation give rise to a system of $2n$ linear equations the whom solution determines the nodal values of the displacement and moment.

2.3.2 The Shape Function and the Finite Element Matrix

It is useful to write in matrix form equation 2.18 :

$$\boldsymbol{K_b} \cdot \boldsymbol{m} + \boldsymbol{K_s} \cdot \boldsymbol{m} - \boldsymbol{K_n} \cdot \boldsymbol{w} = -\boldsymbol{\theta} \tag{2.19}$$

$$-\boldsymbol{K_n} \cdot \boldsymbol{m} - \boldsymbol{Mi} \frac{d^2}{dt^2} \boldsymbol{w} = -\boldsymbol{Q} - \boldsymbol{V} \tag{2.20}$$

in which:

$(\boldsymbol{K_b})_{ij} = \frac{1}{EI} \int_0^L N_i N_j dx$ Bending compliance matrix

$(\boldsymbol{K_s})_{ij} = \frac{1}{\mu G} \int_0^L \frac{\partial N_i}{\partial x} \frac{\partial N_j}{\partial x} dx$ Shear compliance matrix

$(\boldsymbol{K_n})_{ij} = \int_0^L \frac{\partial N_i}{\partial x} \frac{\partial N_j}{\partial x} dx$ Nodal matrix

$(\boldsymbol{Mi})_{ij} = A_c \int_0^L N_i N_j dx$ Mass matrix

$\boldsymbol{Q}_j = \int_0^L q(x) N_j dx$ Distribute load Vector

$\boldsymbol{m}_i = M_i$ Vector of the bending moment nodal values

$\boldsymbol{w}_i = w_i$ Vector of the transverse displacements nodal values

$\boldsymbol{\theta}$ Vector of the boundary condition applied to the end beam rotations

$\boldsymbol{V}$ Vector of the boundary condition applied to the end beam shear force

The matrix elements can be obtained once the function N_i of the Finite Elements has been chosen. Here it is presented, as an example, the case of polynomial function of 2^{th} degrees with the following expressions:

$$N_1(x) = \frac{\left(x - \frac{L}{2}\right)(x - L)}{\frac{L^2}{2}}$$

$$N_2(x) = \frac{x\,(x - L)}{\frac{L}{2}\left(\frac{L}{2} - L\right)}$$

$$N_3(x) = \frac{x\left(x - \frac{L}{2}\right)}{L\left(L - \frac{L}{2}\right)}$$

in which:

l is the length of the finite element

The first derivative of the shape functions are:

$$\begin{aligned}
\frac{d}{dx}N_1(x) &= \frac{2\left(x-\frac{L}{2}\right)}{L^2}+\frac{2\left(x-L\right)}{L^2}\\
\frac{d}{dx}N_2(x) &= -\frac{4\left(x-L\right)}{L^2}-\frac{4x}{L^2}\\
\frac{d}{dx}N_3(x) &= \frac{2\left(x-\frac{L}{2}\right)}{L^2}+\frac{2x}{L^2}
\end{aligned}$$

Now it is straitforwardstraightforward to obtain the matrix:

$$\begin{aligned}
\boldsymbol{K_b} &= \frac{1}{EI}\begin{pmatrix} \frac{2L}{15} & \frac{L}{15} & -\frac{L}{30} \\ \frac{L}{15} & \frac{8L}{15} & \frac{L}{15} \\ -\frac{L}{30} & \frac{L}{15} & \frac{2L}{15} \end{pmatrix}\\
\boldsymbol{K_s} &= \frac{1}{\mu G}\begin{pmatrix} \frac{7}{3L} & -\frac{8}{3L} & \frac{1}{3L} \\ -\frac{8}{3L} & \frac{16}{3L} & -\frac{8}{3L} \\ \frac{1}{3L} & -\frac{8}{3L} & \frac{7}{3L} \end{pmatrix}\\
\boldsymbol{K_n} &= \begin{pmatrix} \frac{7}{3L} & -\frac{8}{3L} & \frac{1}{3L} \\ -\frac{8}{3L} & \frac{16}{3L} & -\frac{8}{3L} \\ \frac{1}{3L} & -\frac{8}{3L} & \frac{7}{3L} \end{pmatrix}\\
\boldsymbol{Mi} &= A_c\begin{pmatrix} \frac{2L}{15} & \frac{L}{15} & -\frac{L}{30} \\ \frac{L}{15} & \frac{8L}{15} & \frac{L}{15} \\ -\frac{L}{30} & \frac{L}{15} & \frac{2L}{15} \end{pmatrix}\\
\boldsymbol{Q} &= \begin{pmatrix} \frac{L}{6} \\ \frac{2L}{3} \\ \frac{L}{6} \end{pmatrix}
\end{aligned}$$

The two vector $\boldsymbol{\theta}$ and $\boldsymbol{V}$ have all null element but the first and last ones associated to the boundary values. The matrix equations 2.19 and 2.20 can be combined to use only one matrix equation by defining the following coefficient matrixes:

$$\begin{aligned}
\boldsymbol{K} &= \begin{bmatrix} \boldsymbol{K_b}+\boldsymbol{K_s} & -\boldsymbol{K_n} \\ -\boldsymbol{K_n} & 0 \end{bmatrix}\\
\boldsymbol{M} &= \begin{bmatrix} 0 & 0 \\ 0 & \boldsymbol{Mi} \end{bmatrix}\\
\boldsymbol{L} &= \begin{bmatrix} -\boldsymbol{\theta} \\ -\boldsymbol{Q}-\boldsymbol{V} \end{bmatrix}
\end{aligned}$$

and for the unknown vector:

$$\boldsymbol{u} = \begin{bmatrix} \boldsymbol{m} \\ \boldsymbol{w} \end{bmatrix}$$

leading to the following usual matrix equation for the discrete system:

$$\boldsymbol{K} \cdot \boldsymbol{u} - \boldsymbol{M} \frac{d^2}{dt^2} \boldsymbol{u} = \boldsymbol{L} \tag{2.21}$$

The form of equation 2.21 is very useful for static problems where the equation reduces to:

$$\boldsymbol{K} \cdot \boldsymbol{u} = \boldsymbol{L}$$

and the boundary conditions can be applied in the usual form with the same subroutines used for any others Finite Element program. In the dynamic case a different formulation has to be used due to the singularity of the mass matrix $\boldsymbol{M}$.

2.3.3 Solution with "Displacement Only Method"

The systems of equations 2.19 and 2.20 can be solved one at a time, deducing the moment from the first system as a function of the displacement and then substituting in the second system, as hereafter described (with no lack in generality an for the sake of simplicity no shear effect is considered):

$$\begin{aligned} \boldsymbol{m} &= \boldsymbol{K_b}^{-1} \cdot (\boldsymbol{K_n} \cdot \boldsymbol{w} - \boldsymbol{\theta}) \\ -\boldsymbol{K_n} \cdot \boldsymbol{K_b}^{-1} \cdot (\boldsymbol{K_n} \cdot \boldsymbol{w} - \boldsymbol{\theta}) - \boldsymbol{Mi} \frac{d^2}{dt^2} \boldsymbol{w} &= -\boldsymbol{Q} - \boldsymbol{V} \end{aligned} \tag{2.22}$$

The solution of system of equations 2.22 requires that the matrix $\boldsymbol{K_b}$ is non singular as it is assured by the linearly independent shape functions. The second matrix equations of 2.22 now has only displacement degrees of freedom and the matrix $\boldsymbol{Mi}$ is non singular too for the same reason stated above. Usual methods for structural time integration can now be used considering the following stiffness matrix: and for The governing system of equations can now be written in the following form:

$$-\boldsymbol{K} \cdot \boldsymbol{w} - \boldsymbol{Mi} \cdot \frac{d^2}{dt^2} \boldsymbol{w} = \boldsymbol{L} \tag{2.23}$$

in which:

$\boldsymbol{K} = \boldsymbol{K_n} \cdot \boldsymbol{K_b}^{-1} \cdot \boldsymbol{K_n}$ the stiffness matrix

$\boldsymbol{L} = -\boldsymbol{Q} - \boldsymbol{V} - (\boldsymbol{K_n} \cdot \boldsymbol{K_b}^{-1} \cdot \boldsymbol{\theta})$ the load vector

Some attention shall be placed in considering the boundary conditions, that allows to make the stiffness matrix non-singular. This topic will be discussed in the following section.

2.3.3.1 Applying End Rotations

In this case the boundary conditions are expressed imposing the rotations at both ends in the form:

$$\begin{aligned} \theta_y(0) &= b_{\theta 1}(t) \\ \theta_y(L) &= b_{\theta 2}(t) \end{aligned}$$

This means that the moments at the same ends are unknown. The application of system 2.22 is straightforward: the vector $\boldsymbol{\theta}$ is completely known, all elements zero but the first and the last ones:

$$\boldsymbol{\theta} = \begin{bmatrix} b_{\theta 1}(t) \\ 0 \\ \vdots \\ -b_{\theta 2}(t) \end{bmatrix} \tag{2.24}$$

The nodal moment values are expressed by:

$$\boldsymbol{m} = \boldsymbol{K_b}^{-1} \cdot (\boldsymbol{K_n} \cdot \boldsymbol{w} - \boldsymbol{\theta}) \tag{2.25}$$

Substituting in the second of the equation 2.22 the final form is obtained:

$$-\boldsymbol{K} \cdot \boldsymbol{w} - \boldsymbol{M}\boldsymbol{i}\frac{d^2}{dt^2}\boldsymbol{w} = -\boldsymbol{Q} - \boldsymbol{V} - (\boldsymbol{K_n} \cdot \boldsymbol{K_b}^{-1} \cdot \boldsymbol{\theta}) \tag{2.26}$$

For the application of displacement boundary conditions the procedure is outlined hereafter in section2.3.3.3.

2.3.3.2 Applying End Moments

More attention has to be payed in the case of end moments constrain that can be expressed as:

$$\begin{aligned} M_x(0) &= b_{m1}(t) \\ M_x(L) &= b_{m2}(t) \end{aligned} \tag{2.27}$$

Now the end rotations are unknown and the boundary condition, expressed by equations 2.27, have to be added to system 2.30 to solve the problem.

Different solution techniques have to be used depending on the type of analysis, they will be described in the next sections.

Static Analysis In this case equations 2.27 have to be added to system 2.23 to obtain the solution in term of displacements and end rotations. The two boundary conditions can be introduced into the first and last equations of the first matrix equation of system2.22, they read:

$$\begin{aligned}(\boldsymbol{K_b}^{-1}\cdot\boldsymbol{K_n})_{1j}\cdot\boldsymbol{w}_j-\boldsymbol{K}_{\boldsymbol{b}11}^{-1}\boldsymbol{\theta}_1 &= b_{m1}(t) \qquad j=1,2..n\\ (\boldsymbol{K_b}^{-1}\cdot\boldsymbol{K_n})_{nj}\cdot\boldsymbol{w}_j-\boldsymbol{K}_{\boldsymbol{b}nn}^{-1}\boldsymbol{\theta}_n &= -b_{m2}(t) \qquad j=1,2..n\end{aligned} \tag{2.28}$$

The two equations in 2.28 can now be added to the system 2.26 as the initial and final rows along with the two additional columns, deduced from the matrix equation 2.22:

$$(\boldsymbol{K_n}\cdot\boldsymbol{K_b}^{-1})_{j1}\cdot\boldsymbol{\theta}_1 \qquad j=1,2..n$$

$$(\boldsymbol{K_n}\cdot\boldsymbol{K_b}^{-1})_{jn}\cdot\boldsymbol{\theta}_n \qquad j=1,2..n$$

The resulting stiffness matrix reads:

$$\boldsymbol{K}=\begin{bmatrix}-\boldsymbol{K}_{\boldsymbol{b}11}^{-1} & (\boldsymbol{K_b}^{-1}\cdot\boldsymbol{K_n})_{1i} & -\boldsymbol{K}_{\boldsymbol{b}1n}^{-1}\\ (\boldsymbol{K_n}\cdot\boldsymbol{K_b}^{-1})_{j1} & -(\boldsymbol{K_n}\cdot\boldsymbol{K_b}^{-1}\cdot\boldsymbol{K_n})_{ji} & (\boldsymbol{K_n}\cdot\boldsymbol{K_b}^{-1})_{jn}\\ -\boldsymbol{K}_{\boldsymbol{b}n1}^{-1} & (\boldsymbol{K_b}^{-1}\cdot\boldsymbol{K_n})_{ni} & -\boldsymbol{K}_{\boldsymbol{b}nn}^{-1}\end{bmatrix} \tag{2.29}$$

The system can now be written, referring to equation 2.22 (the minus sign of the stiffness matrix is put inside the stiffness matrix definition) considering the static conditions:

$$\boldsymbol{K}\cdot\begin{bmatrix}\boldsymbol{\theta}_1\\ \boldsymbol{w}\\ \boldsymbol{\theta}_n\end{bmatrix}=\begin{bmatrix}0\\ \boldsymbol{L}\\ 0\end{bmatrix} \tag{2.30}$$

in which:

$\boldsymbol{L}=-\boldsymbol{Q}-\boldsymbol{V}$ is the load vector

Dynamic Analysis Full Time Integration In the case of dynamic analysis the general discrete equation 2.23 can be used with some slight modifications to the stiffness and mass matrix. The stiffness matrix is exactly the same determined in equation 2.29, for the mass matrix the contribution of the end rotations is nil so the modified matrix is easily obtained:

$$\boldsymbol{M_w}=\begin{bmatrix}0 & 0 & 0\\ 0 & \boldsymbol{Mi} & 0\\ 0 & 0 & 0\end{bmatrix}$$

The final equation reads:

$$-\boldsymbol{K}\cdot\begin{bmatrix}\boldsymbol{\theta}_1\\ \boldsymbol{w}\\ \boldsymbol{\theta}_n\end{bmatrix}-\boldsymbol{M_w}\frac{d^2}{dt^2}\begin{bmatrix}\boldsymbol{\theta}_1\\ \boldsymbol{w}\\ \boldsymbol{\theta}_n\end{bmatrix}=\begin{bmatrix}0\\ -\boldsymbol{Q}(t)-\boldsymbol{V}(t)\\ 0\end{bmatrix} \tag{2.31}$$

The numerical solution of equation 2.31 will be calculated using the standard time integration techniques for structural dynamics, the Wilson-θmethod is the one used in this case. Here only the main results for the development of the method will be addressed and for a deeply discussion the reader is reminded to [Hilber 1976].

The method is based on the assumption that the acceleration varies linearly inside a time step. The time step is comprised between the two temporal instants t_k and $t_k+\theta\Delta t$. The acceleration is expressed by the following equations:

$$\ddot{\boldsymbol{x}}_{k+\theta}=(1-\theta)\ddot{\boldsymbol{x}}_k+\theta\ddot{\boldsymbol{x}}_{k+1} \tag{2.32}$$

in which:

$\ddot{\boldsymbol{x}}$ second time derivative of the unknown vector of equation 2.31

$t_{k+1}=t_k+\Delta t$ discrete time

Integration of acceleration in the interval $[t_k, t_k+\theta\Delta t]$ gives the velocity and the displacement as polynomial expression of $\theta\Delta t$ [Hilber 1976, Paz 1985]:

$$\dot{\boldsymbol{x}}_{k+\theta} = \dot{\boldsymbol{x}}_k+\theta\Delta t[(1-\delta)\ddot{\boldsymbol{x}}_k+\delta\ddot{\boldsymbol{x}}_{k+\theta}] \tag{2.33}$$

$$\boldsymbol{x}_{k+\theta}=\boldsymbol{x}_k+\theta\Delta t v_k+\theta^2\Delta t^2[(\frac{1}{2}-\alpha)\ddot{\boldsymbol{x}}_k+\alpha\ddot{\boldsymbol{x}}_{k+\theta}] \tag{2.34}$$

Substitution of the expression for the kinematics quantities in matrix equation 2.31 reads:

$$\boldsymbol{K}\cdot\boldsymbol{x}_{k+\theta}+\boldsymbol{C}\dot{\boldsymbol{x}}_{k+\theta}+\boldsymbol{M_w}\cdot\ddot{\boldsymbol{x}}_{k+\theta}=\boldsymbol{F}_{k+\theta}$$

in which:

$$\boldsymbol{F}_{k+\theta}=\begin{pmatrix}0\\ \boldsymbol{Q}_{k+\theta}+\boldsymbol{V}_{k+\theta}\\ 0\end{pmatrix}$$

Expressing discrete acceleration and velocity as a function of discrete displacement through equations 2.32, 2.33 and 2.34 leads, after re-arraying of parameters, to the final expression:

$$\begin{aligned}[a_0\boldsymbol{M_w} + b_0\boldsymbol{C} + \boldsymbol{K}] \cdot \boldsymbol{x}_{k+\theta} \quad = \quad & \boldsymbol{F}_{k+\theta} + \\ & + \boldsymbol{M_w}\left[a_0\boldsymbol{x}_k + a_1\dot{\boldsymbol{x}}_k + a_2\ddot{\boldsymbol{x}}_k\right] + \\ & + \boldsymbol{C}\left[b_0\boldsymbol{x}_k + b_1\dot{\boldsymbol{x}}_k + b_2\ddot{\boldsymbol{x}}_k\right] \end{aligned} \tag{2.35}$$

in which:

$a_0 = \frac{1}{\alpha\theta^2\Delta t^2}$

$a_1 = \frac{1}{\alpha\theta\Delta t}$

$a_2 = \frac{1}{2\alpha} - 1$

$b_0 = \frac{\delta}{\alpha\theta\Delta t}$

$b_1 = \frac{\delta}{\alpha} - 1$

$b_2 = (\frac{\delta}{2\alpha} - 1)\theta\Delta t$

The equation 2.35 can be used to determine the unknown vector at time instant $t_{k+\theta}$ once the whole kinematic states are known at time instant t_k. Then using equations 2.32 it is possible to calculate the acceleration at time $t_{k+1} = t_k + \Delta t$:

$$a_{k+1} = c_0(\boldsymbol{x}_{k+\theta} - \boldsymbol{x}_k) - c_1\dot{\boldsymbol{x}}_k - c_2\ddot{\boldsymbol{x}}_k$$

in which:

$c_0 = \frac{a_0}{\theta}$

$c_1 = \frac{a_1}{\theta}$

$c_2 = \left(\frac{1}{2\alpha\theta} - 1\right)$

Then using equations 2.33 and 2.34 with $\theta = 1$ it is possible to calculate the displacements and the velocities at time $t_{k+1} = t_k + \Delta t$. If $\theta = 1$ the algorithm is the classical Newmark. The following worth characteristics of the algorithm can be listed :

Stability for unconditional stability, in choosing the time step Δt, the following inequalities must hold [Hilber 1976]:

$$\begin{aligned} \delta &\geq \frac{1}{2} \\ \alpha &\geq \frac{\delta}{2} \\ \theta &\geq \frac{2\alpha}{1-2\alpha} \end{aligned}$$

Accuracy for every values of θ the order of accuracy is two if [Hilber 1976]:

$$\delta = \frac{1}{2}$$

Dissipation No numerical damping for [Hilber 1976]:

$$\begin{aligned} \delta &= 0.5 \\ \alpha &= 0.25 \end{aligned}$$

and the better values for optimal dissipation characteristics, for both low and high frequency is [Hilber 1976]:

$$\alpha = \frac{(\delta + 0.5)^2}{4}$$

Damping The numerical solution results to be under-damped if the following inequalities hold:

$$\begin{aligned} \delta &\geq \frac{1}{2} \\ \alpha &\geq \frac{(\delta + 0.5)^2}{4} \end{aligned}$$

The better behaviour in terms of frequency induced dissipation for unconditionally stable algorithm is for (damping increasing with frequency):

$$\theta \approx 1.4$$

Example of application of the integration algorithm will be showed in the next sections.

2.3.3.3 Applying End Displacements or Shear Forces

The solution of both matrix equations 2.26 and 2.30 require the application of displacements boundary condition that shall be applied following the standard Finite Element procedures:

1. if the displacement is imposed the relevant system row is taken out from the solution procedure and the unknown values of the shear force will be determined after the time integration

2. if the shear force is imposed the known values is set on the right hand side of equation 2.26

When the displacements are calculated the equation 2.25 allows for the determination of the nodal values of the moment.

length	10 m
Young Modulus	2.1E+11$\frac{N}{m^2}$
density	7250 $\frac{Kg}{m^3}$
width	$0.1m$
height	$.25m$

Table 2.1: Geometrical and Mechanical data

2.4 Numerical Tests

A simple model, for which analytical solution is available, has been chosen to test the performance of the Mixed Finite Element formulation. On that model, eigen mode extraction and time integration analysis have been run comparing the result of the Mixed Finite Elements (heron called MFE), the Classical Finite Elements (heron called CFE) and if available analytical solution.

2.4.1 Eigen Mode Extraction

For the sake of simplicity, without losing in generality, a uniform rectangular cross section beam with free end translations and restrained end rotations is considered. For the MFE equation 2.26 has been solved, for the CFE the solution has been obtained using the general purpose Finite Element Program ANSYS and reference for the analytical solution can be found in [Paz 1985]. The following geometrical and mechanical data has been used:

The beam has been discretized using a Finite Element size equal to $2.5m$ resulting in 5 node, a $2nd$ degree polynomial shape function for the MFE, and the usual 3^{rd} degree polynomial shape function for the CFE. Eigen frequency results, for the various methods, are reported in table 2.2. They show a good agreement between both numerical methods and the exact solution considering that only 9 degree of freedom are present for the MFE and 10 for the CFE. A maximum relative error, on the third mode, of 3.3% for the MFE formulation and 1.37% for the CFE. The higher value for the MFE can be easily explained with the lower degree of the approximating polynomial for the displacement unknowns used respect to the CFE.

This kind of behaviour is completely reversed considering the stresses that is in this case the bending moment value. The approximating polynomial is of order two in the MFE formulation and the shape function is continuous, instead for the CFE the approximating polynomial is of order one and the shape function is discontinuous crossing the element border. As it is clearly

Mode n^{th}	Exact	MFE	ANSYS
1	0.0	0.2247e-05	0.2008E-06
2	6.1011	6.1042	6.0992
3	24.4045	24.588	24.449
4	54.9101	56.739	55.677

Table 2.2: Eigen Frequency results

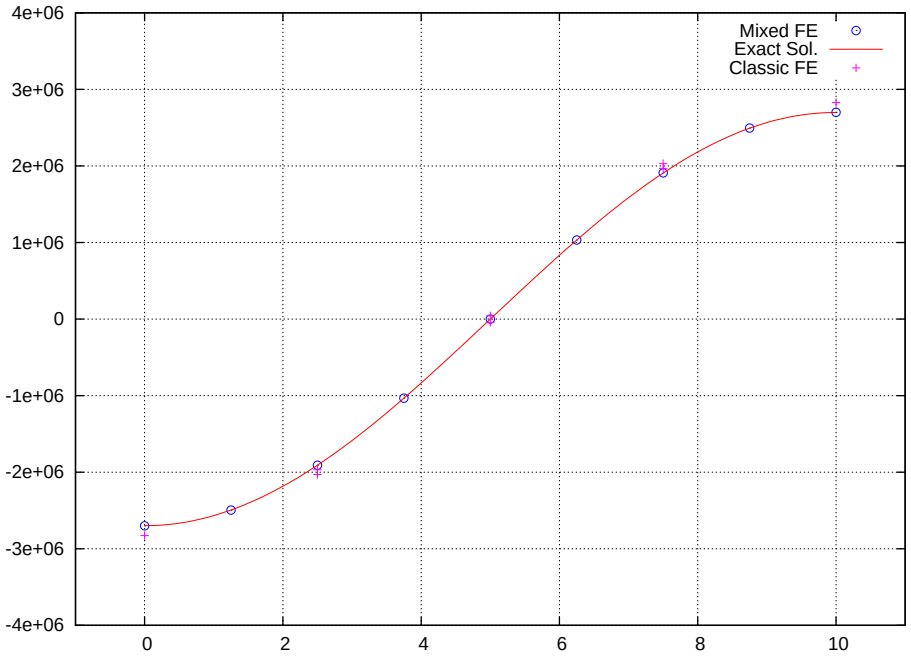

Figure 2.3: Bending moment for the 1^{st} mode. Space coordinate (m) on abscissa and Moment on ordinate (Nm)

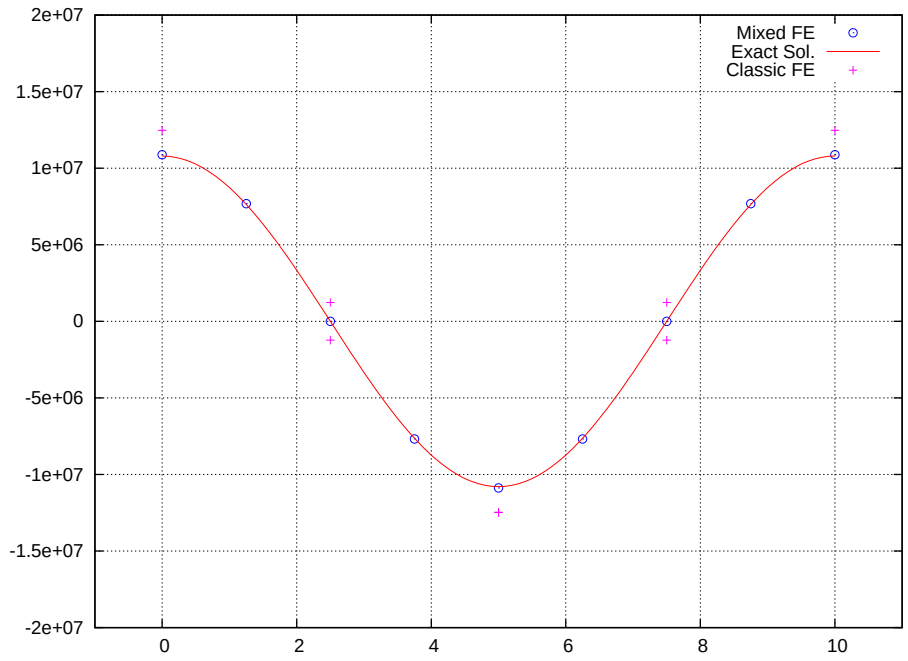

Figure 2.4: Bending moment for the 2^{nd} mode. Space coordinate (m) on abscissa and Moment on ordinate (Nm)

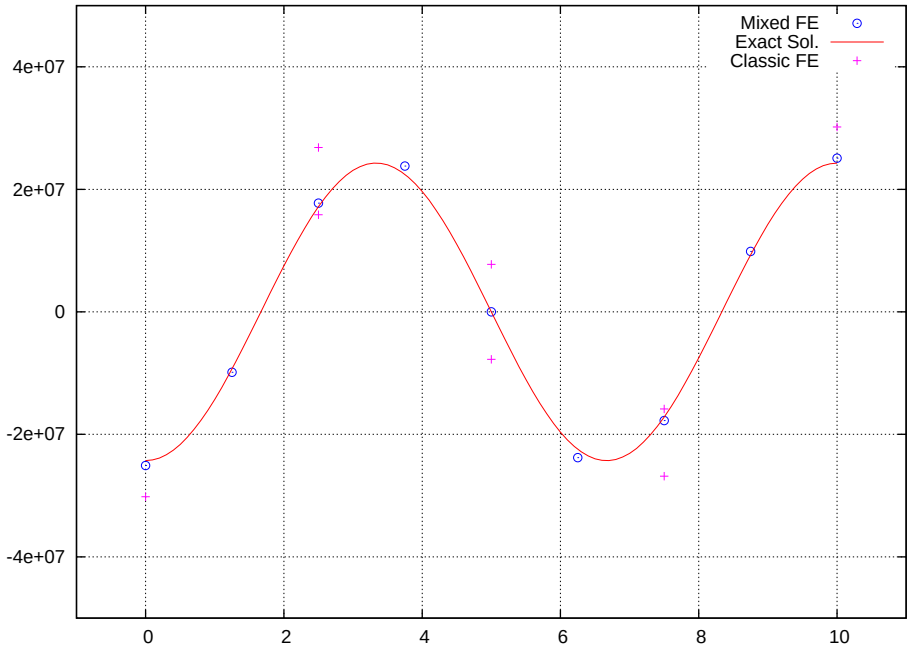

Figure 2.5: Bending moment for the 3^{rd} mode. Space coordinate (m) on abscissa and Moment on ordinate (Nm)

showed by figures 2.3, 2.4 and 2.5 the MFE formulation gives higher level of approximation both in terms of continuity and precision. In the CFE formulation the discontinuity on the nodes and the accuracy of the values decrease quickly with the increasing of the mode number. In the light of the previous results it is possible to draw the conclusion that with a lower degree of approximation in the displacements there is no sensible lack in the frequency accuracy calculation while it is possible to gain a strong increase in the accuracy of the bending moment calculation. This increase is much more impressive if using the same degree of approximation of the CFE for the shape functions, ie third degree polynomials. Numerical and exact solutions are very close in this case as figure 2.6. This behaviour can still be recognized in the bending moment shape mode for the 4^{th} mode as described in figure 2.7.

2.4.2 Time Integration

For the test of the time integration performances of the MFE method the case of the structure presented in section 2.4.1, with simply supported ends, one

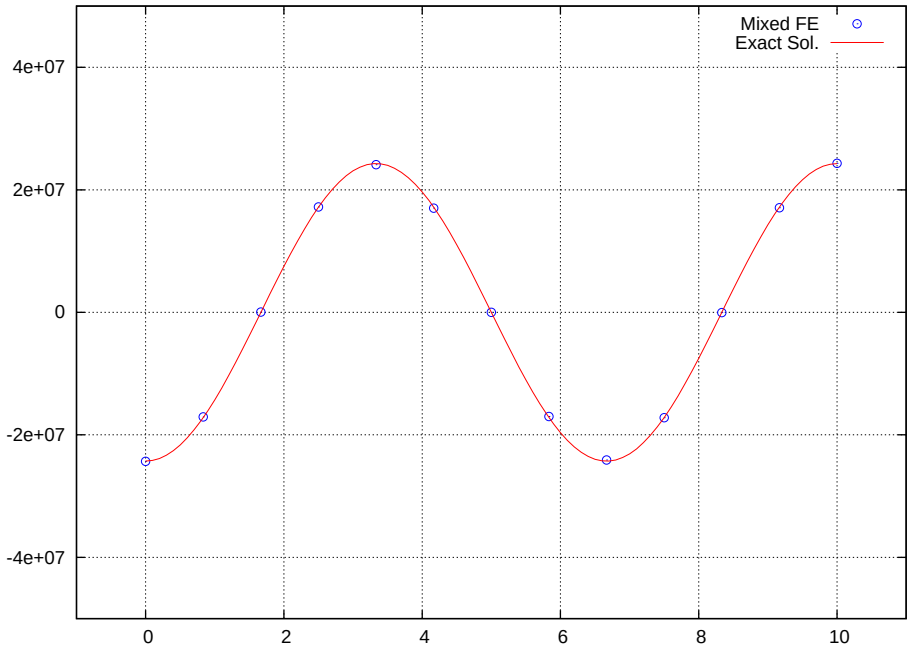

Figure 2.6: Bending moment for the 3^{rd} mode with four node Mixed Element. Space coordinate (m) on abscissa and Moment on ordinate (Nm)

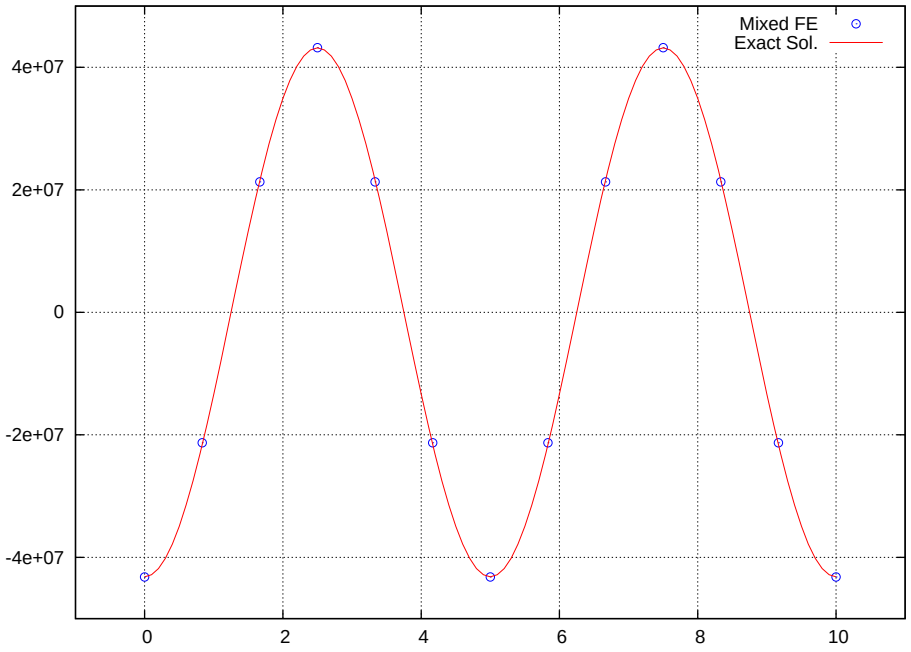

Figure 2.7: Bending moment for the 4^{th} mode with four node Mixed Element. Space coordinate (m) on abscissa and Moment on ordinate (Nm)

node	Exact	MFE	CFE right	CFE left
5	2.9352	2.9566	NA	2.9652
4	2.3512	2.3519	2.3614	2.3600
3	1.6534	1.6528	1.6622	1.6602
2	0.86640	0.86668	0.87646	0.87268
1	0.000000	0.000000	0.027169	NA

Table 2.3: RMS comparison of the Fast Fourier Transform for the bending moment time series data

constant point load suddenly applied at midspan, at time $t = 0$, has been chosen with the same discretization used for the modal analysis. For this particular load configuration an analytical solution [Paz 1985] is available for the beam deflection in the following form:

$$z(x,t) = \frac{2P_0}{A_c L} \sum_{n=1}^{\infty} \left[\frac{1}{\omega^2} sin\frac{n\pi}{2}(1 - cos\omega_n t) sin\frac{n\pi}{L}x \right]$$

and for the bending moment:

$$m(x,t) = EI\frac{2\pi^2 P_0}{A_c L^3} \sum_{n=1}^{\infty} \left[\frac{n^2}{\omega^2} sin\frac{n\pi}{2}(1 - cos\omega_n t) sin\frac{n\pi}{L}x \right]$$

in which ω_n is the n^{th} eigen-value. The numerical results (obtained with the octave script `dyn_solve.m` revision 1.13 with `iload` set to 1) has been obtained, both for the MFE and CFE method, using the classical Newmark method, the only available in the ANSYS software. Neither numerical nor physical damping has been used in both model. Results are showed in terms of displacement and bending moment at the loaded point in figure. The bending moment of the first node of the last element is showed in figure. The time history of the numerical and exact solution are very close, almost identical for the displacement and with some error for the bending moment. For a better understanding of the accuracy of the numerical solutions and for a comparison between the MFE and the CFE the RMS of the FFT of the time history, that describe the energy content of the time series signal, has been calculated and reported in table 2.3. The CFE data are on an element basis so for each node the right and left element data have been considered. Remembering that the numerical solution is always stiffer that the exact one as it is expected the exact solution has the lower energy level. The MFE numerical solution shows a close RMS value to the exact one respect to the CFE method, calculated with the ANSYS software.

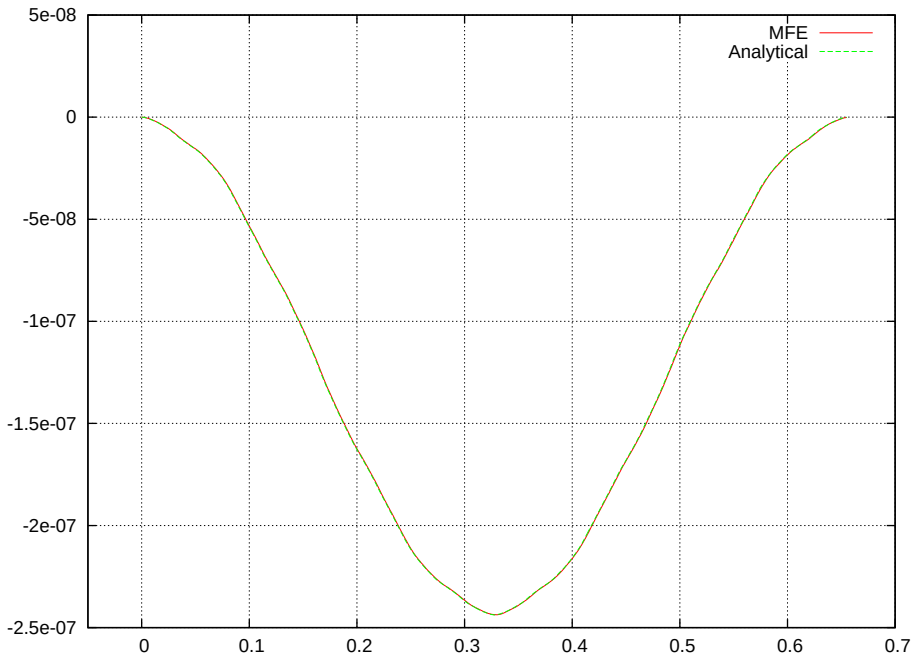

Figure 2.8: Displacement of the loaded point. Time on the abscissa (*sec.*) and displacement on the ordinate (m)

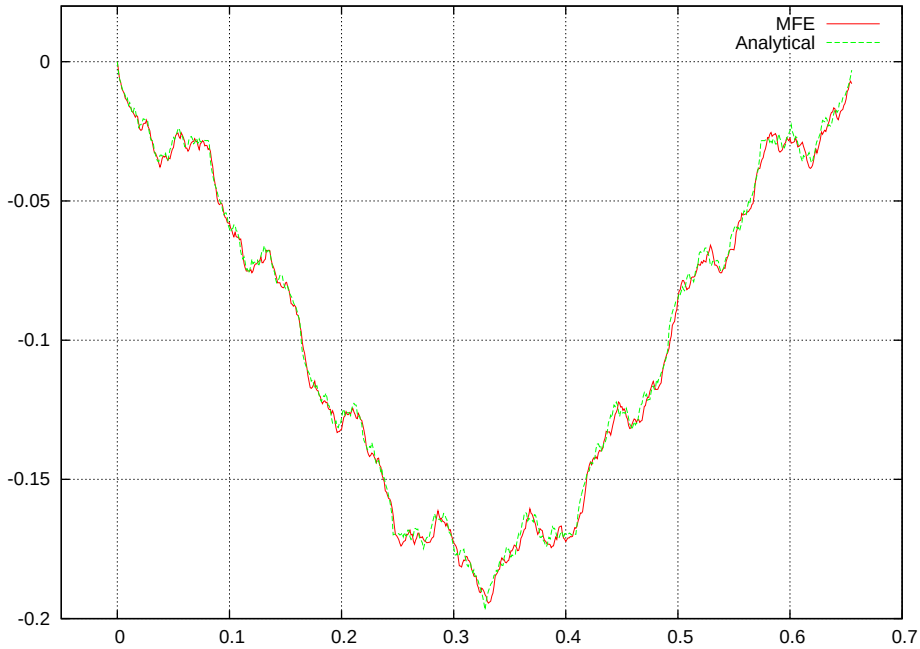

Figure 2.9: Bending moment at the loaded point. Time on the abscissa ($sec.$) and moment on the ordinate (Nm)

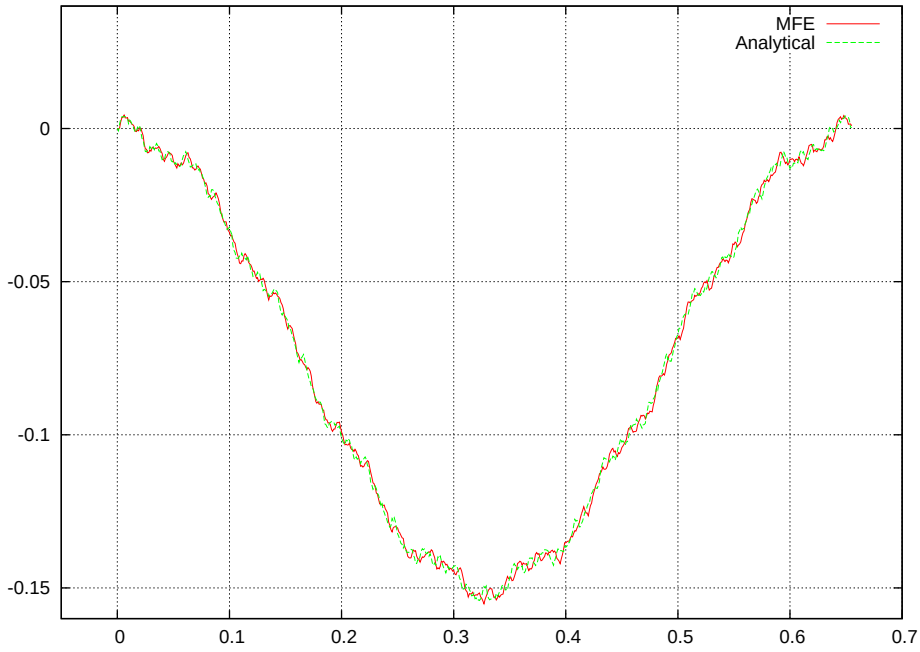

Figure 2.10: Bending moment at the first node of the last element. Time on the abscissa ($sec.$) and moment on the ordinate (Nm)

Chapter 3

Spatial Frame Applications of Beam Element

Application of the "Displacement Only Method" in spatial frame requires that rotation of element matrix and axial stress component should be accounted for.

3.1 The column behaviour

The effect of the axial force has to be considered in spatial beam structures, in this the equilibrium equation is (reference is made to figure 3.1):

$$A_c \frac{\partial^2 u}{\partial t^2} dx = P^* - P$$

in which:

u is the axial displacement

P is the axial force

$P^* = P + \frac{\partial P}{\partial x} dx$

hereafter for other symbols reference is made to section 2.2 and 2.2.1. After some simplification and with the compatibility equation the system that rules the rod behaviour is:

$$\begin{aligned} P - EA\frac{\partial u}{\partial x} &= 0 \\ -\frac{\partial P}{\partial x} + A_c \frac{\partial^2 u}{\partial t^2} &= 0 \end{aligned} \tag{3.1}$$

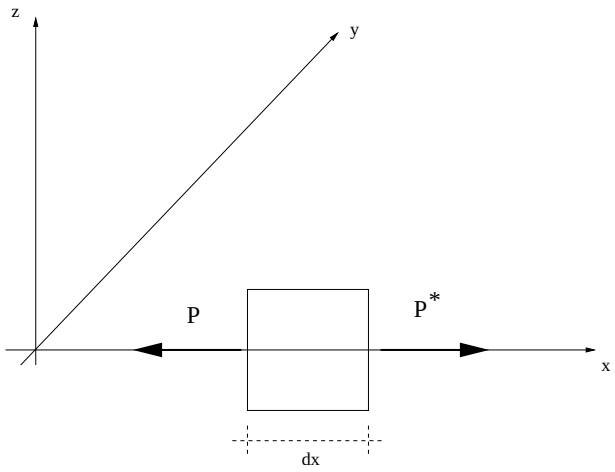

Figure 3.1: Beam axial equilibrium sketch

Using the same weak formulation and finite element approximation of the section 2.3.1 the equation 3.1 is transformed as:

$$\begin{aligned} \int_0^L N_j N_i dx \cdot P_i - EA \int_0^L N_j \frac{\partial N_i}{\partial x} dx \cdot u_i &= 0 \\ -\int_0^L N_j \frac{\partial N_i}{\partial x} dx \cdot P_i + A_c \int N_j N_i dx \cdot \frac{d^2 u_i}{dt^2} + (P^h - b_p(t)) N_j|_0^L &= 0 \end{aligned}$$

in which:

P_i value of the axial force at node i

u_i value of the axial displacement at node i

Using integration by parts in the equilibrium equation, the final form of the system is:

$$\begin{aligned} \int_0^L N_j N_i dx \cdot P_i - EA \int_0^L N_j \frac{\partial N_i}{\partial x} dx \cdot u_i &= 0 \\ + \int_0^L \frac{\partial N_j}{\partial x} \cdot N_i dx \cdot P_i + A_c \int_0^L N_j N_i dx \cdot \frac{d^2 u_i}{dt^2} - b_p(t) N_j|_0^L &= 0 \end{aligned}$$

With the following position:

$(\boldsymbol{K_i})_{ji} = \int_0^L N_j N_i dx$

$(\boldsymbol{K_u})_{ij} = (\boldsymbol{K_p})_{ji} = \int_0^L \frac{\partial N_j}{\partial x} \cdot N_i dx$

$$\begin{aligned} \boldsymbol{K_i} \cdot \boldsymbol{p} - EA \cdot \boldsymbol{K_u} \cdot \boldsymbol{u} &= 0 \\ \boldsymbol{K_p} \cdot \boldsymbol{p} + A_c \boldsymbol{K_i} \cdot \ddot{\boldsymbol{u}} &= 0 \end{aligned}$$

in which :

$\boldsymbol{p}$ is the vector of the axial force nodal value

$\boldsymbol{u}$ is the vector of the axial displacement nodal values

Now it is possible to condensate the axial force in the matrix form:

$$\begin{aligned} \boldsymbol{p} &= EA \cdot \boldsymbol{K_i}^{-1} \cdot \boldsymbol{K_u} \cdot \boldsymbol{u} \\ \boldsymbol{K_p} \cdot \boldsymbol{K_i}^{-1} \cdot \boldsymbol{K_u} \cdot \boldsymbol{u} + A_c \boldsymbol{K_i} \cdot \ddot{\boldsymbol{u}} &= 0 \end{aligned} \tag{3.2}$$

where the stiffness matrix is:

$$\boldsymbol{K_{ax}} = \boldsymbol{K_p} \cdot \boldsymbol{K_i}^{-1} \cdot \boldsymbol{K_u}$$

Considering the same shape function of section 2.3.2 the matrix relationship for a three node element is:

$$\begin{aligned} &\frac{L}{15} \begin{pmatrix} 2 & 1 & -\frac{1}{2} \\ 1 & 8 & 1 \\ -\frac{1}{2} & 1 & 2 \end{pmatrix} \begin{pmatrix} P_1 \\ P_2 \\ P_3 \end{pmatrix} - EA \begin{pmatrix} -\frac{1}{2} & \frac{2}{3} & -\frac{1}{6} \\ -\frac{2}{3} & 0 & \frac{2}{3} \\ \frac{1}{6} & -\frac{2}{3} & \frac{1}{2} \end{pmatrix} \begin{pmatrix} u_1 \\ u_2 \\ u_3 \end{pmatrix} = 0 \\ &\begin{pmatrix} -\frac{1}{2} & \frac{2}{3} & -\frac{1}{6} \\ -\frac{2}{3} & 0 & \frac{2}{3} \\ \frac{1}{6} & -\frac{2}{3} & \frac{1}{2} \end{pmatrix} \begin{pmatrix} P_1 \\ P_2 \\ P_3 \end{pmatrix} + A_c L \frac{1}{15} \begin{pmatrix} 2 & 1 & -\frac{1}{2} \\ 1 & 8 & 1 \\ -\frac{1}{2} & 1 & 2 \end{pmatrix} \begin{pmatrix} \ddot{u}_1 \\ \ddot{u}_2 \\ \ddot{u}_3 \end{pmatrix} = 0 \end{aligned}$$

Eliminating the axial force from the equilibrium equation it is possible to get:

$$\frac{EA}{L} \begin{pmatrix} \frac{7}{3} & -\frac{8}{3} & \frac{1}{3} \\ -\frac{8}{3} & \frac{16}{3} & -\frac{8}{3} \\ \frac{1}{3} & -\frac{8}{3} & \frac{7}{3} \end{pmatrix} \begin{pmatrix} u_1 \\ u_2 \\ u_3 \end{pmatrix} + A_c L \frac{1}{15} \begin{pmatrix} 2 & 1 & -\frac{1}{2} \\ 1 & 8 & 1 \\ -\frac{1}{2} & 1 & 2 \end{pmatrix} \begin{pmatrix} \ddot{u}_1 \\ \ddot{u}_2 \\ \ddot{u}_3 \end{pmatrix} = 0$$

With similar calculations it is possible to deduce the stiffness matrix for shape function of different polynomial degrees.

3.2 Matrix Rotation

In 2D geometry it is necessary to consider for each node two translational Degrees of Freedom, one in the x direction and the other in the z direction, as showed in the figure 3.2, where a general configuration for an element is

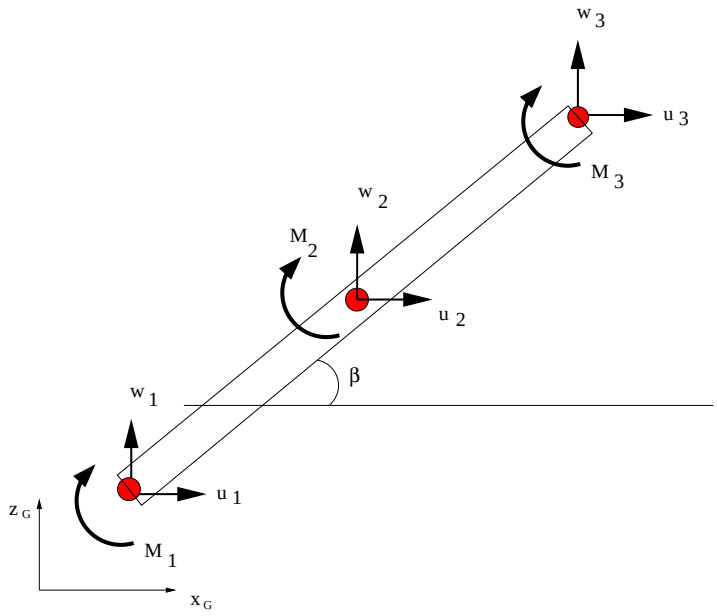

Figure 3.2: DoF sketch for 2D spatial frame

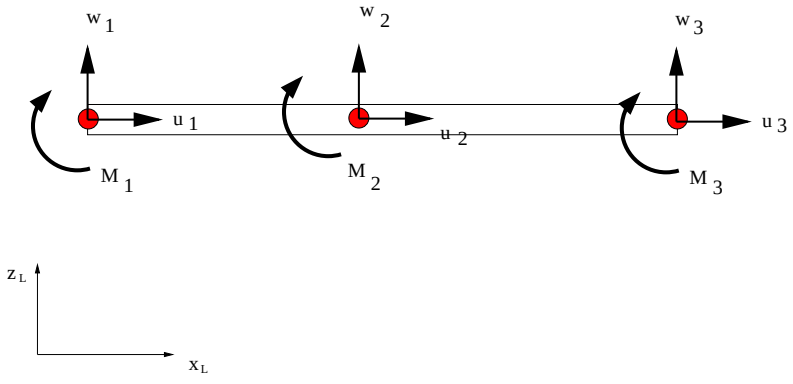

Figure 3.3: Local reference system for the Element

sketched. The stiffness matrix in the global reference system (see figure 3.2) has to be obtained by its rotation from the local reference system (see figure 3.3). The local stiffness matrix is obtained coupling the column behaviour, described in section 3.1, and the beam behaviour described in section 2.3.1 represented by the equation 2.18. For the sake of comprehension of the following analysis it is useful to rewrite equation 2.18 with both end rotations prescribed (the first equation results multiplied for EI respect to equation 2.18):

$$\begin{cases} M_i \int_0^L N_i N_j dx + \frac{M_i EI}{\mu G} \int_0^L \frac{\partial N_i}{\partial x}\frac{\partial N_j}{\partial x} dx - EI \cdot w_i \int_0^L \frac{\partial N_i}{\partial x}\frac{\partial N_j}{\partial x} dx + \\ - EI \cdot b_\theta(t) N_j|^L + EI \cdot b_\theta(t) N_j|_0 = 0 \\ -M_i \int_0^L \frac{\partial N_i}{\partial x}\frac{\partial N_j}{\partial x} dx + \int_0^L q(x) N_j dx - A_c \frac{d^2 w_i}{dt^2} \int_0^L N_i N_j dx + \\ + b_v(t) N_j|^L = 0 \end{cases}$$

Along with the stiffness matrix the load vector has to undergone the same process of transformation too, taking into account that the load vector has a contribution from the end rotations. This effect is quantified by (referring to equations 2.18, 2.19 and 2.24):

$$\boldsymbol{q_\theta} = -(\boldsymbol{K_n} \cdot \boldsymbol{K_b}^{-1} \cdot \boldsymbol{\theta})$$

It has to be considered that the vector $\boldsymbol{\theta}$ has only two elements different from zero, the end rotations (again reference is made to equation 2.24) and that the inversion of the matrix $\boldsymbol{K_b}$ has to be referred to the structure assembled matrix.

3.2.1 Coupling Column and Bending Behaviour

To express the stiffness matrix in an form suitable for the rotation procedure it is worthwhile to re-arraying together both equations, 3.2 and 2.22, in the compatibility equation:

$$\begin{bmatrix} \boldsymbol{K_i} & 0 \\ 0 & \boldsymbol{K_b} \end{bmatrix} \cdot \begin{bmatrix} \boldsymbol{p} \\ \boldsymbol{m} \end{bmatrix} + \begin{bmatrix} -EA \cdot \boldsymbol{K_u} & 0 \\ 0 & -EI \cdot \boldsymbol{K_n} \end{bmatrix} \cdot \begin{bmatrix} \boldsymbol{u} \\ \boldsymbol{w} \end{bmatrix}_L = \begin{bmatrix} 0 \\ -EI \cdot \boldsymbol{\theta} \end{bmatrix}_L \tag{3.3}$$

and in the equilibrium equation:

$$\begin{bmatrix} \boldsymbol{K_p} & 0 \\ 0 & -\boldsymbol{K_n} \end{bmatrix} \cdot \begin{bmatrix} \boldsymbol{p} \\ \boldsymbol{m} \end{bmatrix}_L + \begin{bmatrix} \boldsymbol{Mi} & 0 \\ 0 & -\boldsymbol{Mi} \end{bmatrix} \cdot \frac{d^2}{dt^2} \begin{bmatrix} \boldsymbol{u} \\ \boldsymbol{w} \end{bmatrix}_L = \begin{bmatrix} 0 \\ -\boldsymbol{Q} - \boldsymbol{V} \end{bmatrix}_L \tag{3.4}$$

Obtaining $\boldsymbol{p}$ and $\boldsymbol{m}$ from the first equation:

$$\begin{bmatrix} \boldsymbol{p} \\ \boldsymbol{m} \end{bmatrix} = \begin{bmatrix} \boldsymbol{K_i} & 0 \\ 0 & \boldsymbol{K_b} \end{bmatrix}^{-1} \cdot \left(\begin{bmatrix} EA \cdot \boldsymbol{K_u} & 0 \\ 0 & EI \cdot \boldsymbol{K_n} \end{bmatrix} \cdot \begin{bmatrix} \boldsymbol{u} \\ \boldsymbol{w} \end{bmatrix}_L + \begin{bmatrix} 0 \\ -EI \cdot \boldsymbol{\theta} \end{bmatrix}_L \right)$$

it is possible to express the equilibrium equation in the displacement nodal value unknowns:

$$\begin{aligned}
&\begin{bmatrix} \boldsymbol{K_p} & 0 \\ 0 & \boldsymbol{K_n} \end{bmatrix} \cdot \begin{bmatrix} \boldsymbol{K_i} & 0 \\ 0 & \boldsymbol{K_b} \end{bmatrix}^{-1} \cdot \\
&\cdot \begin{bmatrix} EA \cdot \boldsymbol{K_u} & 0 \\ 0 & EI \cdot \boldsymbol{K_n} \end{bmatrix} \cdot \begin{bmatrix} \boldsymbol{u} \\ \boldsymbol{w} \end{bmatrix}_L + \\
&+ \begin{bmatrix} \boldsymbol{Mi} & 0 \\ 0 & \boldsymbol{Mi} \end{bmatrix} \cdot \frac{d^2}{dt^2} \begin{bmatrix} \boldsymbol{u} \\ \boldsymbol{w} \end{bmatrix}_L = \begin{bmatrix} 0 \\ \boldsymbol{Q} + \boldsymbol{V} \end{bmatrix}_L + \\
&+ \begin{bmatrix} \boldsymbol{K_p} & 0 \\ 0 & \boldsymbol{K_n} \end{bmatrix} \cdot \begin{bmatrix} \boldsymbol{K_i} & 0 \\ 0 & \boldsymbol{K_b} \end{bmatrix}^{-1} \begin{bmatrix} 0 \\ EI \cdot \boldsymbol{\theta} \end{bmatrix}_L
\end{aligned}$$

Re-arraying the nodal displacement vector as follow (for an n nodes elements):

$$U_L = \begin{bmatrix} u_1 \\ w_1 \\ \vdots \\ u_n \\ w_n \end{bmatrix}$$

The equilibrium equation results:

$$\boldsymbol{K}_L \cdot U_L + \boldsymbol{M}_L \cdot \frac{d^2}{dt^2} U_L = \boldsymbol{Q} + \boldsymbol{K}_R \cdot G \cdot \boldsymbol{Q_\theta} \tag{3.5}$$

in which (for the sake of simplicity a three node element has been chosen):

$$\boldsymbol{Q_\theta} = \begin{bmatrix} \theta_1 \\ \theta_n \end{bmatrix}$$

$$G = \begin{bmatrix} 0 & 0 \\ EI & 0 \\ \vdots & \vdots \\ 0 & -EI \end{bmatrix}$$

$$\boldsymbol{K}_L = \begin{bmatrix} (\boldsymbol{K_{ax}})_{11} & 0 & (\boldsymbol{K_{ax}})_{12} & 0 & (\boldsymbol{K_{ax}})_{13} & 0 \\ 0 & (\boldsymbol{K_{fl}})_{11} & 0 & (\boldsymbol{K_{fl}})_{12} & 0 & (\boldsymbol{K_{fl}})_{13} \\ (\boldsymbol{K_{ax}})_{21} & 0 & (\boldsymbol{K_{ax}})_{22} & 0 & (\boldsymbol{K_{ax}})_{23} & 0 \\ 0 & (\boldsymbol{K_{fl}})_{21} & 0 & (\boldsymbol{K_{fl}})_{22} & 0 & (\boldsymbol{K_{fl}})_{23} \\ (\boldsymbol{K_{ax}})_{12} & 0 & (\boldsymbol{K_{ax}})_{12} & 0 & (\boldsymbol{K_{ax}})_{33} & 0 \\ 0 & (\boldsymbol{K_{fl}})_{31} & 0 & (\boldsymbol{K_{fl}})_{32} & 0 & (\boldsymbol{K_{fl}})_{33} \end{bmatrix} \tag{3.6}$$

the same arrangement has to be used for the mass matrix $\boldsymbol{M}_L$and for the node rotation coefficient matrix. In the analysis of frame structures, respect to the analysis developed for supported beams in section 2.3.3.1, the minus sign of the left node rotation and EI have to be moved to the rotation coefficient matrix, $\boldsymbol{K}_R$, due to the assembling process of the rotation equilibrium equation of the frame joint. The rotation coefficient matrix, $\boldsymbol{K}_R$, results:

$$\boldsymbol{K}_R = \begin{bmatrix} (\boldsymbol{K_p}\cdot\boldsymbol{K_i}^{-1})_{11} & 0 & (\boldsymbol{K_p}\cdot\boldsymbol{K_i}^{-1})_{12} \\ 0 & (\boldsymbol{K_n}\cdot\boldsymbol{K_b}^{-1})_{11} & 0 \\ (\boldsymbol{K_p}\cdot\boldsymbol{K_i}^{-1})_{21} & 0 & (\boldsymbol{K_p}\cdot\boldsymbol{K_i}^{-1})_{22} \\ 0 & (\boldsymbol{K_n}\cdot\boldsymbol{K_b}^{-1})_{21} & 0 \\ (\boldsymbol{K_p}\cdot\boldsymbol{K_i}^{-1})_{12} & 0 & (\boldsymbol{K_p}\cdot\boldsymbol{K_i}^{-1})_{12} \\ 0 & (\boldsymbol{K_n}\cdot\boldsymbol{K_b}^{-1})_{31} & 0 \end{bmatrix} \ldots$$
$$\begin{bmatrix} 0 & (\boldsymbol{K_p}\cdot\boldsymbol{K_i}^{-1})_{13} & 0 \\ (\boldsymbol{K_n}\cdot\boldsymbol{K_b}^{-1})_{12} & 0 & (\boldsymbol{K_n}\cdot\boldsymbol{K_b}^{-1})_{13} \\ 0 & (\boldsymbol{K_p}\cdot\boldsymbol{K_i}^{-1})_{23} & 0 \\ (\boldsymbol{K_n}\cdot\boldsymbol{K_b}^{-1})_{22} & 0 & (\boldsymbol{K_n}\cdot\boldsymbol{K_b}^{-1})_{23} \\ 0 & (\boldsymbol{K_p}\cdot\boldsymbol{K_i}^{-1})_{33} & 0 \\ (\boldsymbol{K_n}\cdot\boldsymbol{K_b}^{-1})_{32} & 0 & (\boldsymbol{K_n}\cdot\boldsymbol{K_b}^{-1})_{33} \end{bmatrix}$$

$\boldsymbol{K_i}$ *and* $\boldsymbol{K_b}$ *must result from the assembling process of the elements belonging to the stretch under analysis.* In the previous matrix definitions the following position has been made:

$$\boldsymbol{K_{ax}} = \boldsymbol{K_p}\cdot(EA\cdot\boldsymbol{K_i}^{-1})\cdot\boldsymbol{K_u}$$

$$\boldsymbol{K_{fl}} = \boldsymbol{K_n}\cdot(EI\cdot\boldsymbol{K_b}^{-1})\boldsymbol{K_n}$$

Equation 3.5 is the building block for the assembling process, necessary for the solution of 2-D frame structures.

3.2.2 Local to Global system Transformation

Considering the transformation between the local and global reference systems, the relationship connecting the local displacements components of the j node to global ones reads:

$$U_{Lj} = \boldsymbol{R}\cdot U_{Gj}$$

in which the rotation matrix is:

$$\boldsymbol{R} = \begin{bmatrix} cos\ x_L\hat{x}_G & cos\ x_L\hat{y}_G & cos\ x_L\hat{z}_G \\ cos\ y_L\hat{x}_G & cos\ y_L\hat{y}_G & cos\ y_L\hat{z}_G \\ cos\ z_L\hat{x}_G & cos\ z_L\hat{y}_G & cos\ z_L\hat{z}_G \end{bmatrix}$$

Applying the transformation to the vector of displacements of the finite element gets (considering for simplicity a three node element):

$$\begin{bmatrix} U_{L1} \\ U_{L2} \\ U_{L3} \end{bmatrix} = \begin{bmatrix} R & 0 & 0 \\ 0 & R & 0 \\ 0 & 0 & R \end{bmatrix} \begin{bmatrix} u_{G1} \\ U_{G2} \\ U_{G3} \end{bmatrix}$$

In a more concise form:

$$U_L \quad = \quad T \cdot U_G \tag{3.7}$$

in which:

T is the transformation matrix

Thus for a plane-structural problem the transformation matrix is:

$$T = \begin{bmatrix} cos\beta & sin\beta & 0 & 0 & 0 & 0 & 0 & 0 & 0 \\ -sin\beta & cos\beta & 0 & 0 & 0 & 0 & 0 & 0 & 0 \\ 0 & 0 & 1 & 0 & 0 & 0 & 0 & 0 & 0 \\ 0 & 0 & 0 & cos\beta & sin\beta & 0 & 0 & 0 & 0 \\ 0 & 0 & 0 & -sin\beta & cos\beta & 0 & 0 & 0 & 0 \\ 0 & 0 & 0 & 0 & 0 & 1 & 0 & 0 & 0 \\ 0 & 0 & 0 & 0 & 0 & 0 & cos\beta & sin\beta & 0 \\ 0 & 0 & 0 & 0 & 0 & 0 & -sin\beta & cos\beta & 0 \\ 0 & 0 & 0 & 0 & 0 & 0 & 0 & 0 & 1 \end{bmatrix}$$

If a 2D element is considered as in figure 3.2:

U_{Lj} local vector of node j displacements $\begin{pmatrix} u_{Lj} \\ w_{Lj} \end{pmatrix}$

U_{Gj} global vector of node j displacements $\begin{pmatrix} u_{Gj} \\ w_{Gj} \end{pmatrix}$

Paying attention to the 2D case and considering β the angle between the x_L and the x_G axis the transformation equation becomes:

$$U_{Lj} = \begin{bmatrix} cos\beta & sin\beta \\ -sin\beta & cos\beta \end{bmatrix} U_{Gj}$$

Using the orthogonality feature of the rotation matrix results:

$$U_{Gj} = \begin{bmatrix} cos\beta & -sin\beta \\ sin\beta & cos\beta \end{bmatrix} U_{Lj}$$

Applying the transformation from global to local of the vector of displacements for the whole finite element gets:

$$\begin{bmatrix} u_{L1} \\ w_{L1} \\ u_{L2} \\ w_{L2} \\ u_{L3} \\ w_{L3} \end{bmatrix} = \begin{bmatrix} cos\beta & sin\beta & 0 & 0 & 0 & 0 \\ -sin\beta & cos\beta & 0 & 0 & 0 & 0 \\ 0 & 0 & cos\beta & sin\beta & 0 & 0 \\ 0 & 0 & -sin\beta & cos\beta & 0 & 0 \\ 0 & 0 & 0 & 0 & cos\beta & sin\beta \\ 0 & 0 & 0 & 0 & -sin\beta & cos\beta \end{bmatrix} \begin{bmatrix} u_{G1} \\ w_{G1} \\ u_{G2} \\ w_{G2} \\ u_{G3} \\ w_{G3} \end{bmatrix}$$

here

$$T = \begin{bmatrix} cos\beta & sin\beta & 0 & 0 & 0 & 0 \\ -sin\beta & cos\beta & 0 & 0 & 0 & 0 \\ 0 & 0 & cos\beta & sin\beta & 0 & 0 \\ 0 & 0 & -sin\beta & cos\beta & 0 & 0 \\ 0 & 0 & 0 & 0 & cos\beta & sin\beta \\ 0 & 0 & 0 & 0 & -sin\beta & cos\beta \end{bmatrix} \tag{3.8}$$

Then applying the transformation relationship to the stiffness matrix results:

$$\boldsymbol{K}_G = T^T \cdot \boldsymbol{K}_L \cdot T \tag{3.9}$$

The same transformation of equation 3.9 is applied to the mass matrix:

$$\boldsymbol{Mi}_G = T^T \cdot \boldsymbol{Mi}_L \cdot T \tag{3.10}$$

The frame rotation, mathematically described in equations 3.9 and 3.10, has to be applied to the element characteristic quantities before the assembling process will be performed. To this aim bring back equation 3.5 and applying to it the rules of equation 3.7 it reads:

$$\boldsymbol{K}_L \cdot T \cdot U_G + \boldsymbol{M}_L \cdot T \cdot \frac{d^2}{dt^2} U_G = T \cdot \boldsymbol{Q}_G + \boldsymbol{K}_R \cdot G \cdot \boldsymbol{Q_\theta}$$

then multiplying both sides for T^T:

$$T \cdot \boldsymbol{K}_L \cdot T \cdot U_G + T \cdot \boldsymbol{M}_L \cdot T \cdot \frac{d^2}{dt^2} U_G = T^T \cdot T \cdot \boldsymbol{Q}_G + T^T \cdot \boldsymbol{K}_R \cdot G \cdot \boldsymbol{Q_\theta}$$

and finally using the definition of equation 3.9 and the relation $T^T \cdot T = I$:

$$\boldsymbol{K}_G \cdot U_G + \boldsymbol{M}_G \cdot \frac{d^2}{dt^2} U_G \quad = \quad \boldsymbol{Q}_G + T^T \cdot \boldsymbol{K}_R \cdot G \cdot \boldsymbol{Q}_{\boldsymbol{\theta}} \tag{3.11}$$

Here in a 2D condition the end rotation vector undergoes an identity transformation during reference frame rotation.

The equation 3.11 allows for using a standard element stiffness, mass matrix and load vector assembling process only for the end rotations contribution some attention has to be payed.

3.2.2.1 End Rotations Condition

Considering a linear structure with constant cross section, the matrix product $T^T \cdot \boldsymbol{K}_R$ is identical for two adjacent elements of the structure. Moreover the vector of end rotations has the following form (where the adjacent elements are labeled i and j with the common node l):

$$G{\cdot}\boldsymbol{Q}_{\boldsymbol{\theta}j} = \begin{bmatrix} 0 & 0 \\ EI & 0 \\ \vdots & \vdots \\ 0 & -EI \end{bmatrix} \begin{bmatrix} \theta_h \\ \theta_l \end{bmatrix} \qquad G{\cdot}\boldsymbol{Q}_{\boldsymbol{\theta}i} = \begin{bmatrix} 0 & 0 \\ EI & 0 \\ \vdots & \vdots \\ 0 & -EI \end{bmatrix} \begin{bmatrix} \theta_l \\ \theta_m \end{bmatrix} \tag{3.12}$$

as a consequence the assembling process will cancel out the contribution of the element common end rotations but the case of element with different cross section and "T" joint configurations. In the latter cases the matrix product $T^T \cdot \boldsymbol{K}_R$ is different for two adjacent elements although the common node rotation is identical, as a consequence the joint (or discontinuity node) rotations will still appear in the right hand member of equation 3.11, unknown at the solution stage. For this reason some other conditions have to be introduced to account for the node rotations.

The rotational equilibrium of the "joint" is the condition that makes the system 3.11 solvable.

To this aim, firstly it is necessary to account for the global components of the node displacements, in a manner similar to the one used for equation 3.5, introducing the following position:

$$\boldsymbol{s} \quad = \quad \begin{bmatrix} \boldsymbol{p}_1 \\ \boldsymbol{m}_1 \\ \vdots \\ \boldsymbol{p}_n \\ \boldsymbol{m}_n \end{bmatrix}$$

to re-array the coefficient matrix of equation 3.3 :

$$\boldsymbol{K}_S \cdot \boldsymbol{s}_L + \boldsymbol{K}_D \cdot U_L = -G \cdot \boldsymbol{Q}_{\boldsymbol{\theta}} \tag{3.13}$$

Considering a three node element the matrix $\boldsymbol{K}_S$ and $\boldsymbol{K}_D$ are as follow:

$$\boldsymbol{K}_S = \begin{bmatrix} (\boldsymbol{K_i})_{11} & 0 & (\boldsymbol{K_i})_{12} & 0 & (\boldsymbol{K_i})_{13} & 0 \\ 0 & (\boldsymbol{K_b})_{11} & 0 & (\boldsymbol{K_b})_{12} & 0 & (\boldsymbol{K_b})_{13} \\ (\boldsymbol{K_i})_{21} & 0 & (\boldsymbol{K_i})_{22} & 0 & (\boldsymbol{K_i})_{23} & 0 \\ 0 & (\boldsymbol{K_b})_{21} & 0 & (\boldsymbol{K_b})_{22} & 0 & (\boldsymbol{K_b})_{23} \\ (\boldsymbol{K_i})_{12} & 0 & (\boldsymbol{K_i})_{12} & 0 & (\boldsymbol{K_i})_{33} & 0 \\ 0 & (\boldsymbol{K_b})_{31} & 0 & (\boldsymbol{K_b})_{32} & 0 & (\boldsymbol{K_b})_{33} \end{bmatrix}$$

$$\boldsymbol{K}_D = \begin{bmatrix} EA(\boldsymbol{K_u})_{11} & 0 & EA(\boldsymbol{K_u})_{12} \\ 0 & EI \cdot (\boldsymbol{K_n})_{11} & 0 \\ EA \cdot (\boldsymbol{K_u})_{21} & 0 & EA(\boldsymbol{K_u})_{22} \\ 0 & EI \cdot (\boldsymbol{K_n})_{21} & 0 \\ EA \cdot (\boldsymbol{K_u})_{12} & 0 & EA(\boldsymbol{K_u})_{12} \\ 0 & EI \cdot (\boldsymbol{K_n})_{31} & 0 \end{bmatrix} \cdots$$
$$\begin{bmatrix} 0 & EA \cdot (\boldsymbol{K_u})_{13} & 0 \\ EI \cdot (\boldsymbol{K_n})_{12} & 0 & EI \cdot (\boldsymbol{K_n})_{13} \\ 0 & EA \cdot (\boldsymbol{K_u})_{23} & 0 \\ EI \cdot (\boldsymbol{K_n})_{22} & 0 & EI \cdot (\boldsymbol{K_n})_{23} \\ 0 & EA \cdot (\boldsymbol{K_u})_{33} & 0 \\ EI \cdot (\boldsymbol{K_n})_{32} & 0 & EI \cdot (\boldsymbol{K_n})_{33} \end{bmatrix}$$

It is important to highlight that the previous matrix $\boldsymbol{K}_S$ and $\boldsymbol{K}_D$ must be assembled for each node belonging to the stretch under analysis to get the complete form 3.13. Equation 3.13 expresses the internal action, M_x and P, as a function of the deformation (U and $\boldsymbol{\theta}$) of the element. Considering figure 3.4 the bending moment exerted on joint J_n is a function of the vertical displacements and rotation of the orizontal stretch between J_n and J_m. To calculate the moment on joint J_n the deformation of each element on the orizontal stretch have to be accounted for. Then assembling matrixes $\boldsymbol{K}_S$ and $\boldsymbol{K}_D$ and recalling equation 3.12 only joint rotations, $\theta_{J_n}$and θ_{J_m}, give rise to a contribution different from zero. The resulting matrix equation reads (here the matrix $\boldsymbol{K}_S$ and $\boldsymbol{K}_D$ resutlt from the assembling performed on the element of the stretch from J_n to J_m):

$$\boldsymbol{s}_L = -\boldsymbol{K}_S^{-1} \cdot (\boldsymbol{K}_D \cdot T \cdot U_G + G \cdot \boldsymbol{Q}_{\boldsymbol{\theta}}) \tag{3.14}$$

in which the global compoments of the displacements have been used. From relation3.14 the row correspong to the moments acting on the joints of the

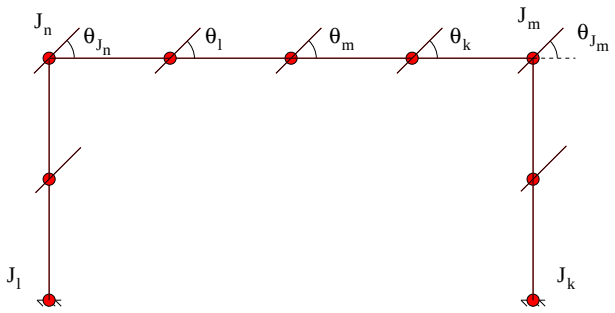

Figure 3.4: Example sketch of a frame structure

structure has to be cut off (for the sake of semplicity the subscript "L", referring to the local component, has been dropped and substituted by the vector component number and by the label of the joint which the moment acts on and the stretch which belongs to) :

$$\begin{aligned}(\boldsymbol{s}_{J_m})_s &= -(\boldsymbol{K}_S)^{-1}_{2j}\cdot(\boldsymbol{K}_D)_{jm}T_{ml}\cdot(U_G)_l-(\boldsymbol{K}_S)^{-1}_{22}\cdot(\boldsymbol{Q_\theta})_1+(\boldsymbol{K}_S)^{-1}_{2k}\cdot(\boldsymbol{Q_\theta})_2\\ (\boldsymbol{s}_{J_m})_s &= -(\boldsymbol{K}_S)^{-1}_{kj}\cdot(\boldsymbol{K}_D)_{jm}T_{ml}\cdot(U_G)_l-(\boldsymbol{K}_S)^{-1}_{k2}\cdot(\boldsymbol{Q_\theta})_1+(\boldsymbol{K}_S)^{-1}_{kk}\cdot(\boldsymbol{Q_\theta})_2\\ & j,m,l=1,2,.....k \end{aligned} \tag{3.15}$$

in which k is the number of the nodes in the stretch "s". On the right end of the element the internal positive bending moment laied in the negative side of global reference system, for this reason the second equation have to be multiplyed by -1:

$$\begin{aligned}(\boldsymbol{s}_{J_m})_s &= -(\boldsymbol{K}_S)^{-1}_{2j}\cdot(\boldsymbol{K}_D)_{jm}T_{ml}\cdot(U_G)_l-(\boldsymbol{K}_S)^{-1}_{22}\cdot(\boldsymbol{Q_\theta})_1+(\boldsymbol{K}_S)^{-1}_{2k}\cdot(\boldsymbol{Q_\theta})_2\\ (\boldsymbol{s}_{J_m})_s &= +(\boldsymbol{K}_S)^{-1}_{kj}\cdot(\boldsymbol{K}_D)_{jm}T_{ml}\cdot(U_G)_l+(\boldsymbol{K}_S)^{-1}_{k2}\cdot(\boldsymbol{Q_\theta})_1-(\boldsymbol{K}_S)^{-1}_{kk}\cdot(\boldsymbol{Q_\theta})_2\end{aligned}$$

Getting equation 3.15 for each stretch that converge to the joint it is possible to write down the rotational equilibrium condition (referring is made to the example figure 3.4):

$$(\boldsymbol{s}_{J_n})_1+(\boldsymbol{s}_{J_n})_2 = 0 \tag{3.16}$$

Adding, for each "joint", the equilibrium equation 3.16 to the system of equations 3.11 the solution of the structural problem can be obtained using the usual methods for inversion of the system of algeabric equations. When the displacements and joint rotations of the structure has been obtained the moment should be calculated using the first equation of the system 3.15.

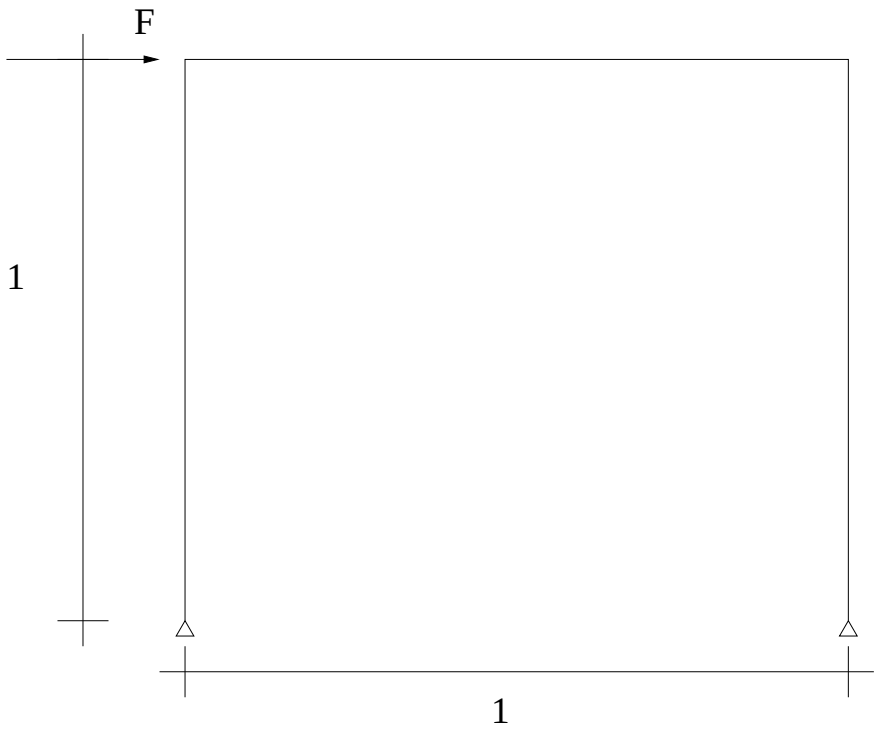

Figure 3.5: Sketch of the Frame geometry

3.3 Numerical Example

The MBEM (Mixed Beam Element Method) has been tested versus the standard Finite Element Methods using its implementation in the general purpose package ANSYS. A simple frame geometry has been used with unitary dimension as represented in figure 3.5, with a suddenly applied unitary force at time $t = 0$. The frame characteristics are listed in table 3.1. The element size used was $\Delta h = 0.3333$ with a total of 10 node for both model and 3 element for the MBEM and 9 for the ANSYS model. The results are reported, in

E	$4.6 \cdot 10^9$
ρ	$1.6 \cdot 10^3$
b	0.1
h	$.7 \cdot 10^{-2}$

Table 3.1: Mechanical and geometric characteristic of the cross section of the frame

figure 3.6, in terms of horizontal displacements and bending moments of the upper left node. Both figure show how the MBEM gets better results above all in term of bending moment that for the ANSYS model is discontinuos at the node, two values have to be reported.

The dynamic displacements oscillates about the value results from the statical application of the load. Such value is 0.019015 the average value of the dynamic analysis is 0.018998 with a percent error of 0.09% for the MBEM while for the ANSYS model the average value is 0.018635 with a percent error of 1.998%. This kind of result is more stressed for the bending moment which, in the ANSYS model, is discontinuos while in the MBEM is continuos and with an error of 0.773% on the average value.

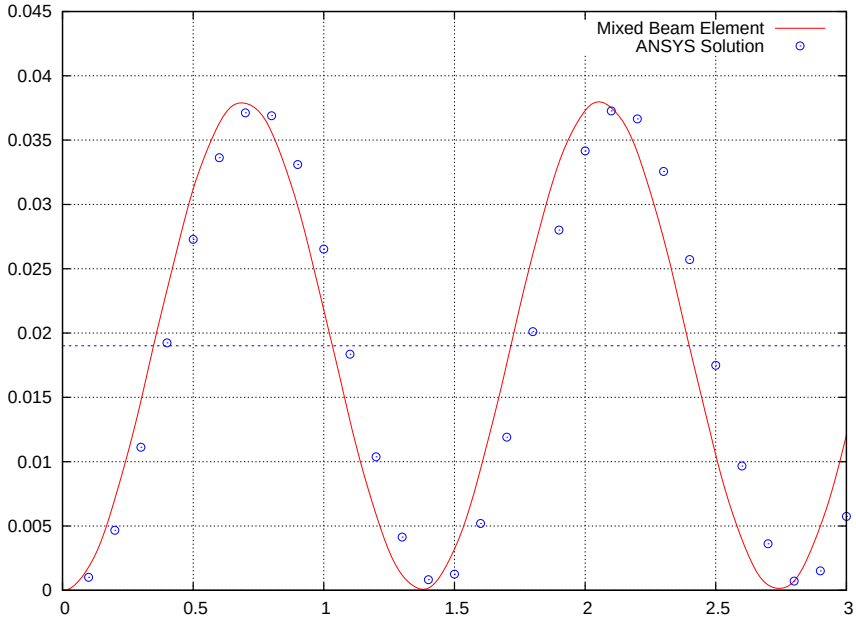

(a) Displacement

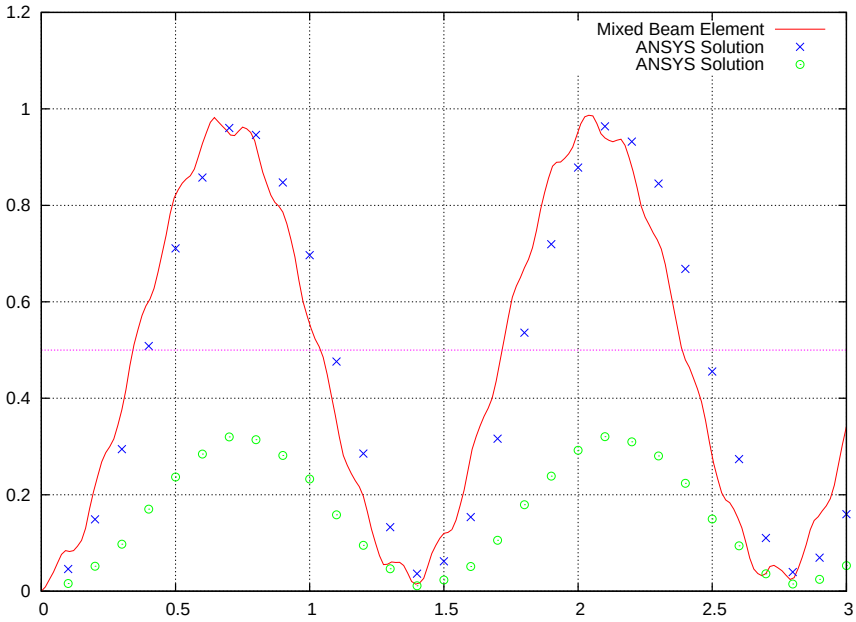

(b) Bending Moment

Figure 3.6: Time history of the ANSYS and Mixed-FE model solutions at the upper-left node

Bibliography

[Auricchio 1994] F. Auricchio, R.L. Taylor, "A shear deformable plate element with an exact thin limit", Computer Methods in Applied Mechanics and Engineering, vol 118,pg 393-412, 1994

[Kwon 1997] Y. W. Kwon, H. Bang, "The Finite Element Method using Matlab", CRC Press 1997

[Paz 1985] M. Paz, "Structural Dynamics Theory & Computation", Van Nostrand Reinhold New York, 1985

[Landau 1979] L. D. Landau, E. M. Lifsits, "Fisica teorica/teoria dell'elasticità", Editori Riuniti, Roma 1979

[Hilber 1976] Hans M. Hilber, "Analysis and design of numerical integration method in structural dynamics", College of engineering University of California, Report No. EErc 76-29 November 1976

Part II

The Experimental Data Post-Processing

Chapter 4

Laboratory Test Normal Surface Displacement Determination

4.1 Introduction

To fully test the algorithm for the defect detection it is necessary to have use beam/shell with different position and size of defects. Usually this goal is get laying teflon made spot in the resin region of the layered structure. This kind of arrangement is not able to represent the different level of discontinuity usually present in layered structures.

On the contrary it is very difficult to realize controlled delamination defect in laboratory experiments, moreover considering the fact that to fully test the post-processing method different length and depth position of the defect have to be realized.

To overtake these problems a *virtual laboratory* is realized that has been validated with experimental data gathered from aluminum-resin layered beams. After the validation process the virtual laboratory has been used to supply the data over which the post-processing model has been run considering different length and depth of the defects.

4.2 Sample building

Aluminum bars sized 15mm x 2mm and 192mm length are used. In order to build a composite structure two bars are glued by epossydic resin E227 that is the standard glue for these applications. The micro-spheres were added to increase the density and to avoid air bubbles inside the resin. Two samples were built. The samples were made like a sandwich, that means the resin between two bars was continuous. The epossydic resin was left stand for 48

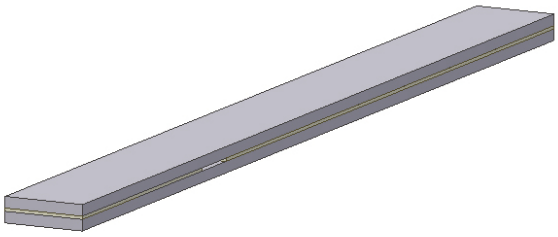

Figure 4.1: Sample Bar

hours at room temperature.

The thickness of resin was measured in order to have this parameter for the numerical model. Its constant thickness was not guaranteed, because the resin was spread by hand. The direct measurement was not possible, so the bar thickness was subtracted from the total one.

In this way the measurement uncertainty is compound by the error on the sandwich thickness measurement and the bar thickness measurement. In Figure 4.2, thickness measurement points are shown. Several points were chosen along the symmetric axe and along the edges (higher and lower) in order to have not only the resin thickness each 10mm, but also to check the flatness errors. The longitudinal sections of resin was computed and shown in Figure 4.3.

It is possible to note, the outlines of curves are not regular, but that was expected as aforementioned, because the resin was handily spread. In the contrary, the flatness error was negligible. So it is possible to conclude the resin thickness is variable along the longitudinal section and constant along the cross section (average variation is less than 0.01mm, that means 0.067% of the whole resin thickness). This is a great result, because it means the numerical model can be studied in 2D. Considering the longitudinal measurements, the maximum error is 10% for sample 1 and lower for the other sample. That means, if this value is taking in account it is possible to model the resin thickness like constant. So the mean thickness were computed as following:

- 0.41 mm for sample 1;

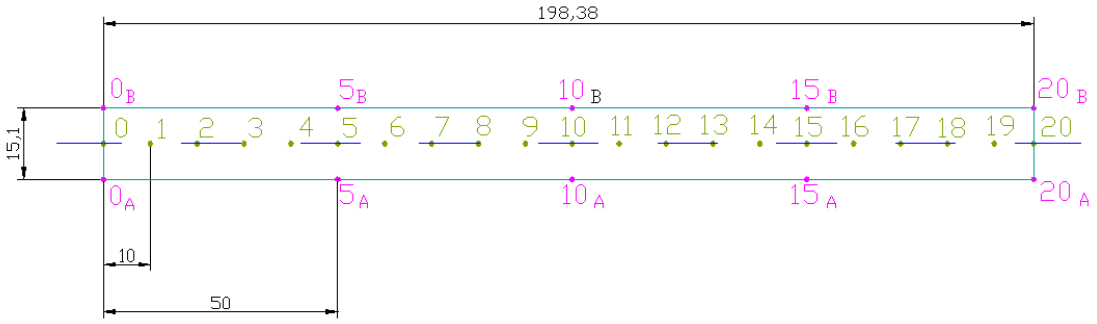

(a) Measurement thickness points

Figure 4.2:

- 0.43 mm for sample 2.

4.3 measurement chain

Measurement chain was composed by the equipments shown in Figure 7 and they are: instrumented hammer (named "woodpecker") with supplier that permits to repeat automatically the impulses; load cell amplifier; Scanning Laser Doppler Vibrometer (SLDV); computer; test rig. Samples were laid on the foam rubber that permits to consider the sample in free-free constraint system (as well demonstrate in the next section) The load cell (on the hammer head) output signal, through the amplificatory arrives in the channel A of the controller and it is used for many tasks:

- reference signal to get the input load condition for FEM validation and to compute the FRF;
- trigger for scanning;
- to know the real instant of force applied on the sample.

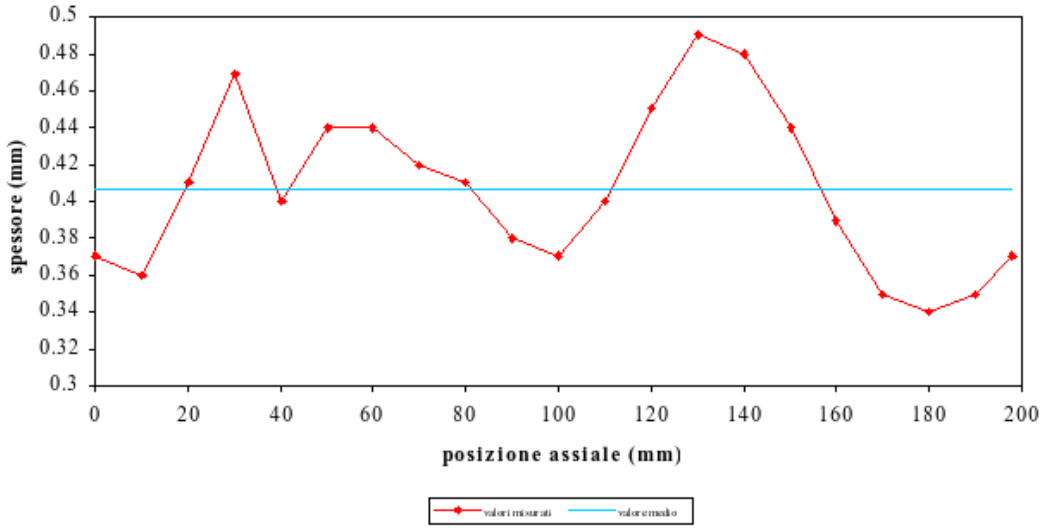

(a) Bar 1

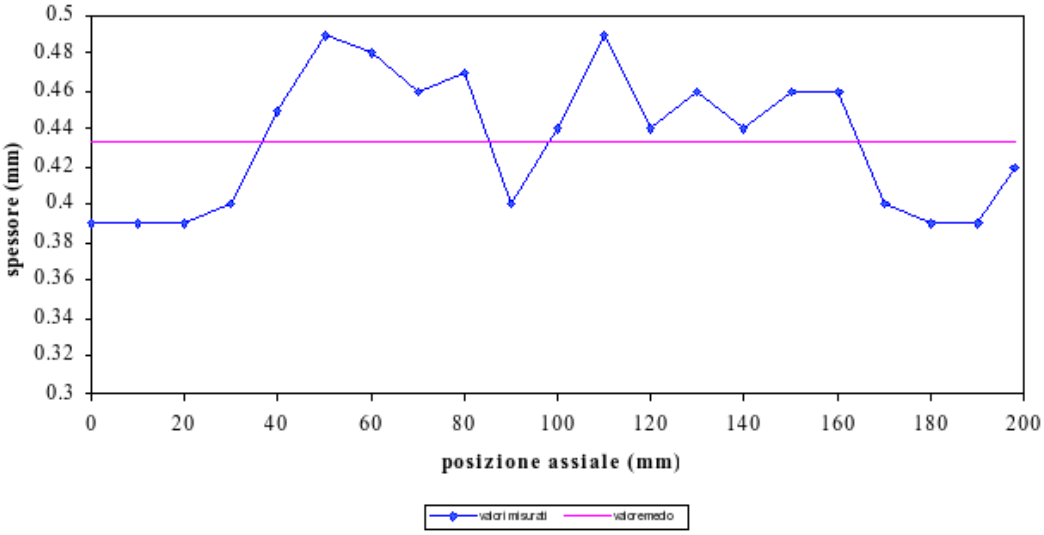

(b) Bar 2

Figure 4.3: Resin thickness of sample bar

Figure 4.4: measurement chain

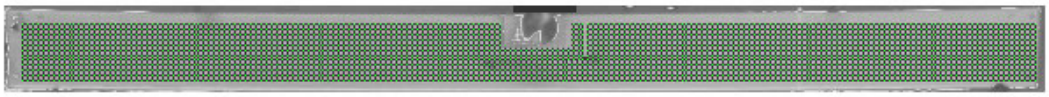

Figure 4.5: Measurement grid

The out of plane speed of the surface it is measured by the SLDV. The pick-up grid is showed in figure 4.5

The input force is applied in the middle of the sample and an area greater than that of the hammer is subtracted from the grid to avoid to pick up the hammer movement.

Chapter 5

The Finite Element Model

5.1 Introduction

A full 2D model using solid elements for the ply and contact element for the delamination has been used. For the contact simulation two different elements has been chosen the surface-to-point and the point-to-point.

5.2 The Elements

The Finite Element Model has been realized using the general purpose Finite Element code ANSYS. The beam has been considered under a plane stress state in the $x - y$ coordinate plane. for this reason the ANSYS element PLANE42, a four node isoparametric Finite Element (see figure 5.1), has been used. The delamination surface has been modeled using the contact surface element CONTAC48 that can describe a general contact between a set of points and a surface (see figure 5.2). The shear and normal interaction, between the two surface of the delamination, has been modeled using spring elements featuring multi-linear force-displacement curve like the one reported in figure 5.3. The mesh has been obtained using an element size equal to $2.0 \cdot 10^{-3} m$, the mesh is showed in figure 5.4.

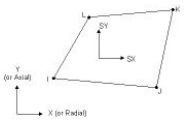

Figure 5.1: Four node isoparametric plane stress element sketch

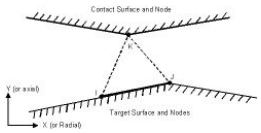

Figure 5.2: Contact surface element sketch

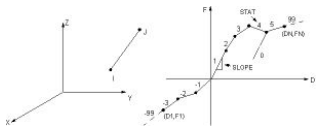

Figure 5.3: Multi-linear spring element

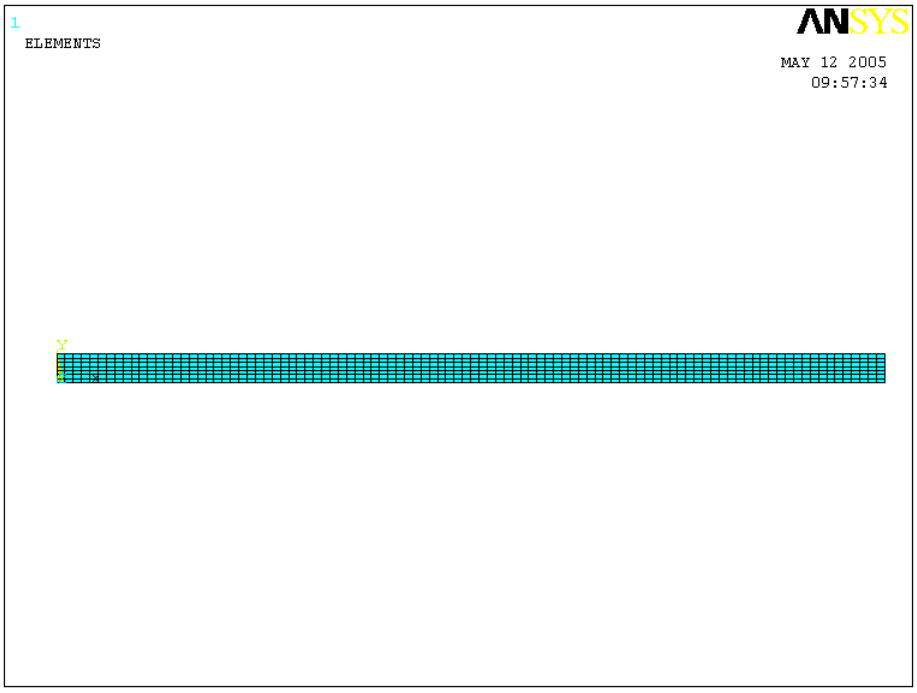

Figure 5.4: Mesh of the FE model

5.3 Typical analysis results

To test the model some runs has been performed by imposing displacements close to the right end of the beam. The input function is a monocromatic signal. Two different cases have been considereds with $1.0 \cdot 10^3 Hz$ and $1.0 \cdot 10^4 Hz$ frequency exitation. Two samples of the resulting stress fields are reported in figure 5.5. The results show very well how the defect perturb the well known beam stress field resulting in a different cross section stiffness that acts inducing a discontinuity in the displacement distribution on the surface.

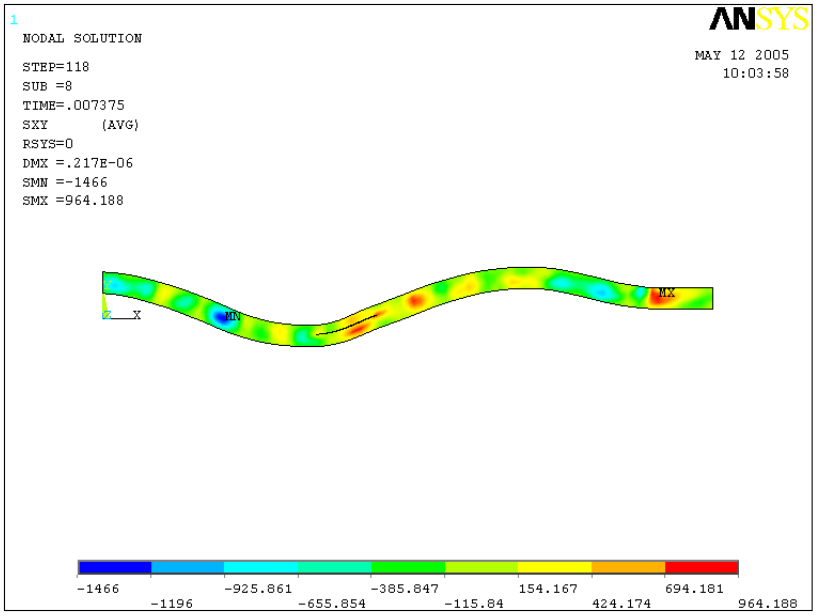

(a) case (a)

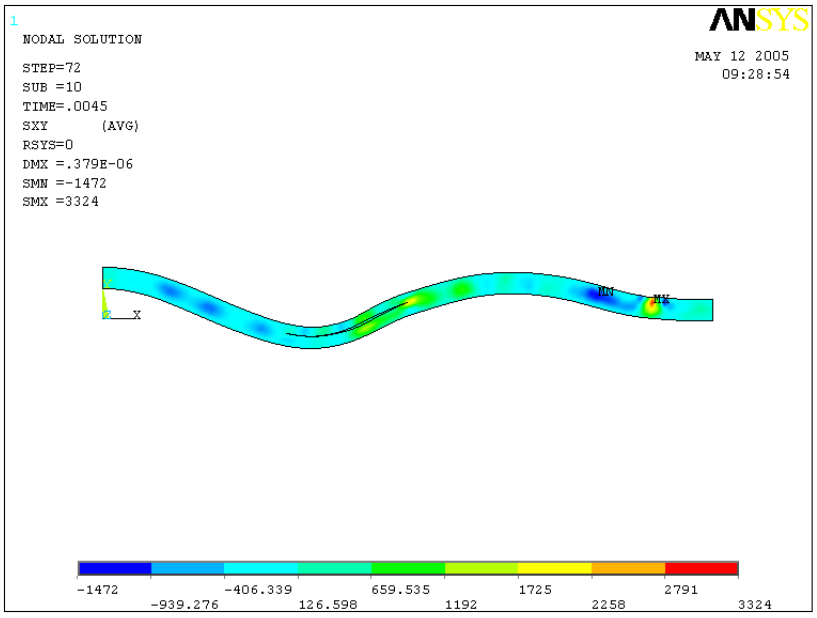

(b) case (b)

Figure 5.5: τ_{xy} stress field for defect depth of $4.0 \cdot 10^{-3}$ and defect length $2.0 \cdot 10^{-2}$(a) and $4.0 \cdot 10^{-2}$(b)

Chapter 6

Experimental vs Virtual Laboratory results

To test the performances of the virtual laboratory the results gathered from the Polytec devices has been compared with the ones obtained from the numerical simulation.

6.1 The Input Force

To reproduce the input signal of the laboratory experiments as close as possible a rectangular PSD with the same overall energy of the input signal has been used in the FEM simulation.

The time history was obtained reconstructing the signal from the rectangular PSD and from the hypothesis of a random equi-distribution of the phase using the following formula:

$$F(t) = \sum_{j=1}^{N} \sqrt{4S_0(\omega_j)}\Delta\omega \cdot cos(\omega_j \cdot t - \theta_j)$$

in which:

$S_0(\omega_j)$ is constant and equal to the height of the rectangle

$\Delta\omega$ is the step in the frequency domain of the PSD data

θ_j is the phase

S_0 has been calculated imposing the same area for the measured PSD data and the rectangular PSD with the upper limit at $5 \cdot 10^3 Hz$.

$k_0 \cdot L$	0.0
$k_1 \cdot L$	4.730
$k_2 \cdot L$	7.853
$k_3 \cdot L$	10.996
$k_4 \cdot L$	14.137
$k_5 \cdot L$	17.279

Table 6.1: Boundary condition coefficient for eigenfrequencies calculation

6.2 Experimental results

A first level of characterization was done comparing the modal frequencies obtained by using the FRF of the output, the structural dynamics theoretical value and the ANSYS FEM model. A second, more accurate comparison was done inputting to the FEM model the force deduced by the procedure described in section 6.1 and comparing the FFT of the measured velocities with the FEM ones.

6.2.1 Eigen-frequencies comparison

The theoretical beam model frequencies result from the following relation:

$$f_i = \frac{k_i^2 \cdot L^2}{2\pi} \sqrt{\frac{EI}{\rho A L^4}} \tag{6.1}$$

in which k_i is a coefficient accounting for the different boundary conditions of the beam. In the present case of a free-free beam the values can be deduced from table 6.1 from [Paz 1985]. The second order moment and the area of the section are calculated using the relation:

$$I = 2 \cdot b \cdot \left(\frac{1}{12} h_a^3 + h_a \cdot \frac{(h_a + h_r)^2}{4} \right) + \frac{1}{12} \cdot \frac{E_r}{E_a} h_r^3$$

$$\rho A = \rho_a b \cdot h_a + \rho_r b \cdot h_r$$

in which:

$E_a = 7 \cdot 10^{10}$ Aluminum Young Modulus

$\rho_a = 2744$ Aluminum density

Mode	Theoretical	FEM	Experimental
1	585.28	585.35	575
2	1613.4	1602.3	1550
3	3162.8	3108.8	2981

Table 6.2: Comparison between theoretical, experimental and FEM eigen-frequencies (Hz) for beam 1

Mode	Theoretical	FEM	Experimental
1	590.08	588.34	587.5
2	1626.6	1610.1	1600
3	3188.8	3122.9	3075

Table 6.3: Comparison between theoretical, experimental and FEM eigen-frequencies (Hz) for beam 2

$E_r = 8 \cdot 10^9$ Resin Young Modulus

$\rho_r = 1860$ Resin density

$h_a = 2 \cdot 10^{-3}$ Aluminum layer height

$h_r = 4 \cdot 10^{-4}$ Resin layer height

Using the above values the first three eigen-frequencies are listed in table 6.2 for the beam number 1 and in table 6.3 for the beam number 2. The experimental data are gathered from the peaks Frequency Response Function of the Polytec instrument.

It is possible to draw the conclusion of a neat convergence between the different models. The ability of the full 2D beam FEM model, to simulate the second order effects of the beam section deformation (release of the Euler-Bernoulli hypothesis). accounts for the little differences in the eigen-frequencies and for the lower stiffness of the FEM and Experimental system. A very good level of agreement can be found between the theoretical (both beam theory and FEM model) and the experimental one, in fact the higher values of inaccuracy is 4.1% for the third frequency of the beam 1.

6.2.2 Frequency Response to Impulsive Input

A second more complete comparison has been done performing simulations, using the FEM model, that should reproduce the laboratory vibrations of the

Node	x coordinate (m)
13	0.013
52	0.052
99	0.099
137	0.137
175	0.175

Table 6.4: Nodes position for FFT comparison

beam 1 and 2. The input has been reproduced using the algorithm described in section 6.1. The results have been compared in terms of z-direction velocity at 5 different points along the axis of the beam. The velocity output of the FEM simulation has been compared with the velocities measured with the SLDV instrumentation in terms of the FFT of the velocities in the "z" direction. The results are showed in figures 6.1, 6.2, 6.3, 6.4 and 6.5. The position of the nodes is reported in table 6.4. All figures show a good agreement between experimental and FEM data both in term of frequencies and amplitude.

The FEM model is able to reproduce the beam behaviour at low and high frequencies showing the effects of the two symmetrical eigen-modes (the first and the third) and the effect of the free constraint for the frequency that tend to zero.

The same agreement can be showed in term of amplitude where there is an acceptable convergence in the FEM results to the experimental one. The relative amplitude of the third mode to the first one of the experimental data respect to the numerical ones is due to the constant Power Spectral Density of the input force used in the numerical analysis and to the inaccuracy of the hammer position.

These results allow to state that it is possible to use the FEM model to reproduce experimental surface measurement for test the post-processing unbalanced force method.

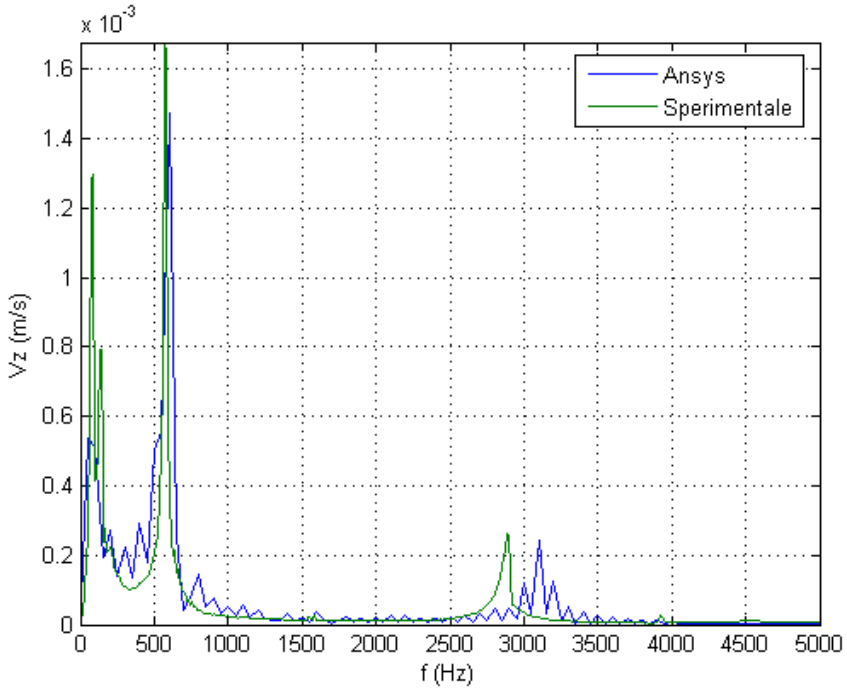

(a) Beam 1

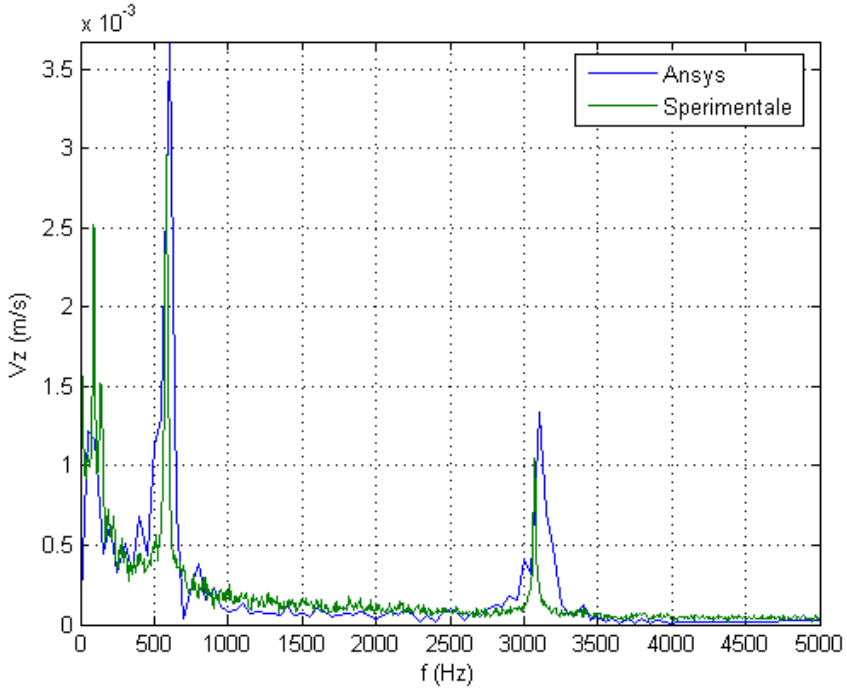

(b) Beam 2

Figure 6.1: Comparison for FEM and Experimental FFT of the z Velocity of node 13

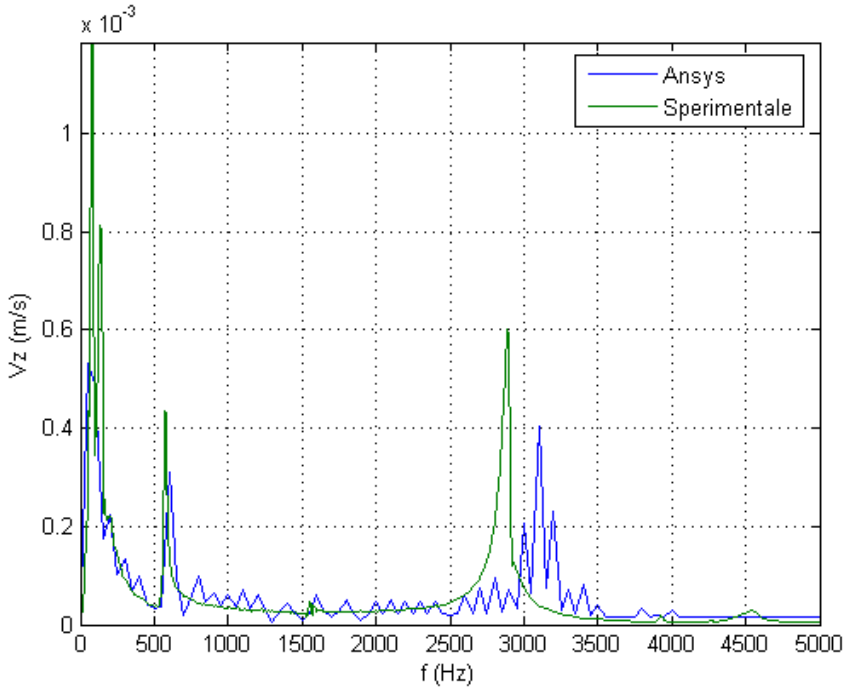

(a) Beam 1

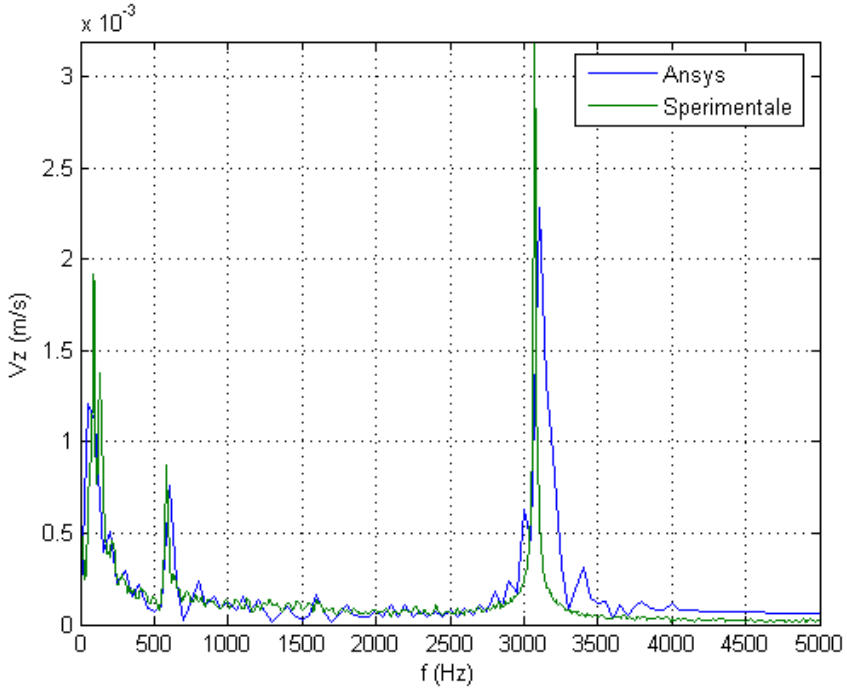

(b) Beam 2

Figure 6.2: Comparison for FEM and Experimental FFT of the z Velocity for node 52

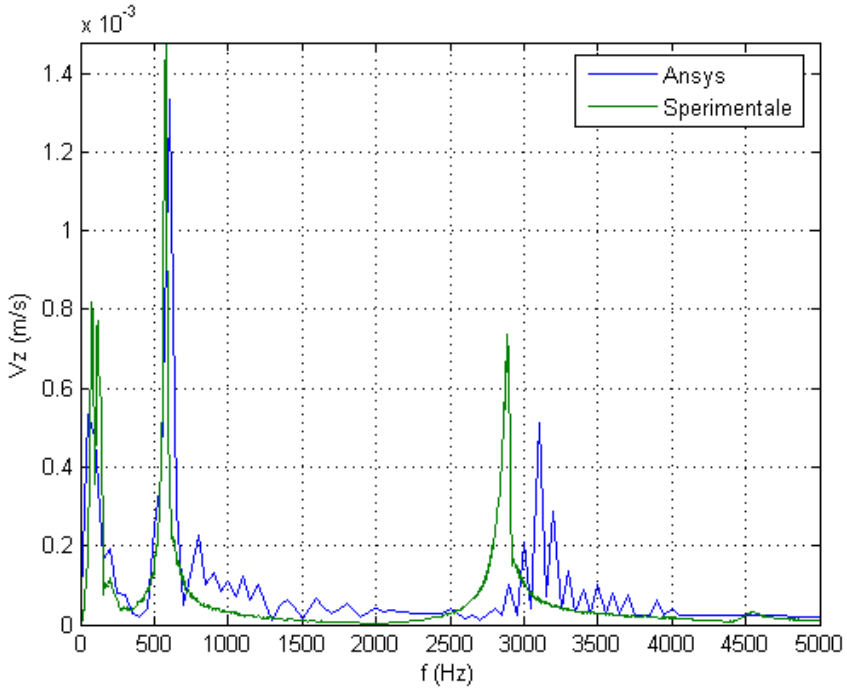

(a) Beam 1

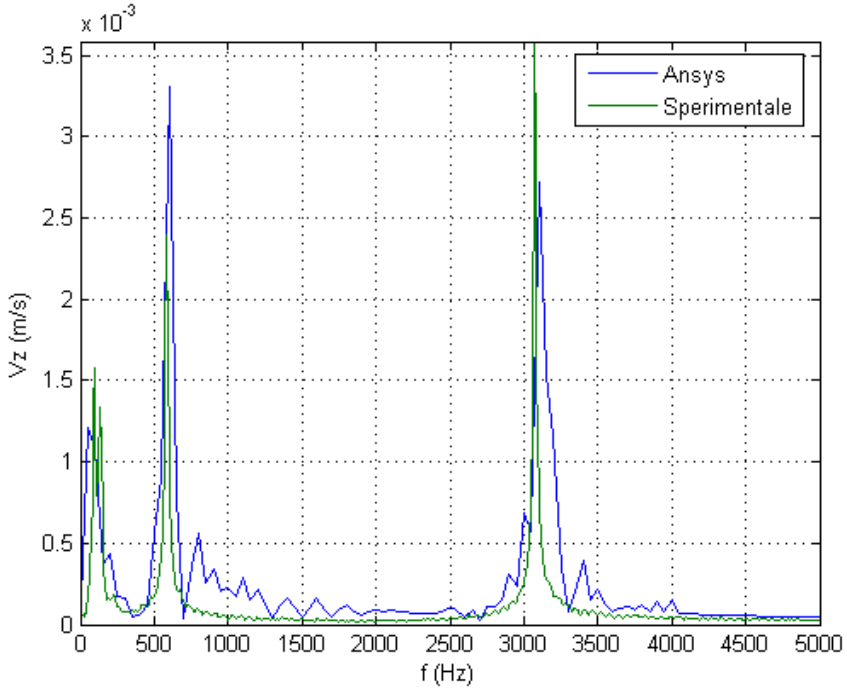

(b) Beam 2

Figure 6.3: Comparison for FEM and Experimental FFT of the z Velocity for node 99

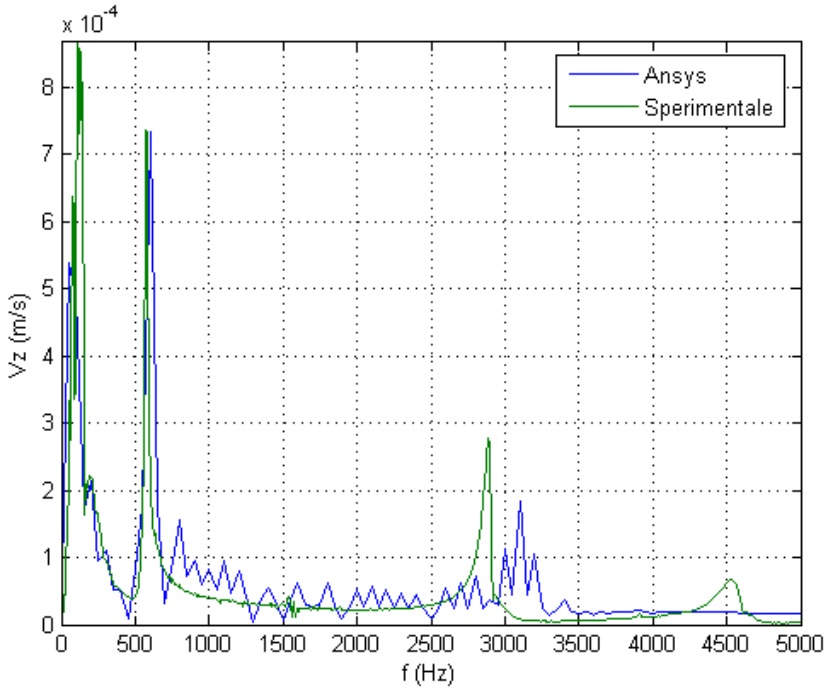

(a) Beam 1

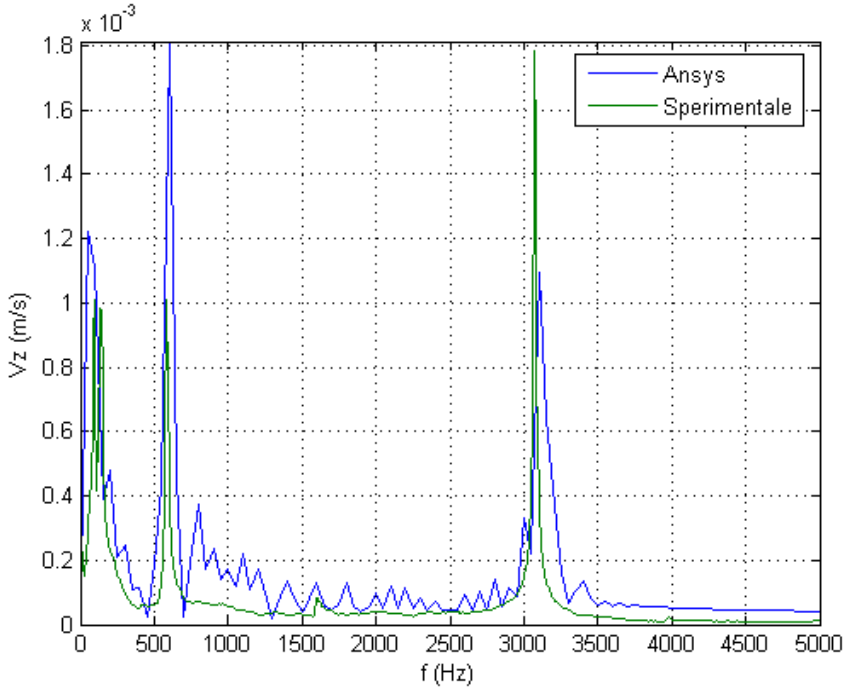

(b) Beam 2

Figure 6.4: Comparison for FEM and Experimental FFT of the z Velocity for node 137

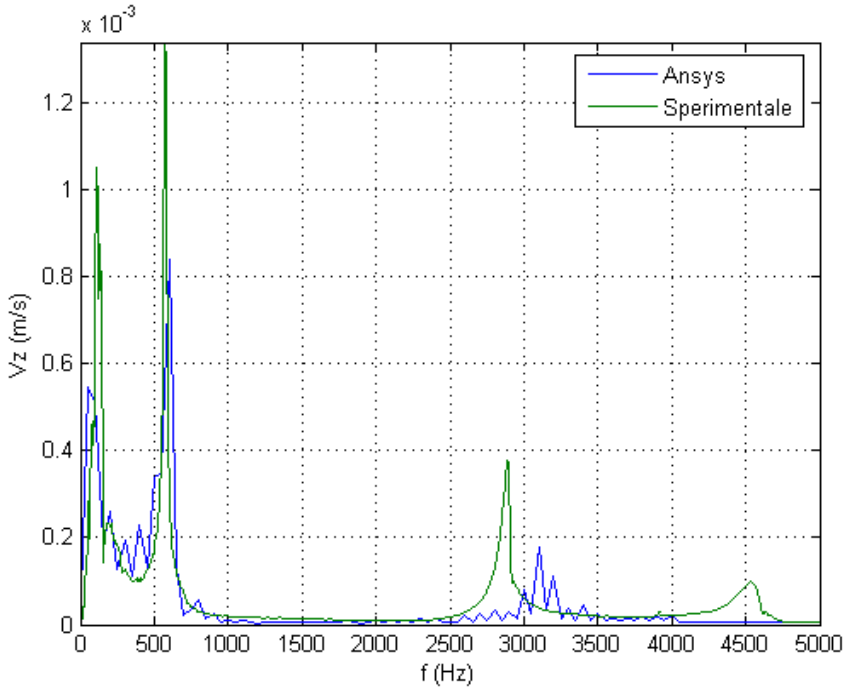

(a) Beam 1

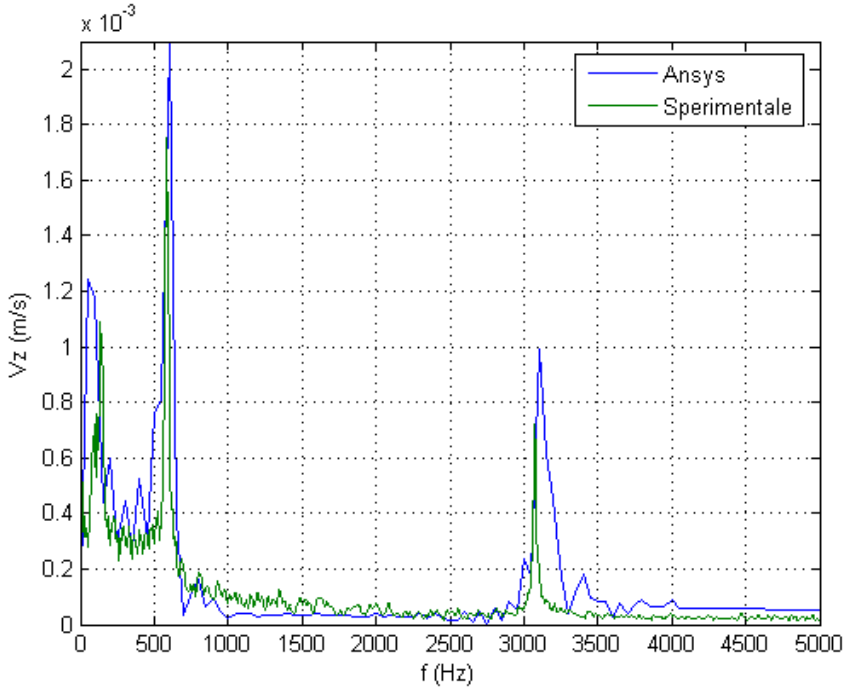

(b) Beam 2

Figure 6.5: Comparison for FEM and Experimental FFT of the z Velocity for node 137

Bibliography

[Paz 1985] M. Paz, "Structural Dynamics Theory & Computation", Van Nostrand Reinhold New York, 1985

Chapter 7

Unbalanced Force Mapping Method

In the previous chapters various levels of accuracy have been presented in the description of stiffness for beams and plates and how the differences in the mathematical modeling lead to different level of error between the physical processes and the numerical approximation. This kind of difference could be used to post-processing the experimental results to connect the difference in the responses of different areas, of the structure under testing, to different characteristics of the areas. In a more straightforward manner the difference between a particular mathematical model displacement output and the experimental results could say how much and where the stiffness, assumed by the model, is actually distributed in the physical system.

7.1 Unbalanced Force Mapping Method (UF2M)

The Unbalanced Force Mapping Method (called hereon UF2M) uses the difference between the surface traction distribution, determined post-processing the experimentally measured displacements and the actual traction distribution on the sample surface to asses where the stiffness of the structure move aside from its average.

To accomplish the previous task the theory, developed in the previous chapter, has been used. For simplicity purpose but without lacking in generality it has been applied to beam layered structure. The governing equations using the mixed approach reads:

$$\begin{cases} \frac{M_x}{E} - \frac{1}{\mu G}\frac{\partial^2 M_x}{\partial x^2} + \frac{\partial^2 w}{\partial x^2} = 0 \\ \frac{\partial^2 M_x}{\partial x^2} + q(x) - A_c \frac{\partial^2 w}{\partial t^2} = 0 \end{cases} \tag{7.1}$$

in which:

w is the transverse beam displacement in the z direction

M_x is the bending moment in the $x-z$ plane

$q(x)$ is the applied external load per unit length

A_c is the mass per unit length of the beam

Considering that the test for the defect detection shall be performed under dynamic condition and with the analyzed area free from external force the previous equation should modified as follow:

$$\begin{cases} \frac{M_x}{E} - \frac{1}{\mu G}\frac{\partial^2 M_x}{\partial x^2} + \frac{\partial^2 w}{\partial x^2} = 0 \\ \frac{\partial^2 M_x}{\partial x^2} - A_c \frac{\partial^2 w}{\partial t^2} = 0 \end{cases} \tag{7.2}$$

Under the hypothesis that the specimen follows the Timoshenko Beam Theory it is possible to assert:

> *introducing into equation 7.2 the displacement gathered from the Laser Doppler Velocimetry measurement as the vector w the right hand term shall result in a zero vector (but experimental uncertainty); if, for any reason, the right hand term will be different from zero it means that in the area in which that happens is present an anomaly in the specimen.*

Here *zero vector* means values inside the *experimental uncertainty* assumed even spatially distribuited on the structure. Due to the fact that the presence of delamination defects will result in a variation of the beam middle surface curvature the errors introduced by the numerical differentiation in equations 7.2 could be of the same order of magnitude of the right hand values unbalanced force. A weighting procedure similar to the one used for the Mixed Finite Element formulation will help to keep the differentiation error low. The resulting system of equations reads:

$$\begin{cases} \frac{M_i}{EI}\int_0^L N_i \Phi_j dx + \frac{M_i}{\mu G}\int_0^L \frac{\partial N_i}{\partial x}\frac{\partial \Phi_j}{\partial x} dx - \hat{w}_i \int_0^L \frac{\partial N_i}{\partial x}\frac{\partial \Phi_j}{\partial x} dx + \\ \qquad + b_\theta(t)\Phi_j\big|_0 = U_j(t) \\ -M_i \int_0^L \frac{\partial N_i}{\partial x}\frac{\partial \Phi_j}{\partial x} dx - \frac{d^2\hat{w}_i}{dt^2}\int_0^L A_c N_i \Phi_j dx + \\ \qquad + b_v(t)\Phi_j\big|^L = U_j(t) \end{cases} \tag{7.3}$$

in which:

$\hat{w}_i$ displacement measured at grid point i

$U_i(t)$ unbalanced force at grid point i

Φ_j $j-th$ weighing function

the experimental data are supplied in the frequency domain so the previous equation will transformed as follow:

$$\begin{cases} \frac{M_i}{EI}\int_0^L N_i\Phi_j dx + \frac{M_i}{\mu G}\int_0^L \frac{\partial N_i}{\partial x}\frac{\partial \Phi_j}{\partial x}dx - \bar{w}_i(\omega)\int_0^L \frac{\partial N_i}{\partial x}\frac{\partial \Phi_j}{\partial x}dx + \\ + b_\theta(\omega)\Phi_j|_0 = \bar{U}_j(\omega) \\ -M_i\int_0^L \frac{\partial N_i}{\partial x}\frac{\partial \Phi_j}{\partial x}dx + \omega^2\bar{w}_i(\omega)\int_0^L A_c N_i\Phi_j dx + \\ + b_v(\omega)\Phi_j|^L = \bar{U}_j(\omega) \end{cases} \tag{7.4}$$

in which:

$\bar{w}_i(\omega)$ is the Fourier Transform of the measured displacements

$\bar{U}_j(\omega)$ is the Fourier Transform of the unbalanced forces

The weighting function Φ_j at its lowest level of approximation can be chosen equal to the shape function N_j. In this way the resulting matrix equation of 7.4 is:

$$-\boldsymbol{K}\cdot\bar{w}(\omega) + \omega^2\,\boldsymbol{M_w}\cdot\ \bar{w}(\omega)\ = \bar{U}(\omega) \tag{7.5}$$

in which:

$\bar{w}(\omega)$ is the vector of the measured displacements

$\bar{U}(\omega)$ is the vector of the unbalanced forces

Equation 7.5 is used to post-processing the experimental data to determine the potential areas in which anomalies can be present.

Chapter 8

Test of UF2M Performances

8.1 Introduction

In this chapter the Virtual Model is used to get the surface displacement measurement to test the Unbalanced Force Method. Various delamination lengths at various depths and with different forcing frequencies have been considered to asses the ability of the UF2M to detect the position and length of the anomalies in the structure.

8.2 The Virtual Laboratory

The Finite Element Model described in section 5 has been used to produce the time history of the surface displacements field. The frequency response of such field has been assumed as the experimental pick up of a surface measurement technique like the LDV. As a virtual laboratory set up a layered beam has been chosen made of 7 layer of the same material bonded together by a suitable resin. Table 8.1 contains the main geometrical and mechanical data assumed for the beam. Three different delamination lengths has been considered with two different depth respect to the measuring surface. Two

length	$2.0 \cdot 10^{-1} m$
Young modulus	$4.6 \cdot 10^{9} Pa$
density	$1.9 \cdot 10^{3} \frac{Kg}{m^3}$
single layer thickness	$1.0 \cdot 10^{-3} m$
number of layers	7

Table 8.1: Mechanical and geometrical characteristic of the layered beam

wave division	16
N^{th} acq. periods	8
S_0	$0.1 \cdot 10^{-6} m$
Piezo Size	$5.0 \cdot 10^{-3} m$
Piezo Position	$1.8 \cdot 10^{-1} m$
α	0.25
δ	0.5
ξ	0.0

Table 8.2: Acquisition and integration parameters

different monochromatic inputs has been considered for each case with the acquisition lasting for 8 period. Table 8.2 lists the more relevant parameters used in the Finite Element simulation for the production of the data used as laboratory results. The whole tests has been coded using four digit:

1^{st} is for the input frequency

2^{nd} for the number of periods of acquisition

3^{rd} for the delamination depth

4^{th} is for the delamination length

The cases performed are summarized in Table 8.3. The "Defect depth" column report the y coordinate of the plane containing the defect, so higher value is for more superficial defects. In the following the response in the measured surface displacement field and in the Unbalanced Force obtained from those measurements will be described.

8.3 The Displacements Frequency Response

As it is expected, above all at low frequencies, the measurements of the surface displacements of defected and undefected samples, show no differences that could be related to the geometric position of the defects. Such behaviour is confirmed by the results showed in figures 8.1, 8.2 and 8.3. Here the FFT has been applied to the time varying differences between the undefected case displacements and the defected ones, normalized respect to the maximum displacement measured in the undefected beam. The figures report in a 2D mapping the spatial variation along the layered beam of such

Code	Defect length	Defect depth (Depth over the bottom plane)	Load frequency
doe1823	$4.0 \cdot 10^{-2}$	$5.0 \cdot 10^{-3}$	$1.0 \cdot 10^{3}$
doe1821	$2.0 \cdot 10^{-2}$	$5.0 \cdot 10^{-3}$	$1.0 \cdot 10^{3}$
doe1822	$0.8 \cdot 10^{-2}$	$5.0 \cdot 10^{-3}$	$1.0 \cdot 10^{3}$
doe0823	$4.0 \cdot 10^{-2}$	$5.0 \cdot 10^{-3}$	$1.0 \cdot 10^{4}$
doe0821	$2.0 \cdot 10^{-2}$	$5.0 \cdot 10^{-3}$	$1.0 \cdot 10^{4}$
doe0822	$0.8 \cdot 10^{-2}$	$5.0 \cdot 10^{-3}$	$1.0 \cdot 10^{4}$
doe1833	$4.0 \cdot 10^{-2}$	$4.0 \cdot 10^{-3}$	$1.0 \cdot 10^{3}$
doe1831	$2.0 \cdot 10^{-2}$	$4.0 \cdot 10^{-3}$	$1.0 \cdot 10^{3}$
doe1832	$0.8 \cdot 10^{-2}$	$4.0 \cdot 10^{-3}$	$1.0 \cdot 10^{3}$
doe0833	$4.0 \cdot 10^{-2}$	$4.0 \cdot 10^{-3}$	$1.0 \cdot 10^{4}$
doe0831	$2.0 \cdot 10^{-2}$	$4.0 \cdot 10^{-3}$	$1.0 \cdot 10^{4}$
doe0832	$0.8 \cdot 10^{-2}$	$4.0 \cdot 10^{-3}$	$1.0 \cdot 10^{4}$

Table 8.3: Codes and relevant parameter

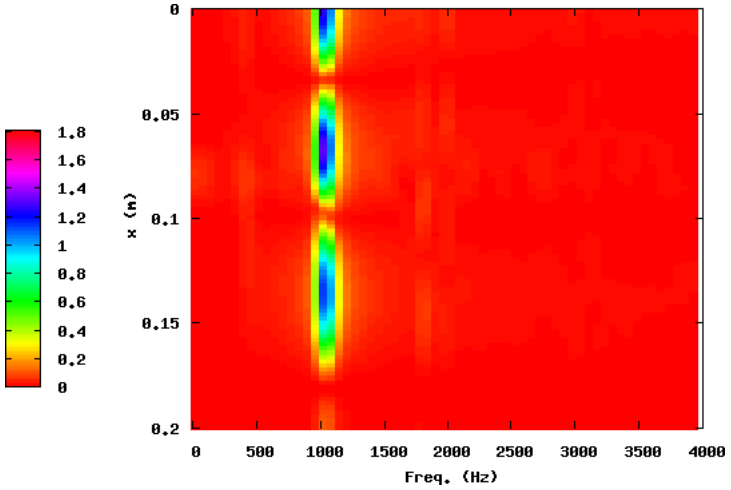

Figure 8.1: Differences (as % on the max displacement of the undefected beam) in the Frequency Response of the undefected beam and the defected ones with a defect length of $4.0 \cdot 10^{-2}$

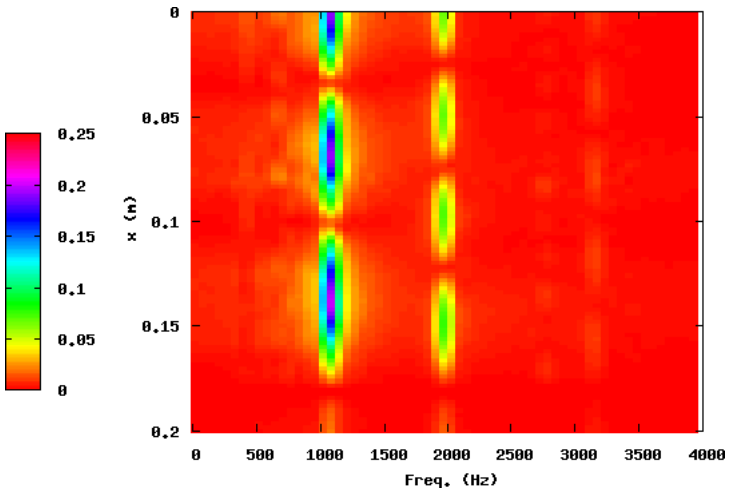

Figure 8.2: Differences (as % on the max displacement of the undefected beam) in the Frequency Response of the undefected beam and the defected ones with a defect length of $2.0 \cdot 10^{-2}$

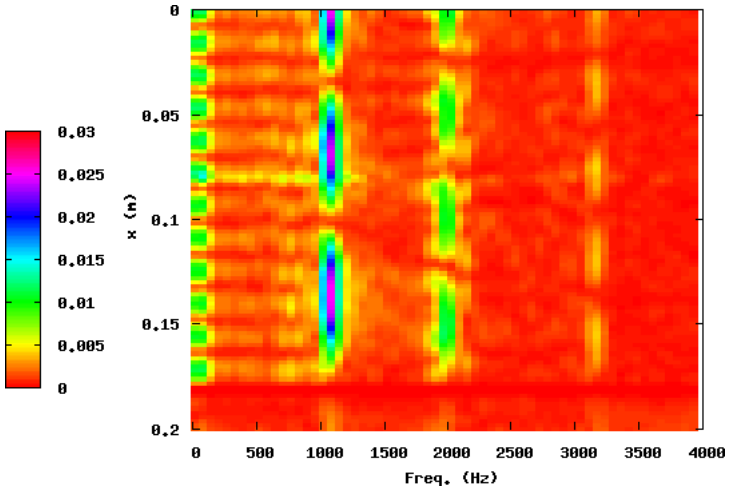

Figure 8.3: Differences (as % on the max displacement of the undefected beam) in the Frequency Response of the undefected beam and the defected ones with a defect length of $0.8 \cdot 10^{-2}$

FFT in term of percentage of the maximum displacement. The figures show a classical pattern of stationary waves with some differences in the amplitude values that cannot have any immediate correlation with the geometrical position of the defects.

8.4 The Unbalanced Force Calculation

From the surface displacement Fast Fourier Transform it is possible to calculate the Unbalanced Force (hereon UF) FFT over the beam length according to the equation of section 7.1.

The structure is excited in a localized area, as a consequence in the area other than the loaded the dynamic equilibrium equation holds stating that *"the resultant of the inertial force and the elastic force has to be zero"*. The method returns the value of the nodal force, in Newton, exceeding the dynamic equilibrium.

Introducing the frequency component amplitude of the measured displacement in the equation 7.2 it is possible to get the nodal values of the UF in term of frequencies.

If the structure has a uniform distribution of its mechanical and geometrical characteristics the UF distribution will be constant, but the area where the UF goes away from the average value the presence of a anomaly is detected. The average value of the UF takes into account for the mathematical model inaccuracy too.

In the following figure a 2D mapping of the frequency values of the UF are reported allowing to determine the position and the frequency where the UF go away from the average value. Post-processing the data the results obtained for cases doe1823 and doe0823 are showed in figure 8.4. The UF Frequency Response distribution shows very clear where the UF are different from the average and in addition, due to the large length of the defects, a peak is presents at the both ends of the delamination. The same results is present in the cases doe1821 and doe0821 where in the low frequency case there is a broader frequency distribution of the UF signal in the defected area. The same pattern is present in the cases doe1822 and doe0822, reported in figures 8.6. Here a decrease in the absolute values of the UF is present due to the small amount of the defect length. Some differencies appear in the higher excitation frequency (10000 Hz) cases. Here some conditions are present in which the method is unable to give rise to peak values that account for anomalies. These conditions appear for different frequencies and defect length. In figure 8.7 the higher frequency case and in figure 8.9 the lower frequency one give rise to no evidence of anomaly. Instead in figure 8.8 the

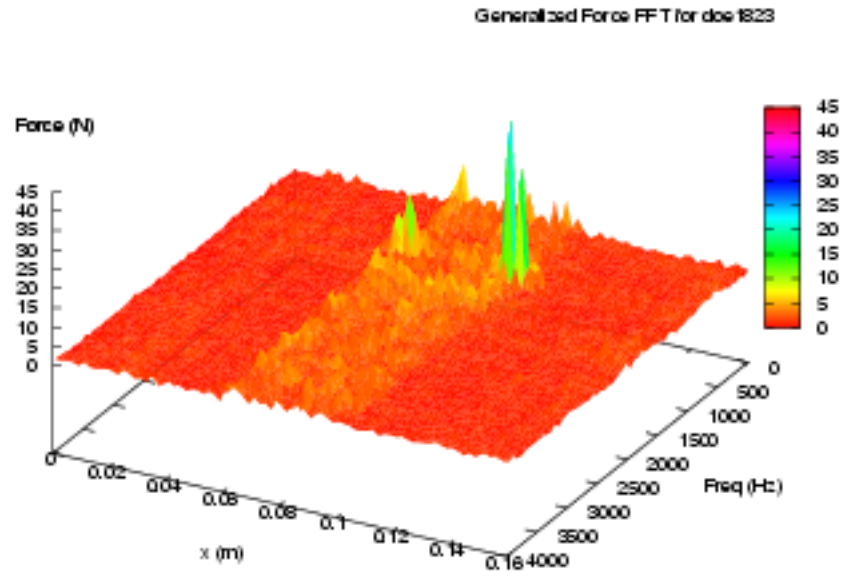

(a) 1,000 Hz forcing frequency

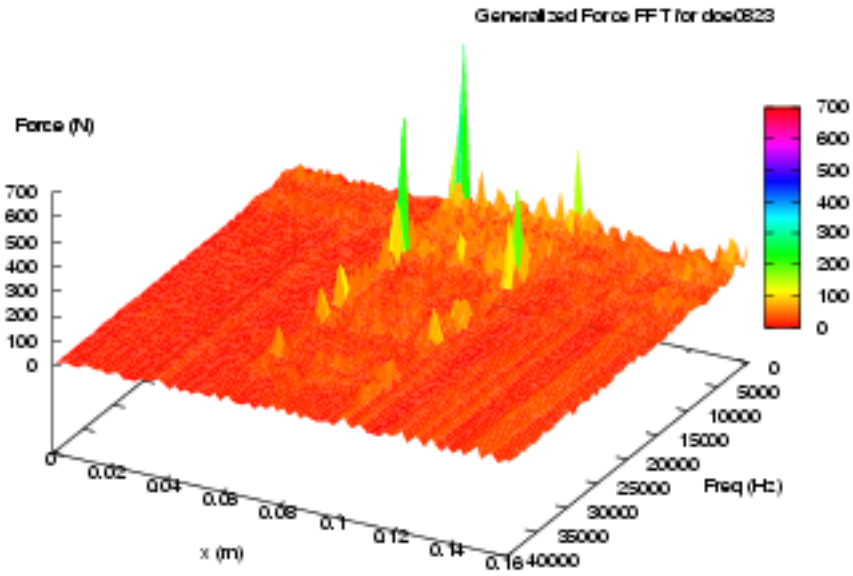

(b) 10,000 Hz forcing frequency

Figure 8.4: Frequency Spectrum for defect length of $4.0 \cdot 10^{-2}$ and depth of $5.0 \cdot 10^{-3}$

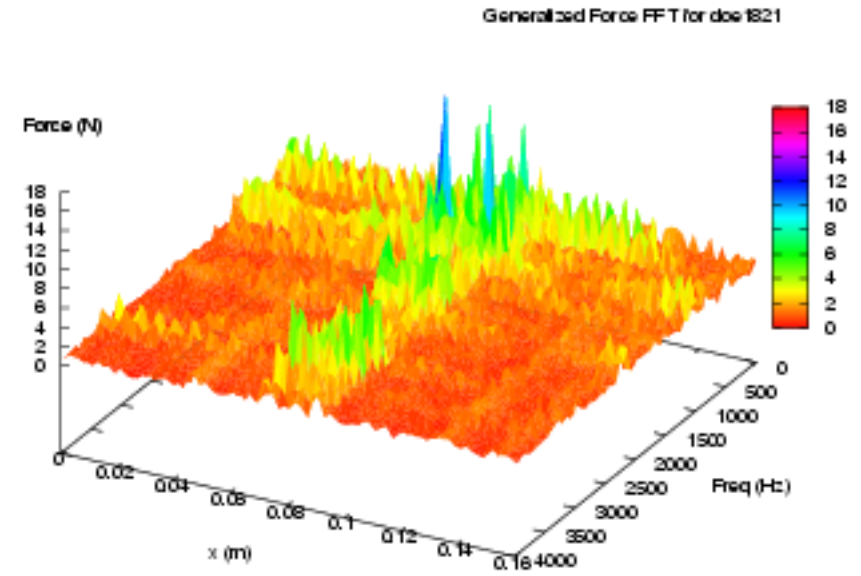

(a) 1000 Hz forcing frequency

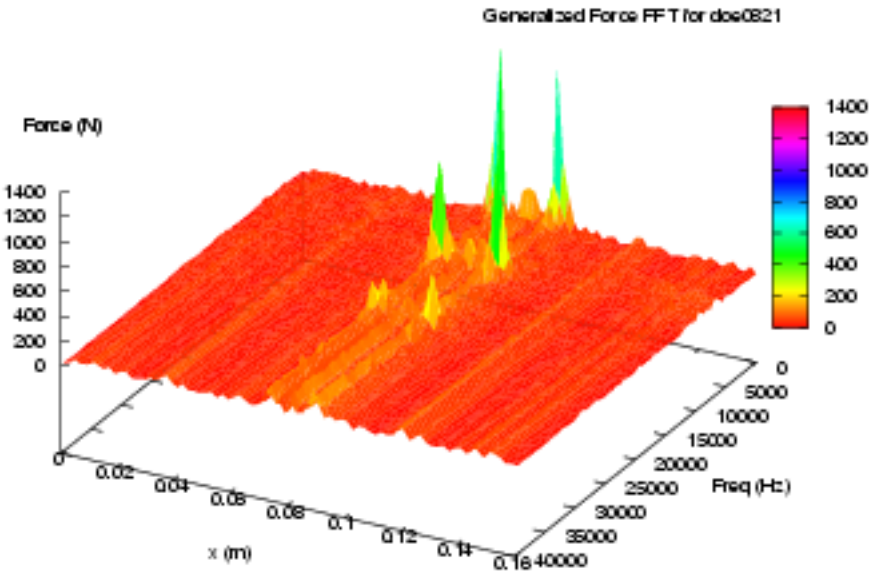

(b) 10,000 Hz forcing frequency

Figure 8.5: Frequency Spectrum for defect length of $2.0 \cdot 10^{-2}$ and depth of $5.0 \cdot 10^{-3}$

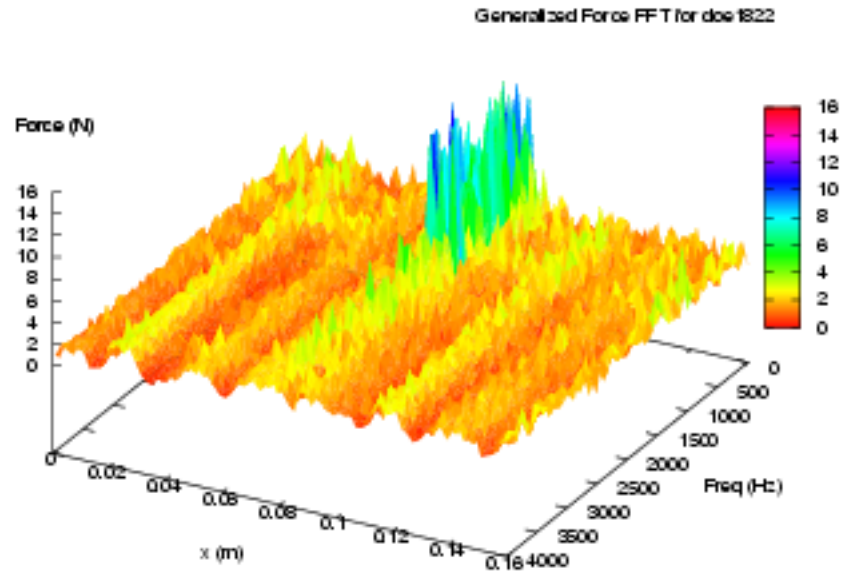

(a) 1,000 Hz forcing frequency

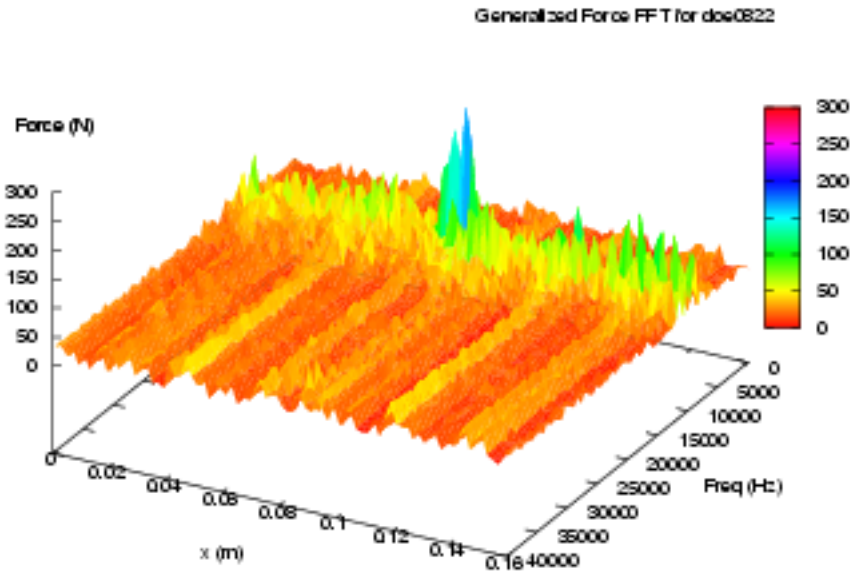

(b) 10,000 Hz Forcing frequency

Figure 8.6: Frequency Spectrum for defect length of $0.8 \cdot 10^{-2}$ and depth of $5.0 \cdot 10^{-3}$

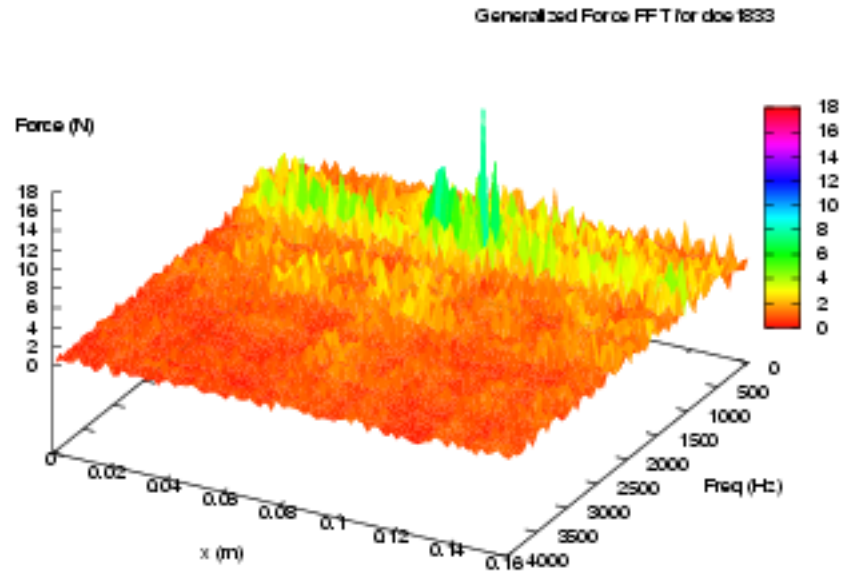

(a) 1,000 Hz forcing frequency

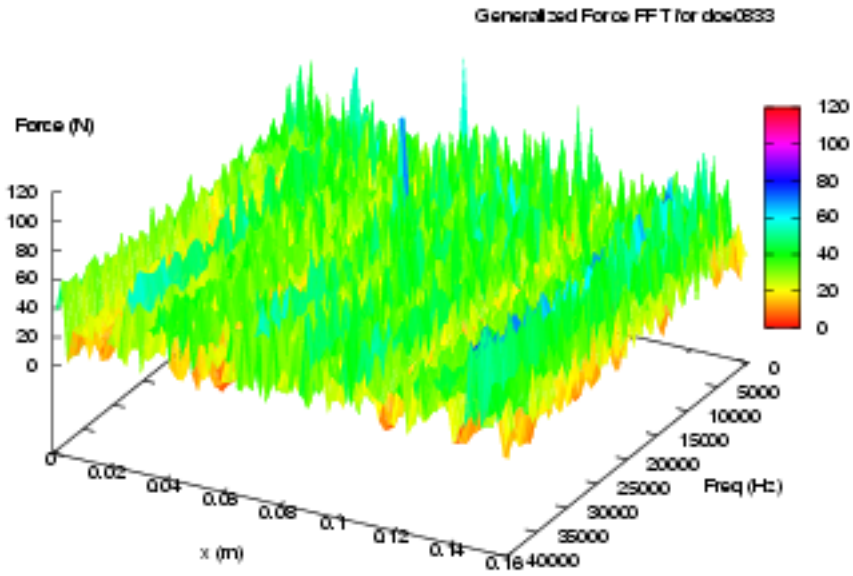

(b) 10,000 Hz forcing frequency

Figure 8.7: Frequency Spectrum for defect length of $4.0 \cdot 10^{-2}$ and depth of $4.0 \cdot 10^{-3}$

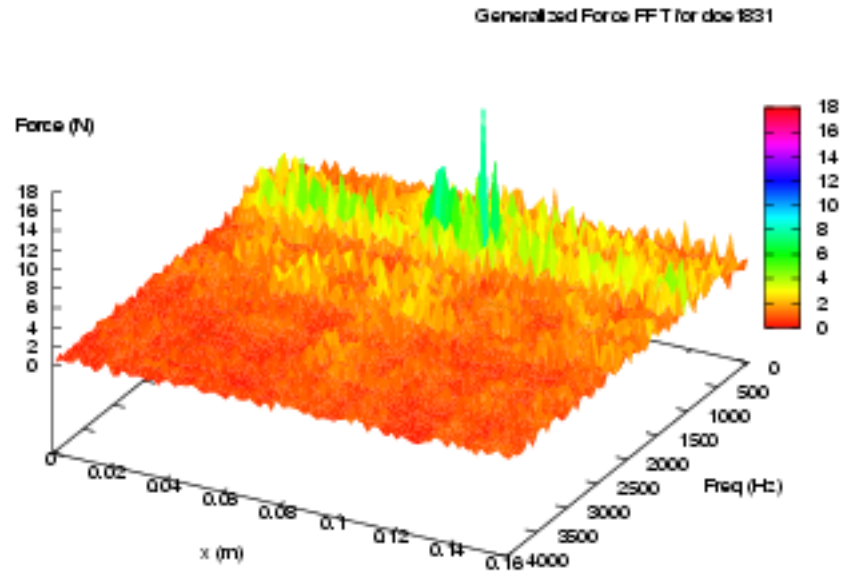

(a) 1,000 Hz forcing frequency

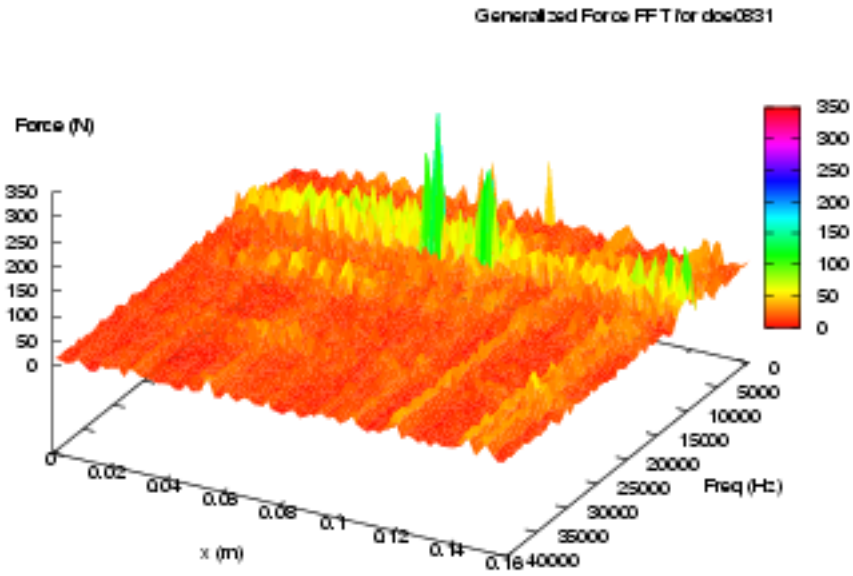

(b) 10,000 Hz forcing frequency

Figure 8.8: Frequency Spectrum for defect length of $2.0 \cdot 10^{-2}$ and depth of $4.0 \cdot 10^{-3}$

same pattern of the lower frequency case (1000 Hz) is showed. For a better understanding of the overall performance of the method a graph is reported with the power density of the frequency signal of the unbalanced force. The results are repoirted in figure 8.10 for the whole length of the beam and for the no-load are in term of the spatial distribution of the energy of the FFT of the UF. It is evident that the area of delamination is clearly characterized by a higher amount of the powere density.

8.5 Conclusion

As previously stated the method is a local method, its goal is to detect the area in which is high the chance of presence of discontinuous geometrical or mechanical characteristic. The expected pattern is a uniform random distribution of unbalanced force with the presence of high peak value exactly over the extention of the defected are.

This is exactly what is represented in the graphs of the section 7.1 in which a uniform random value is present which represents the moving of the mathematical model away from the physical one. Along with this pattern a peak values area is present exactly over the delamination length.

The defected area is very well found out in the case of delamination at 1.5mm from the neutral plane. The unbalanced force "noise" value is always less then 20% of the average peak value. A maximum in the peak value is present at both ends of the area where the discontinuity, due to the start in the delamination, gives rise to higher unbalanced forces. In the inner area the peak are less evident because the ply, over the delamination, tries to conform to the thin/thick plate model rules, although according to the different characteristics.

This kind of pattern ensure a better detection performances of the method highlighting a characteristic shape of the unbalanced spectrum that easily bring back to the presence of delamination.

The case of lower distance from the neutral axis (0.5mm from the neutral axis) presents some odd results. This inconsistencies are clearly due to the presence of delamination in the null bending strain area. In fact, in cases doe1832 and doe0833, no patterns that could bring back to delamination defect are present. The first case is with higher excitation frequency and the latter with the lower one.

For all the other cases the same consideration drawn out for the more superficial case are applicable. the noisy value is less than the 20% of the peak average. This deficiency of the method is acceptable due to the fact that vibration induced deflection in field of small displacement are not able

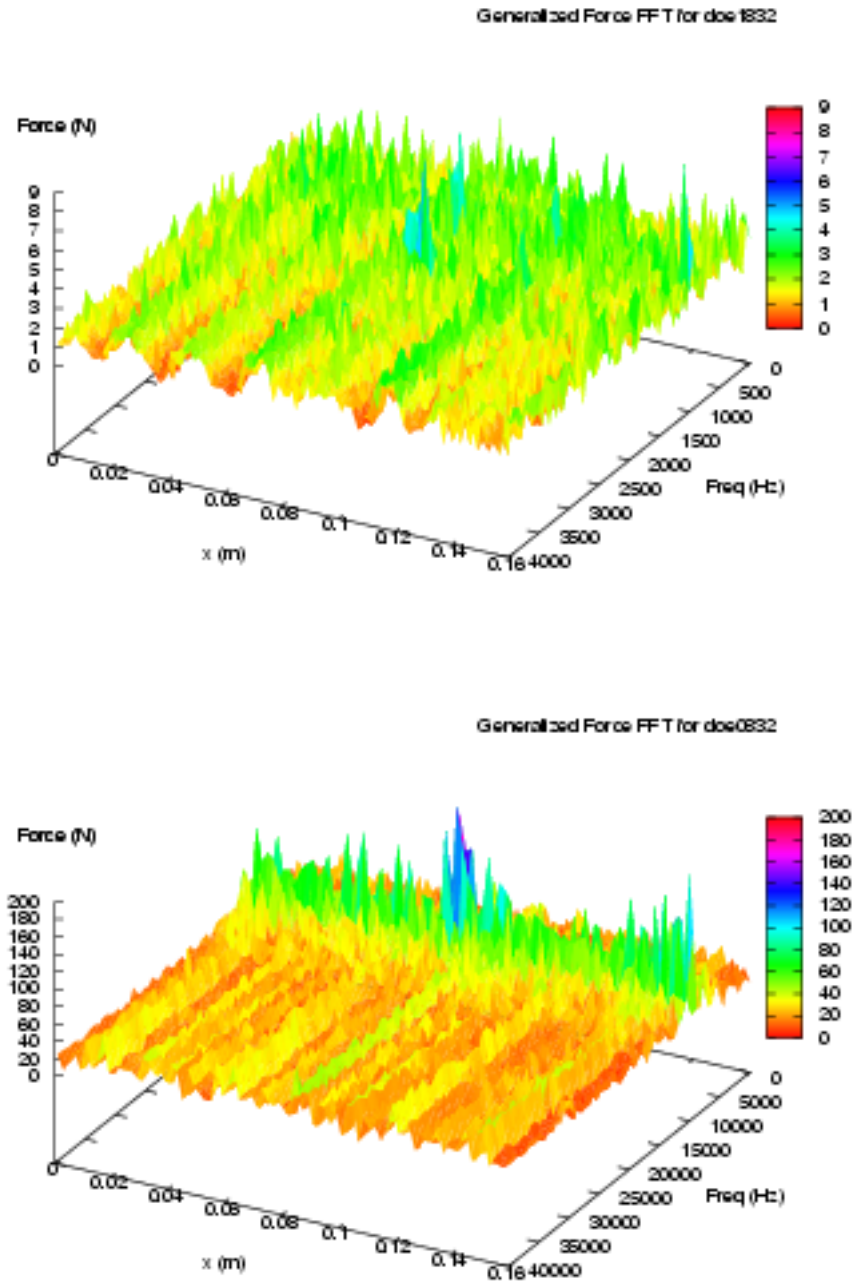

(a) 10,000 forcing frequency

Figure 8.9: Frequency Spectrum for defect length of and $0.8 \cdot 10^{-2}$ depth of $4.0 \cdot 10^{-3}$

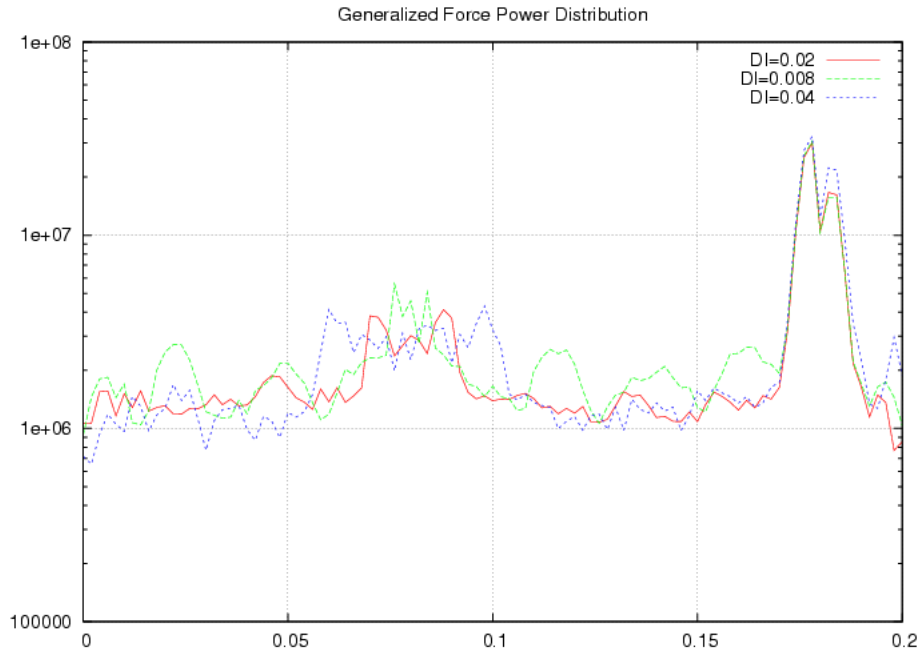

(a) Whole beam length

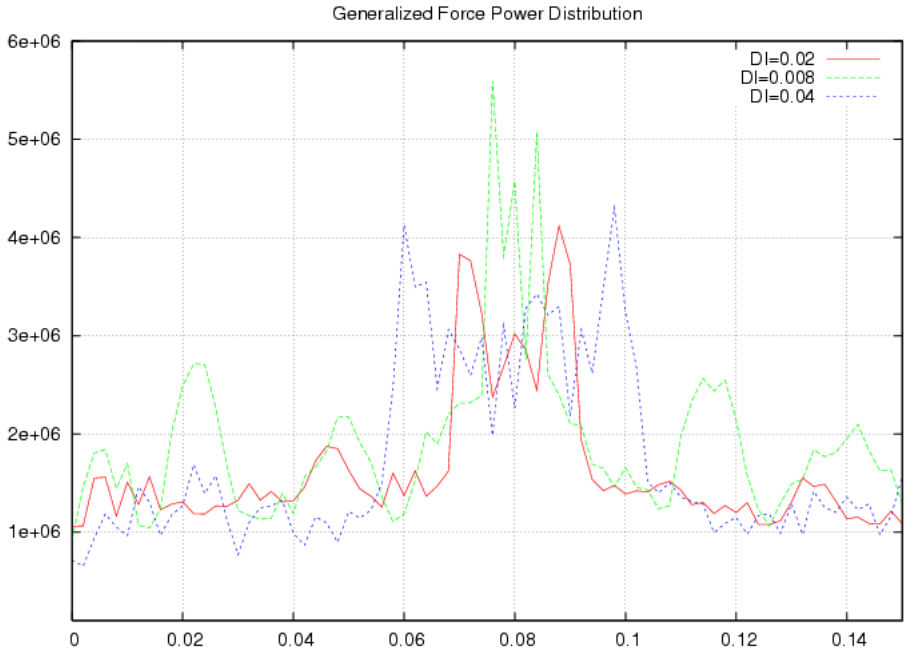

(b) Load application area excluded

Figure 8.10: Power densit yof the unbalanced force signal for the case with depth of $4.0 \cdot 10^{-3}$

to highlight defect in the area of neutral axis where bending stresses are null.

Bibliography

[Bucaro et ali 2004] J. A. Bucaro, A. J. Romano, P. Abraham, S. Dey, "Detection and localization of inclusions in plates using inversion of point actuated surface displacements" Journal of Acoustic Society of America115 (1) January 2004 pag. 201-206

[Romano et ali 1998] A. J. Romano, J. J. Shirron, J. A. Bucaro, "On the non invasive of material parameters from a knowledge of elastic displacements: Theory and numerical simulation", IEEE Transaction on ultrasonicsa and frequency control, vol 45, no 3 may 1998